Accumulation of ^{241}Am in the Southern Baltic Sea Sediments

M.Sc. Klaudia Block

Supervisor: dr hab. Dagmara Strumińska-Parulska, prof. UG

Co-supervisor: dr hab. Agata Zaborska, prof. IO PAN

Laboratory of Toxicology and Radiation Protection

Faculty of Chemistry, University of Gdańsk

Gdańsk 2024

Acknowledgments

I am deeply grateful to everyone who contributed to the completion of my doctoral journey. First of all, to my beloved supervisor - dr hab. Dagmara Strumińska-Parulska, prof. UG for her patience, support and guidance. It is thanks to you I have spread my wings.

I would like to thank my co-supervisor - dr hab. Agata Zaborska, prof. IO PAN for her constructive feedback and scientific advice at various stages of this research.

I would also like to thank Professor Ljudmila Benedik for providing knowledge and care during my stay in Slovenia.

I am grateful to my colleagues and friends for their encouragement, discussions, and moral support during challenging times. From University of Gdańsk: dr. Grzegorz Olszewski, thank you for always answering my questions and relieving stress with your sense of humour. Dr. Aleksandra Moniakowska, we laughed and cried together, if it weren't for you, I would be bored! Thank you.

My friends from the Jožef Stefan Institute in Slovenia: Majda Nikezić, Adna Alilović, Nurgul Nursapina, Saeed Waqar Ali, Sreekhanth Vijayakumaran Nair, Radojko Jaćimović and all the people I met at the institute, thank you for receiving me so warmly and that we had such a great time. I am very happy to have met you! And special thanks to my best friend from Slovenia - Jan Gačnik, without you I would have given up a long time ago, you are my daily support and with you life is easier, thank you for your life and scientific help. Love you!

To my dear friends - Klaudia, Mischel, Wiktoria and Ola, thank you for your moral support and for being with me in the hardest times. I know I can always count on you guys!

At the end thank my parents and my sisters Patrycja and Natalia thank you for your understanding. Doing my doctorate would have been much more difficult without all your support.

Table of Contents

Acknowledgments 1
Abbreviations 4
Abstract 6
Streszczenie pracy 8
1. INTRODUCTION 10
1.1 Discovery and Production of Americium 11
1.2 Physical and Chemical Properties of Americium 17
1.3 Primary Sources of Americium Radionuclides to the Marine Environment 24
1.3.1 Nuclear Weapons Testing 26
1.3.2 Nuclear Accidents 27
1.3.3 Radioactive Waste 29
1.3.4 Nuclear Reprocessing Plants 30
1.3.5 Ingrowth of ^{241}Am from ^{241}Pu 31
1.3.6 Sources of Americium in the Baltic Sea 32
1.4 Processes and Factors Affecting ^{241}Am Transport in Aquatic Ecosystem 36
1.5 Bioaccumulation and Biomagnification of ^{241}Am 39
1.6 Health Risks Associated with Radiation 40
1.7 Geochronological Methods 41
1.7.1 ^{241}Am as a Time-Marker for Sediment Dating 42
1.7.2 Radiolead Method 43
1.7.3 Cesium Method 46
1.8 Alpha Spectrometry for ^{241}Am Measurement 48
1.8.1 Alpha-particle Spectrometry 49
2. CHARACTERISTICS OF THE STUDY AREA 53
2.1 Overview of the study area 53
2.1.1. The geological history of the Baltic landscape 54
2.1.2. Water supply and exchange 55
2.1.3. Geological Composition and Sedimentation Dynamics: Key Factors Influencing Pollution Management in the Baltic Sea 57
2.1.4. Surface Water Circulation and Sedimentary Dynamics: Implications for Sediment Transport and Distribution in the Baltic Sea 58
2.1.5. Human-Induced Pressures and Environmental Challenges in the Baltic Sea 59

2.2. Bornholm Basin 61
2.3. Gdańsk Basin 62
2.4. Gotland Basin 63
2.5. Research Material 65
3. AIMS AND SCOPE OF WORK 66
4. CHARACTERISATION AND APPLICATION OF A SEQUENTIAL PROCEDURE FOR ^{241}Am DETERMINATION IN MARINE SEDIMENT 67
4.1 Sample Pre-treatment 67
4.2 Sample Decomposition 71
4.3 Preconcentration of Am by Oxalate Precipitation 72
4.4 Anion Exchange Chromatography 73
4.5 Extraction Chromatography 74
4.6 Source Preparation 78
4.7 The Efficiency of the Radiochemical Procedure 80
4.8 Analysis of Americium Isotopes by α-particle Spectrometry 82
4.9 Analysis of ^{210}Pb and ^{137}Cs Isotopes by γ-spectrometry 84
5. DATA ANALYSIS 86
5.1 Radiochemical Recovery 86
5.2 Minimum Detectable Activity (MDA) 87
5.3 Activity Concentration 87
5.4 Uncertainty Analysis 89
5.5 Quality Assurance and Control on ^{241}Am Analyses 91
6. RESULT AND DISCUSSION 97
6.1 Assessment of Age-Depth Relationships 97
6.1.1 Sediment Accumulation Rates 97
6.1.2 Distribution of ^{137}Cs 107
6.2 ^{241}Am Activity Concentrations in Sediments 112
6.2.1 Sediments Cores Collected in 2010 112
6.2.2 Sediment Cores Collected in 2019 115
6.3 Comparison of the Obtained ^{241}Am Activities with Literature Values 122
6.4 Statistical Analysis of ^{241}Am Activity Concentrations 124
6.5 Historical View on ^{241}Am Activity Concentration Changes 127
6.7 Limitations and Future Directions 135
7. CONCLUSIONS 137

REFERENCES 139
List of Figures 139
List of Tables 178

Abbreviations

AG	analytical grade
ALARA	as low as reasonably achievable
ATSDR	Agency for Toxic Substances and Disease Registry
CAS	Chemical Abstracts Service
CF:CS	constant flux and constant sedimentation
CRM	certified reference materials
CRS	constant rate of supply
CTBT	Comprehensive Nuclear-Test-Ban Treaty
CWA	Chemical Warfare Agents
DOE	Department of Energy
DTPA	diethylenetriaminepentaacetic acid
EDTA	ethylenediaminetetraacetic acid
FDNPP	Fukushima Daiichi Nuclear Power Plant
FWHM	Full Width at Half Maximum
GUM	Expression of Uncertainty in Measurement
HELCOM	Baltic Marine Environment Protection Commission
HIBA	hydroxyisobutyric acid
HPGe	High Purity Germanium Radiation Detectors
IAEA	International Atomic Energy Agency
INES	International Nuclear and Radiological Event Scale
INSAG	International Nuclear Safety Advisory Group
IQ	intelligence quotient
ISO	International Organization for Standardization
LOD	limit of detection
MAR	mass accumulation rates
MDA	minimum detectable activity
MOX	mixed oxide fuel

NIST	National Institute of Standards and Technology
NPL	National Physical Laboratory
NRC	Nuclear Regulatory Commission
OECD	Organization for Economic Cooperation and Development
PSU	practical salinity unit
QA	quality assurance
RBMK	high-power channel reactor
RM	reference material
SAR	sediment accumulation rate
TRU	TRans Uranium elements
UNSCEAR	United Nations Scientific Committee on the Effects of Atomic Radiation
USSR	Union of Soviet Socialist Republics
UTEVA	Uranium und TEtraValents Actinides
VIM	International Vocabulary of Metrology

Abstract

The presented PhD thesis aims to determine the activity levels and the distribution of alpha-emitting americium radionuclide, ^{241}Am, in dated sediments from the southern Baltic Sea. The accumulation rates determination allowed to assess the status and historical variability of bottom sediment contamination with ^{241}Am. The contamination of the Baltic Sea with radioactive substances occurred due to the global fallout of atmospheric nuclear weapon tests and the Chernobyl disaster. Although radioactivity levels decrease due to radioactive decay, the radionuclides' ecological half-lives in the entire Baltic Sea are prolonged due to slow water exchange and rapid sedimentation – also, ^{241}Pu decay, leading to the ingrowth of ^{241}Am activities over time. The knowledge of the quantity of ^{241}Am in the sediments of the Baltic Sea is limited. Thus, this study aimed to determine ^{241}Am in sediment cores collected from various locations of the southern Baltic Sea. Time-based distributions were derived from age-depth profiles using the ^{210}Pb dating method and further validated by ^{137}Cs profiles. The estimated accumulation rates differed among the three Baltic basins, ranging from 1.07±0.11 mm·year^{-1} to 4.34±0.33 mm·year^{-1}. The activities of ^{241}Am were measured by alpha spectrometry after radiochemical separation and purification. The results showed geographical divergences in the concentrations of ^{241}Am, varying from 0.020±0.001 Bq·kg^{-1} at the Gotland Basin to 3.19±0.23 Bq·kg^{-1} in the Gdańsk Basin. These findings enhance our understanding of the radioactive contamination levels in the Baltic Sea and serve as a crucial reference dataset for future assessments and management strategies to mitigate the environmental impact of radionuclides in the region.

The thesis is organized into six chapters, with the initial three chapters focusing on the theoretical aspects of the research. The first chapter presents the presence of americium in the marine environment. It covers the discovery and production of americium, its properties, and the primary sources of americium in the marine environment. The chapter also discusses the behaviour of ^{241}Am in the marine environment, including its transport, fate, and bioaccumulation. In addition, the potential health risks of exposure to americium are addressed, and the methods used to test for its presence and geochronological dating are also discussed. Chapter two

provides a detailed analysis of the geographic locations studied. It includes describing specific areas such as the Bornholm Basin, the Gdańsk Basin, and the Gotland Basin.

The chapter outlines the unique features of each area, highlighting their importance to the overall study. It also identifies the research needs, discusses the materials used in the study, and outlines the objectives and scope of the research work. The chapter serves as a basis for understanding the environmental context crucial to subsequent analysis and findings. The third chapter outlines the specifics of the step-by-step process designed to accurately determine ^{241}Am in marine sediments. This chapter shows the practical part of the research. Chapter four focuses on the processing and interpretation of the collected information. This chapter introduces the principles of data analysis, including aspects such as radiochemical recovery, minimum detectable activity (MDA), activity concentration, uncertainty analysis, and validation. This chapter is crucial to understanding the study's results and providing the necessary analysis for accurate interpretation. Chapter five is dedicated to the presentation and discussion of the findings. It is a closer look at the data. Lastly, chapter six closes the thesis by summarizing the essential findings and insights derived from the study. It offers a final assessment and draws conclusions based on the research outcomes, concisely summarizing the investigation.

Keywords: americium ^{241}Am, radioactive contamination, nuclear weapon tests, Chernobyl accident, bottom sediments, southern Baltic Sea

Streszczenie pracy

Prezentowana rozprawa doktorska ma na celu określenie poziomów aktywności i rozmieszczenia emitera promieniowania alfa izotopu ameryku, ^{241}Am, w datowanych osadach z południowego Bałtyku. Określenie wskaźników akumulacji pozwoliło ocenić stan i historyczną zmienność zanieczyszczenia osadów dennych ^{241}Am. Skażenie Morza Bałtyckiego substancjami radioaktywnymi nastąpiło głównie w wyniku globalnego opadu będącego skutkiem testów broni jądrowej w atmosferze i katastrofy elektrowni jądrowej w Czarnobylu. Chociaż poziomy radioaktywności maleją w efekcie rozpadu radioaktywnego, ekologiczne okresy półtrwania radionuklidów w całym Morzu Bałtyckim są wydłużone z powodu powolnej wymiany wody i szybkiej sedymentacji, a także również rozpadu ^{241}Pu, co prowadzi do wzrostu aktywności ^{241}Am w czasie.

Wiedza na temat ilości ^{241}Am w osadach Morza Bałtyckiego jest ograniczona. W związku z tym niniejsze badanie miało na celu określenie ^{241}Am w rdzeniach osadów zebranych z różnych miejsc południowego Bałtyku. Rozkłady czasowe zostały wyprowadzone na podstawie profili wiekowo-głębokościowych przy użyciu metody datowania ^{210}Pb i dodatkowo zweryfikowane przez profile ^{137}Cs. Oszacowane wskaźniki akumulacji różniły się między trzema basenami bałtyckimi, wahając się od 1.07±0.11 mm·rok^{-1} to 4.34±0.33 mm·year^{-1}. Aktywność ^{241}Am zmierzono metodą spektrometrii alfa po uprzedniej radiochemicznej separacji i oczyszczeniu. Wyniki wykazały geograficzne zróżnicowanie stężeń aktywności ^{241}Am, wahające się od 0,020±0,001 Bq·kg^{-1} w Basenie Gotlandzkim do 3,19±0,23 Bq·kg^{-1} w Basenie Gdańskim. Wyniki te zwiększają nasze zrozumienie poziomów skażenia radioaktywnego w Morzu Bałtyckim i służą jako kluczowy zbiór danych referencyjnych dla przyszłych ocen i strategii zarządzania w celu złagodzenia wpływu radionuklidów na środowisko w regionie.

Praca składa się z sześciu rozdziałów, z których pierwsze trzy koncentrują się na teoretycznych aspektach badań. Rozdział pierwszy przedstawia obecność ameryku w środowisku morskim obejmuje odkrycie i produkcję ameryku, jego właściwości oraz główne źródła. W rozdziale omówiono również zachowanie ^{241}Am w środowisku morskim, w tym jego transport, los i bioakumulację. Ponadto omówiono potencjalne zagrożenia dla zdrowia wynikające z narażenia na działanie ameryku, a także metody

stosowane do badania jego obecności i datowania geochronologicznego. Rozdział drugi zawiera szczegółową analizę badanych lokalizacji geograficznych. Obejmuje ona opis konkretnych obszarów, takich jak Basen Bornholmski, Basen Gdański i Basen Gotlandzki. Rozdział przedstawia unikalne cechy każdego obszaru, podkreślając ich znaczenie w aspekcie przeprowadzonych badań. Określono również potrzeby badawcze, omówiono materiały wykorzystane w badaniu oraz nakreślono cele i zakres prac badawczych. Rozdział ten jest podstawą do zrozumienia kontekstu środowiskowego, kluczowego dla późniejszej analizy i ustaleń. Trzeci rozdział przedstawia specyfikę analizy radiochemicznej, procesu krok po kroku zaprojektowanego w celu dokładnego oznaczenia ^{241}Am w osadach morskich. Rozdział ten przedstawia praktyczną część badań. Rozdział czwarty koncentruje się na przetwarzaniu i interpretacji zebranych informacji. Rozdział ten wprowadza zasady analizy danych, w tym aspekty takie jak odzysk radiochemiczny, minimalna wykrywalna aktywność (MDA), stężenie aktywności, analiza niepewności i walidacja. Rozdział ten ma kluczowe znaczenie dla zrozumienia wyników badania i zapewnienia niezbędnej analizy w celu dokładnej interpretacji. Rozdział piąty poświęcony jest prezentacji i omówieniu wyników. Jest to bliższe spojrzenie na dane. Wreszcie, rozdział szósty zamyka rozprawę, podsumowując najważniejsze ustalenia i spostrzeżenia wynikające z badania. Zawiera on końcową ocenę i wyciąga wnioski na podstawie wyników badań, zwięźle podsumowując dochodzenie.

Słowa kluczowe: ameryk ^{241}Am, skażenie radioaktywne, testy broni jądrowej, awaria w Czarnobylu, osady denne, Bałtyk Południowy

1. INTRODUCTION

The Baltic Sea is one of the most heavily polluted seas globally, grappling with severe contamination, eutrophication, and the spread of hypoxia. Persistent inflows of hazardous substances and nutrients steadily infiltrate the Baltic Sea, where they accumulate over decades due to its restricted water exchange. A thorough comprehension of the oceanic processes within the Baltic Sea holds paramount significance for effective marine environment management. Marine sediments are the largest reservoir for heavy metals and radionuclides. Adsorbed onto suspended particulate matter, radionuclides sink and settle into the sediments. Here, they can be re-mobilized into the overlying water column through physical and biochemical processes or part of the pool of radionuclides buried deeper in the sediments. Pollution of bottom sediments, especially in coastal, port, and estuarine areas, may directly threaten bottom organisms and indirectly threaten the entire trophic chain (Snelgrove, 1999).

Environmental radiochemistry mainly aims to analyze radioisotope concentrations in the environment. So far, no studies have assessed the status and historical variability of the southern Baltic Sea bottom sediments with the radioactive isotope americium ^{241}Am. The ^{241}Am is a long-lived α-emitting nuclide that has become one of the critical marine contaminants. Since the 1940s, continuous releases of ^{241}Am into the marine environment have occurred due to various human nuclear activities, including atmospheric nuclear weapon tests, discharges from nuclear reprocessing plants, and nuclear accidents (such as Palomares in 1966, Thule in 1968, Chernobyl in 1986, and Fukushima in 2011) (Cundy et al., 2002; Kashparov et al., 2003b; Muravitsky et al., 2005; UNSCEAR, 2000). Furthermore, with the beta-decay of the increasing ^{241}Pu resulting from weapon-fallout-derived releases or nuclear accidents, additional environmental contamination with ^{241}Am is anticipated (Bouisset ET AL., 2021; Kashparov et al., 2003b; Muravitsky et al., 2005). These releases of ^{241}Am pose a long-term radioactive risk to the environment and potential threats to public health due to its toxicity. Therefore, it is imperative to regularly monitor the levels of ^{241}Am in the environment and assess its radiological risk and environmental impact. Additionally, ^{241}Am is a critical indicator in oceanography, identifying the source of artificial radioactivity and playing a significant role in sediment dating studies (Arnaud et al., 2006). The variation of radionuclide contents in bottom sediments depends on several

factors such as latitude, local input, sediment accumulation and mixing rates, removal efficiencies due to particle types and sizes, lateral transport of water and particles, and organic carbon content in sediment (Carpenter et al., 1987; Baskaran et al., 1996).

Regarding studies on the presence of americium in the marine environment, more knowledge is needed on the concentration of ^{241}Am activity in its major constituents. This isotope could significantly affect marine biota and adversely affect countries bordering the Baltic Sea. Determination of ^{241}Am in the environment is essential for monitoring its release (both controlled and accidental releases) and for assessing environmental impact and radiological risk. Based on the obtained data on ^{241}Am in consequent sediment layers, it is possible to delve into the historical accumulation of isotopes in sediments. The main points of the study include assessing the contamination levels and distribution patterns of ^{241}Am in dated sediment cores. In addition, the study aims to provide a comprehensive assessment of sediment contamination and offer detailed insight into the historical distribution of ^{241}Am in dated sediment cores. A key aspect of this research is to estimate the activity of ^{241}Am concerning its source, namely the Chernobyl Nuclear Power Plant accident. This multifaceted approach aims to uncover detailed information on the temporal evolution of ^{241}Am in sediments, shedding light on contamination levels and distribution dynamics, ultimately increasing our understanding of the long-term impact of the Chernobyl Nuclear Power Plant accident on Baltic Sea sediments.

1.1 Discovery and Production of Americium

Actinides are elements with atomic numbers ranging from 89 to 103 that follow actinium. All elements in the actinide series are unstable, releasing considerable energy during radioactive decay ranging from millions of years to a few nanoseconds. Americium and plutonium belong to the transuranic elements created artificially through nuclear processes, with atomic numbers greater than 92, the atomic number of uranium (Lehto and Hou, 2010).

Glenn Theodore Seaborg, an American chemist, made significant contributions to nuclear science. For his work on the synthesis, discovery, and investigation of ten transuranium elements, he received the Nobel Prize in Chemistry in 1951. Glenn Seaborg joined the Manhattan Project in 1940 after he and his colleagues produced

plutonium at the University of California, Berkeley (Hoffman, 2002). Seaborg created the plutonium bomb that was used to attack Nagasaki in Japan. After the war, he returned from Chicago to Berkeley as a full professor of chemistry, bringing some of his associates with him. Seaborg and his colleagues started producing and identifying other transuranic elements with atomic numbers 95 (americium) and 96 (curium). They were ineffective until Seaborg came up with the development of the actinide concept and the arrangement of the actinide series in the periodic table of the elements in which the 14 elements heavier than actinium are placed in the periodic table of elements as a transition series under the lanthanide transition series, as shown in Figure 1 (Seaborg, 1946).

The history of the announcement of the discovery is fascinating. During World War II, the information of essential findings, such as new elements on the periodic table, had to remain until the conflict was over. On November 11, 1945, an announcement was made unintentionally over live radio during an episode of NBC's 'Quiz Kids'. Seaborg appeared as a guest on a program that featured children with high IQs. The researcher questioned whether any new elements, besides plutonium and neptunium, had been identified in Seaborg's lab during the war (Runde and Schulz, 2008).

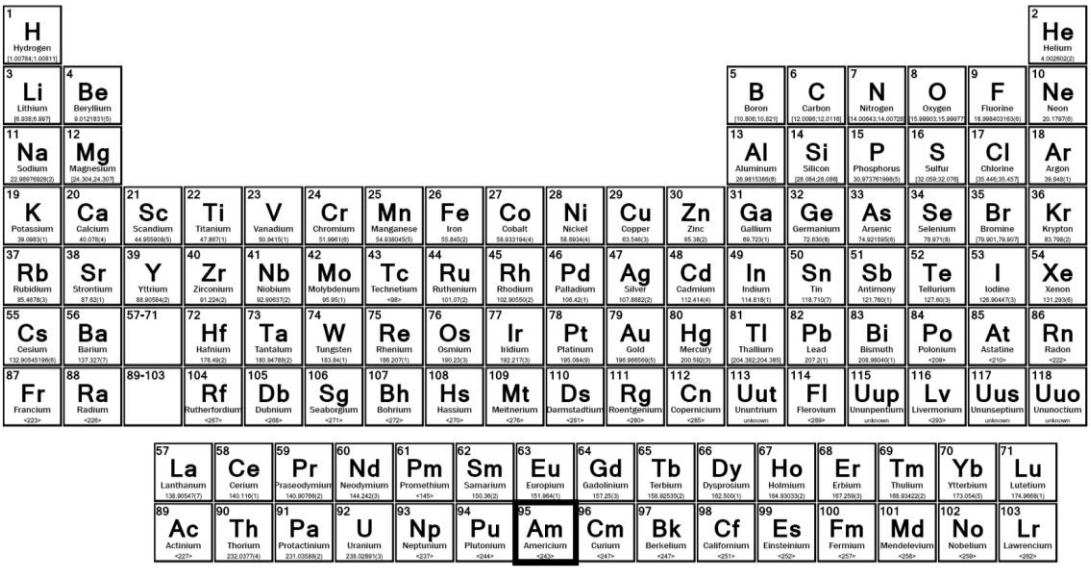

Figure 1. Periodic table of elements - element of americium highlighted by a bold border (National Center for Biotechnology Information, 2024)

Thus, americium was discovered by G. Seaborg, L. Morgan, R. James, and A. Ghiorso in 1944 and isolated by B.B. Cunningham as the isotope ^{241}Am in $Am(OH)_3$ in the fall of 1945. The name "americium" was proposed for element 95, in tribute to America by analogy with naming its rare earth homolog "europium" after Europe. ^{241}Am is produced by bombarding ^{239}Pu with neutrons, causing some ^{239}Pu atoms to capture a neutron and transform into ^{240}Pu. The ^{240}Pu changed into ^{241}Pu, which then decayed into ^{241}Am through beta decay, according to the following reactions (Ghiorso et al. 1950):

$$Pu^{239} + n \rightarrow Pu^{240} + \gamma$$

$$Pu^{240} + n \rightarrow Pu^{241} + \gamma$$

$$Pu^{241}(14\ years) \xrightarrow{\beta^-} Am^{241}\ (432.2\ years, \alpha)$$

$$Am^{241} + n \rightarrow Am^{242} + \gamma$$

$$Am^{242} + n \rightarrow Am^{243} + \gamma$$

^{241}Am and ^{243}Am can be produced through neutron activation involving an operating nuclear reactor or bomb detonation. This process starts with the neutron activation of ^{239}U or ^{239}Pu (Vajda and Kim, 2011).

Specifically, ^{241}Am can also be produced more directly through the alpha bombardment of ^{238}U to produce ^{241}Pu (^{238}U [α,n] ^{241}Pu), followed by its subsequent beta decay. Each americium isotope, including ^{241}Am, can be neutron-activated to produce isotopes up through at least ^{246}Am. The quantity of any produced isotope depends on the initial mass of either ^{238}U or ^{239}Pu and the neutron fluence during the activation period, balanced by the natural radioactive decay of the isotopes being formed (Malátová and Bečková, 2014; Parrington et al., 1996). For example, an atom of ^{239}Pu will naturally decay to ^{235}U unless its first neutron is activated to ^{240}Pu. An isotope of ^{240}Pu will alpha decay to ^{236}U unless it is first activated to ^{241}Pu. ^{241}Pu, in turn, will beta decay to ^{241}Am unless it undergoes neutron activation to ^{242}Pu. These processes can be managed through focused radiochemical separation or special processing, such as proton bombardment, to direct the effort toward a specific isotopic product (Parrington et al., 1996).

In general, lower mass isotopes are preferentially produced in the relatively low fluxes available inside nuclear reactors, while higher masses are more feasibly produced in extreme flux conditions present during a nuclear detonation (Parrington et al. 1996). The processes involved are summarized in Figure 2.

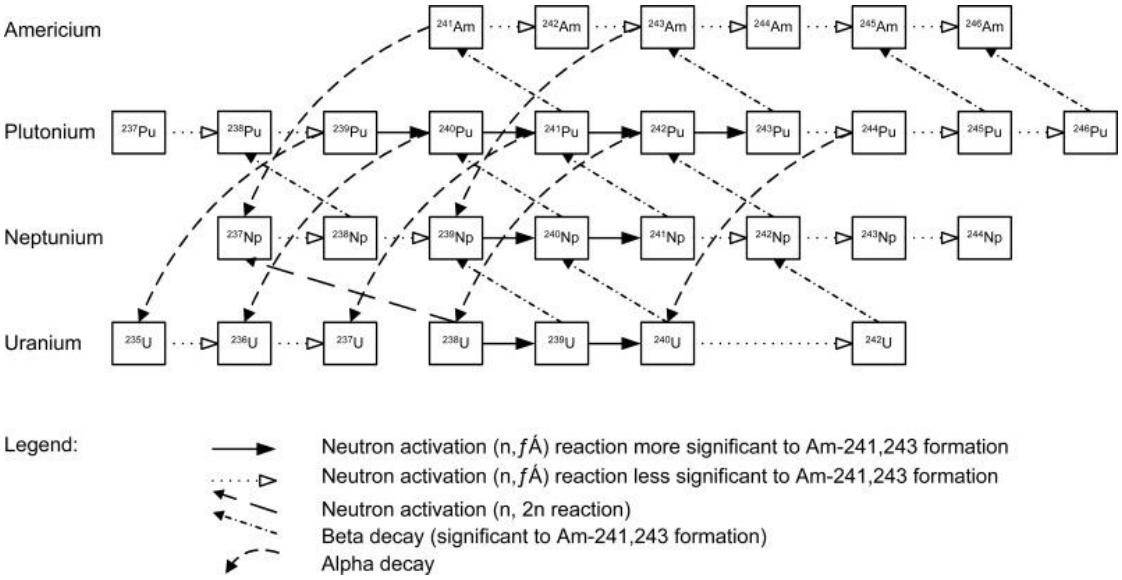

Figure 2. Production table for ^{241}Am (Parrington et al. 1996)

It is worth adding that among americium isotopes, ^{241}Am is widely used in industrial fields, such as static charge eliminators and smoke detectors (Aggarwal, 2018; Bennett, 1978).

The ^{241}Am and ^{243}Am decay scheme is complex, as shown in Tables 1 and 2.

Table 1. ^{241}Am decay scheme - minimum intensity 2%, up to five energies, with at least one entry per radiation type (ATSDR, 2004)

Nuclide	**Half-life**	**Energies and intensities of the emitted radiation**					
		Alpha (α)		Beta (β) max		Gamma (γ)	
		keV	%	MeV	%	keV	%
^{241}Am	432.2 years	5.485	84.5			13.9	42
↓		5.443	13.0			59.5	35.9
						26.3	2.4
^{237}Np	$2.144 \cdot 10^{6}$ years	4.788	47			13.3	58
↓		4.771	25			29.4	15
		4.766	8			86.5	12.4
		4.639	6.2			8.2	9
		4.664	3.3			95.9	2.7

Table 2. continued

^{233}Pa ↓	26.97 days			232 156 260 174 572	40 27.7 17 16.4 4	13.6 312.2 98.4 94.7 111.0	56 38.6 17.7 10.9 8.2
^{233}U ↓	$1.592 \cdot 10^5$ years	4.824 4.784	84.4 13.2			13.0	6.0
^{229}Th ↓	7.340 years	4.845 4.901 4.815 5.053 4.968	56.2 10.2 9.3 6.6 6.0			12.3 88.5 85.4 100.0 11.1	79 24.7 15.0 11.3 8
^{225}Ra ↓	14.9 days			331 371	69.5 30.5	40.0 12.7	30.0 15.2
^{225}Ac ↓	10.0 days	5.830 5.792 5.791 5.732 5.637	50.7 18.1 8.6 8.0 4.4			12.0 10.6	20.9 9.3
^{221}Fr ↓	4.9 minutes	6.341 6.126	83.4 15.1			218.2 11.4	11.6 2.2
^{217}At ↓	0.323 seconds	7.066				258.5	0.056
^{213}Bi 97.84% ↓ 2.16%	45.59 minutes	5.869	1.94	1422 982	65.9 31.0	440.5 79.3	26.1 2.0
^{213}Po ↓	3.65 microseconds	8.376	100.0			778.8	0.005
^{209}Tl ↓	2.2 minutes			660	98.8	1567.1 465.1 117.2 75.0 10.6	99.8 96.9 84.3 10.7 9.4
^{209}Pb ↓	3.253 hours			0.644	100		
^{209}Bi	stable						

Table 3. ^{243}Am decay scheme - minimum intensity 2%, up to five energies, with at least one entry per radiation type (ATSDR, 2004)

Nuclide	**Half-life**	**Energies and intensities of the emitted radiation**					
		Alpha (α)		Beta (β) max		Gamma (γ)	
		keV	%	MeV	%	keV	%
^{243}Am ↓	7.370 years	5.275 5.233 5.181	87.4 11.0 1.1			74.7 13.9 43.5	68.2 21.4 5.9
^{239}Np ↓	2.3565 days			436.5 330.4 391.9 714.1	45 40.5 11 2.0	14.3 106.1 103.8 277.6 99.6	63 27.2 22.5 14.4 14.0
^{239}Pu ↓	24.110 years	5.157 5.144 5.106	73.3 15.1 11.5			13.6	4.9
^{235}U ↓	703.800.000 years	4.398 4.366 4.215 4.596 4.325	55 17.0 5.7 5.0 4.4			185.7 13.0 143.8 93.4 163.3	57.2 36 11.0 5.8 5.1
^{231}Th ↓	25.52 hours			288.1 305.3 206.0 287.2 142.2	40 33 12.8 12 2.8	13.3 25.6 84.2	72 14.1 6.6
^{231}Pa ↓	32.760 years	5.014 4.951 5.028 5.059 4.736	25.4 22.8 20.0 11.0 8.4			12.7 27.4 300.0 302.6	36 10.3 2.5 2.2
^{227}Ac 98+% ↓ 1.4%	21.772 years	4.953	0.658	44.8 35.5 20.3	53 35 10	12.0	0.088
^{227}Th ↓		18.68 days	6.038 5.978 5.757 5.709 5.713	24.2 23.5 20.4 8.3 4.9		12.3 236.0 50.1 256.2 329.8	40 12.9 8.4 7.0 2.9
	^{223}Fr ↓	22.00 minutes			1.099.,0 1.069.4 914.3	70 15.0 10.1	50.1 12.3 79.7 234.8 49.8	34 30 8.7 3.0 2.8

Table 4. continued

^{223}Ra ↓	11.43 days	5.716 5.607 5.747 5.540 5.434	51.6 25.2 9.0 9.0 2.2			83.8 11.7 81.1 269.5 94.9	25.4 25 15.3 13.9 11.5
^{219}Rn ↓	3.96 seconds	6.819 6.553 6.425	79.4 12.9 7.5			271.2 401.8	10.8 6.6
^{215}Po ↓	1.781 milliseconds	7.386	100.0				
^{211}Pb ↓	36.1 minutes			1379 547	91.3 6.3	404.9 832.0	3.8 3.5
^{211}Bi ↓	2.14 minutes	6.623 6.278	83.5 16.2			351.1	12.9
^{207}Tl ↓	4.77 minutes			1427	99.7	897.8	0.26
^{207}Pb	stable						

1.2 Physical and Chemical Properties of Americium

Americium is part of the actinide series of elements, and it is located in period seven and group 3 of the periodic table. Its atomic number is 95, and the electron configuration is $1s^1\ 2s^2\ 2p^6\ 3s^2\ 3p^6\ 4s^2\ 3d^{10}\ 4p^6\ 5s^2\ 4d^{10}\ 5p^6\ 6s^2\ 4f^{14}\ 5d^{10}\ 6p^6\ 5f^7\ 7s^2$. Many known isotopes of americium range from atomic mass 232 to 247. However, the most studied isotopes are ^{241}Am and ^{243}Am, and both isotopes have the same chemical behavior in the environment (Aggarwal, 2018; Runde and Schulz, 2008).

Following the discovery of americium and its inclusion in the actinide series, research into comparisons between americium and other actinides and lanthanide species began. The oxidation states of americium are +II (only in solid-state compounds), +III, +IV, +V, and +VI (Runde and Mincher, 2008; Seaborg, 1991). The most stable oxidation state for americium is +III, forming stable compounds with many other elements, and Am(III) has been reported to sorb strongly to natural sediments, with sorption often increasing with pH (Das et al., 2011; Moulin et al., 1992). The challenge of actinide analysis lies in the absence of highly complex-forming tetravalent

species of americium and curium, along with their chemical similarities to each other and the lanthanides. These factors significantly impede the possibility of separation, making Am and Cm chemistry the most challenging part of the analysis of actinides (Vajda et al., 2012).

Americium in an aqueous solution occurs in oxidation states in the following forms:

$$+\text{III} : Am^{3+} \qquad +\text{IV} : Am^{4+} \qquad +\text{V} : AmO_{2}^{+} \qquad +\text{VI} : AmO_{2}^{2+}$$

The first study of the absorption spectrum of Am(III) revealed similarities to rare earth solutions (Tian et al., 2002; Stumpf et al., 2008). In perchloric acid, the absorption spectrum of Am(III) revealed an intense absorption at 503 nm (Werner and Perlman, 1951). They investigated AmO_2^+ by oxidizing an Am(III) carbonate solution with sodium hypochlorite. The hexavalent state of Am was reported in 1951 (Asprey et al., 1951). The trivalent state of americium has a characteristic pink color that, when oxidized, changes to a yellow color (AmO_2^+) and then to a reddish-brown color (AmO_2^{2+}). Although Asprey et al. discovered stability issues with the higher oxidation states of Am(V) and Am(VI) in an acidic solution, the specific issues were not discussed (Asprey et al., 1951). Later work discovered that the kinetics of the disproportionation of Am(V) to Am(III) and Am(VI), followed by auto reduction of Am(VI) to Am(V), were caused by radiolysis products (Asprey and Penneman, 1962). However, Am(III) could theoretically oxidize to the tetravalent Am oxidation state. It is unstable in acidic media. The standard electrode potential of the Am^{4+}/Am^{3+} couple in an acidic solution is very high (2.44 V) and significantly lower (0.4─0.5 V) in basic ones. Therefore, forming Am(IV) in basic solutions is possible when a strong complexing agent, such as phosphates, is present. However, this species is unstable and can be readily reduced to the trivalent state (Warwick et al., 1996). After plutonium, americium is the second element to coexist in all four oxidation states simultaneously in carbonate solutions (Bourges et al.,1983).

Despite the stability issues associated with higher oxidation states, many methods for separating Am and Cm by oxidizing americium have been developed (Goff et al., 2012; Mincher et al., 2014). Stephanou et al., 1952 reported separating Am and Cm by oxidizing Am to the hexavalent state with peroxy disulfate, followed by precipitation of CmF_3. Precipitation of lanthanide trifluoride has also been shown to

separate Am(VI) from large quantities of lanthanides (Shehee et al., 2010). The physical and chemical properties of americium and selected americium compounds are shown in Table 3.

Although fluoride precipitations can achieve > 90% separation, the precipitating agent is 3-4 M hydrofluoric acid (HF), making the process unsuitable for commercial reprocessing or recycling due to the difficulty of handling and the corrosive nature of fluoride solutions.

Over time, several new separation methods that used oxidation of species to higher states were reported. Liquid-liquid extraction, for example, used ammonium persulfate as an oxidizing agent to oxidize Am(III) to Am(VI), followed by reduction to produce Am(V) (Stokely and Moore, 1967). Potassium persulfate (Scott, 2011), sodium perxenate (Holcomb, 1965), sodium bismuthate (Mincher et al., 2008), and electrolytic oxidation (Myasoedov et al., 1986) are some other oxidizing agents used in the separation of trivalent actinides (Holcomb, 1965; Musikas et al., 1980). Figure 3 and Figure 4 show the standard reduction potentials for Am oxidation states at an acidic and basic solution, respectively.

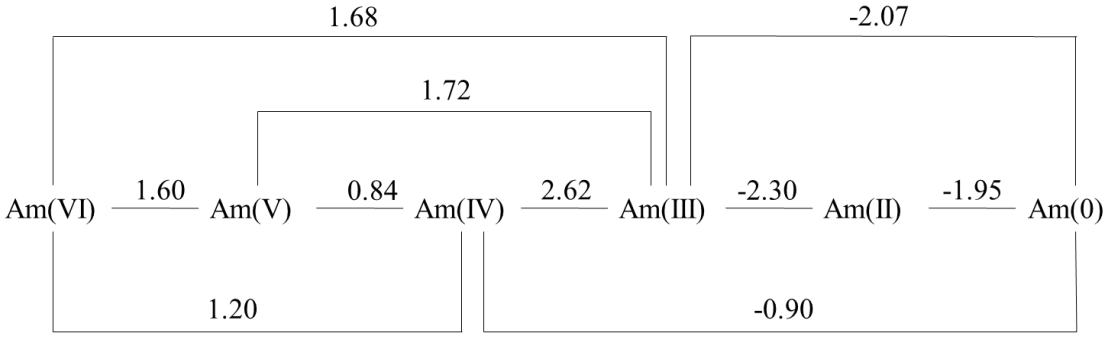

Figure 3. Standard reduction potentials of Am at the acidic solution (E_0/V) (Schulz, 1976; Silva and Nitsche, 1995)

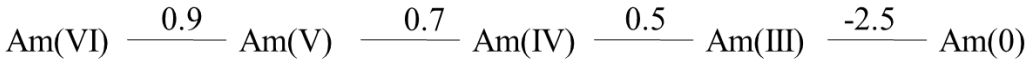

Figure 4. Standard reduction potentials of Am at the basic solution (E_0/V) (Penneman and Keenan, 1960; Schulz, 1976)

Table 5. Physical and chemical properties of americium and selected americium compounds (ATSDR, 2004)

	Value			
Property	**Americium**	**Americium(II) oxide**	**Americium(III) oxide**	**Americium(III) chloride**
Atomic/molecular weight[a]	243	275	534	349
Chemical formula	Am	AmO_2	Am_2O_3	$AmCl_3$
Synonyms	No data	No data	No data	No data
CAS Registry No.	7440-35-9[b]	12005-67-3	12254-64-7	13464-46-5
Color	Silvery	Black	Tan	Pink
Physical form	Solid metal	Cubic crystals	Hexagonal crystals	Hexagonal crystals
Odor	No data	No data	No data	No data
Melting point, EC	1,176	>1,000 (decomposes)	No data	500
Boiling point, EC	2,011	Not relevant	No data	No data
Autoignition temperature	No data	Not relevant	Not relevant	Not relevant
Solubility: Water Other solvents	 Insoluble Soluble in acid	 No data Soluble in acid	 No data Soluble in acid	 Soluble No data
Density [$g \cdot cm^{-3}$]	12	11.68	11.77	5.87
Partition coefficients	No data	No data	No data	No data
Vapor pressure	No data	No data	No data	No data
Refractive index	No data	No data	No data	No data
	Americium(III) fluoride	**Americium nitrate**	**Americium citrate**	
Atomic/molecular weight[a]	300	429	432	
Chemical formula	AmF_3	$Am(NO_3)_3$	$AmC_6H_5O_7$	
Synonyms	No data	Americium trinitrate	No data	
CAS Registry No.	13708-80-0	25933-53-3	11078-88-9	

Table 6. (continued)

Property	Americium(III) fluoride	Americium nitrate	Americium citrate
Color	Pink	No data	No data
Physical form	Hexagonal crystals	No data	No data
Odor	No data	No data	No data
Melting point, EC	1,393	No data	No data
Boiling point, EC	No data	No data	No data
Autoignition temperature	Not relevant	Not relevant	Not relevant
Solubility: Water Other solvents	 No data No data	 No data No data	 No data No data
Density [$g \cdot cm^{-3}$]	9.53	No data	No data
Partition coefficients	No data	No data	No data
Vapor pressure	No data	No data	No data
Refractive index	No data	No data	No data

[a]calculated for ^{243}Am

[b]this is also a generic CAS Registry Number for americium (unspecified form)

An essential property of Am is its ability to form complex ions in aqueous solutions with inorganic ions or organic compounds. The relative tendency of Am species to form complexes varies depending on their charge density and can be ranked as follows:

$$AmO_2^{2+} \sim Am^{3+} > AmO_2^{+}$$

The absence of the highly complex-forming tetravalent Am species and americium chemical similarity to the lanthanides greatly hinders the separation of Am. No highly stable Am complexes are available, and highly selective separations with extremely high distribution coefficients towards the lanthanides are lacking. Table 4 summarizes the stability constants of the most stable complexes of Am(III) with both inorganic and simple organic complexes. As a result, americium chemistry remains the most challenging aspect of actinide analysis, especially in the actinide technology of spent fuel reprocessing/partitioning and radioactive waste management.

Table 7. Summarized stability constants of the most stable complexes of Am(III) with inorganic and simple organic complexes (according to Runde and Schulz, 2008)

Complex	**Temperature [°C]**	**Ionic strength [M]**	**Ig [β_H] stability constants**
$AmOH^{2+}$	25	0.005	10.7
$Am(OH)_2^{+}$	25	0.005	20.9
$AmCO_3^{+}$			7.8
$Am(CO_3)_3^{3-}$			15.2
AmF^{2+}	25	1	2.9
AmF_3	23	0	2.1
$AmCl^{2+}$			-2 -1.2
$AmCl_2^{+}$			-1 -0.3
$AmBr^{2+}$	25		3.3
$AmNO_3^{2+}$			-1.3 -0.6
$Am(NO_3)^{2+}$			0.2
$AmSCN^{2+}$			0.2–0.9
$Am(SCN)_3$	25	5	0.6
$Am(SCN)_4^{-}$	25	5	0
$AmSO_4^{+}$			1.2–1.9
$Am(SO_4)_2^{-}$			1.8–2.1
$AmH_2PO_4^{2+}$	20	0.2	1.7
$Am(H_2PO_4)_4^{-}$		1	3.4
Am-acetate^{2+}			1.8–2.1

Table 8. (continued)

Am-acetate$_6^{3-}$		1	7.7
Am-oxalate^{+}			4.6–7.3
Am-oxalate$_3^{3-}$			11.1–12.3
Am-oxalate$_4^{-}$		1	11
Am-HIBA^{2+}		0.5	2.7
Am-HIBA$_3$			5–6.3
Am-citrate^{0}		1	7.1
Am-citrate$_2^{3-}$			9.7–14
Am-EDTA^{-}			16.9–18.1
AmHEDTA			9.3–14
AmDTPA^{2-}			21.3–24.0
AmHDTPA^{-}	25	0.1	14.3

HIBA α-hydroxyisobutyric acid, EDTA ethylenediaminetetraacetic acid, DTPA diethylenetriaminepentaacetic acid

Cations in any aqueous environment will be complexed by water molecules (hydration) or other present ligands. The environment contains a number of common ligands, such as CO_3^{2-}, OH^{-}, Cl^{-}, and natural organic matter, which can complex radionuclides. In addition, synthetic organic ligands may also be present as co-contaminants (Silva and Nitsche, 1995). The stability series of the inorganic complexes of Am(III) (which is similar to that of Pu(III)) is as follows:

$$OH^{-}, CO_3^{2-} > F^{-}, H_3PO_4^{2-}, SO_4^{2-} > Cl^{-}, NO_3^{-} > ClO_4^{-}$$

Although the stability of Am thiocyanate (SCN) complexes is not high, they play a significant role in Am chemistry due to their relatively high separation factors towards lanthanides (Harmon et al., 1972).

The balance between the various oxidation forms of americium is well illustrated by the Pourbaix diagram in the redox potential (Eh) and pH coordinate system in Figure 5, illustrating the stability of americium oxidation states in carbonate solution. The chart shows three oxidation levels of americium in equilibrium, allowing the disproportionation reaction to proceed under these conditions (Runde and Mincher, 2011).

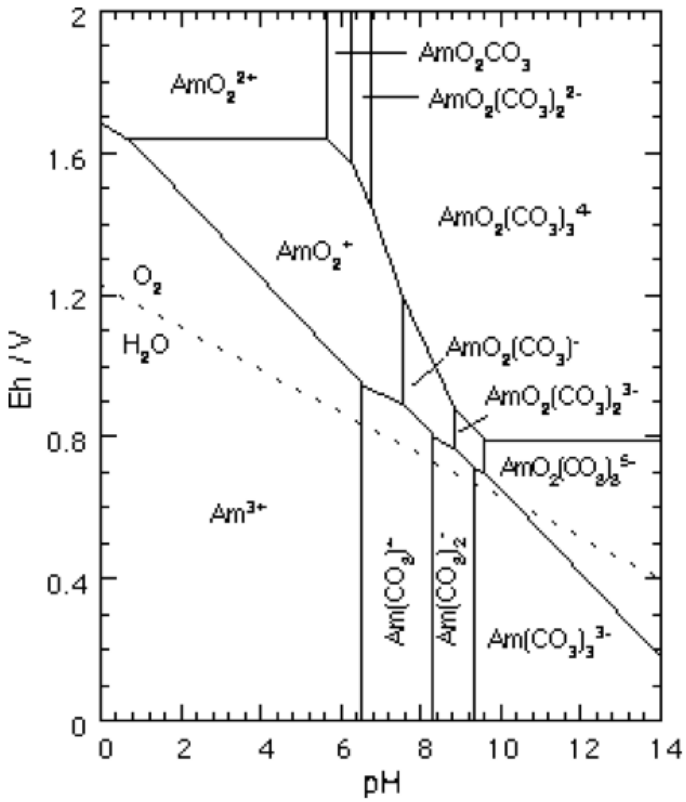

Figure 5. Pourbaix diagram (Eh-pH) in a solution in the Am-H_2O-CO_2 system by Runde and Mincher, 2011

1.3 Primary Sources of Americium Radionuclides to the Marine Environment

Radionuclides from natural and anthropogenic sources influence the marine environment. Radionuclides, occurring naturally or produced artificially in industrial facilities, are omnipresent in the world's oceans and seas. While natural radioactivity is the primary source of radioactivity in the environment, human activities can contribute to additional radioactivity. Artificial radionuclides find their way into the oceans through various pathways, such as atmospheric fallout from nuclear weapons testing, routine and accidental releases from nuclear facilities, and run-off from land. Understanding natural processes and assessing the impact of human activities on seas and oceans is crucial for comprehending marine radioactivity distribution. The study of radionuclide content and distribution in the sea serves as a valuable tool to unravel the marine environment's radioecological state and the radionuclides' environmental fate. These processes, ranging from water mass movement to diffusion and turbulence phenomena, sea-atmosphere interactions, and chronological sequences of events, are

elucidated through the chemical properties and decay constants of radionuclides. An essential element of radioecological assessment involves understanding the current concentrations and isotopic composition of radioactive elements in seawater. This not only aids in identifying the radioecological status but also contributes to developing protective measures against adverse impacts resulting from nuclear technology in human economic activities.

Additionally, the marine environment often serves as a repository for nuclear waste generated by installations. Over several decades, global activities such as weapons production and testing, accidents, electricity generation, and spent fuel reprocessing have introduced radioactive contaminants into the environment. These undesired radionuclides dispersed through the atmosphere or local water systems, accelerate movement through various transfer mechanisms (Hu et al., 2010). Figure 6 summarizes the main sources of radionuclides, the environmental pathways, and the key processes controlling radionuclide migration.

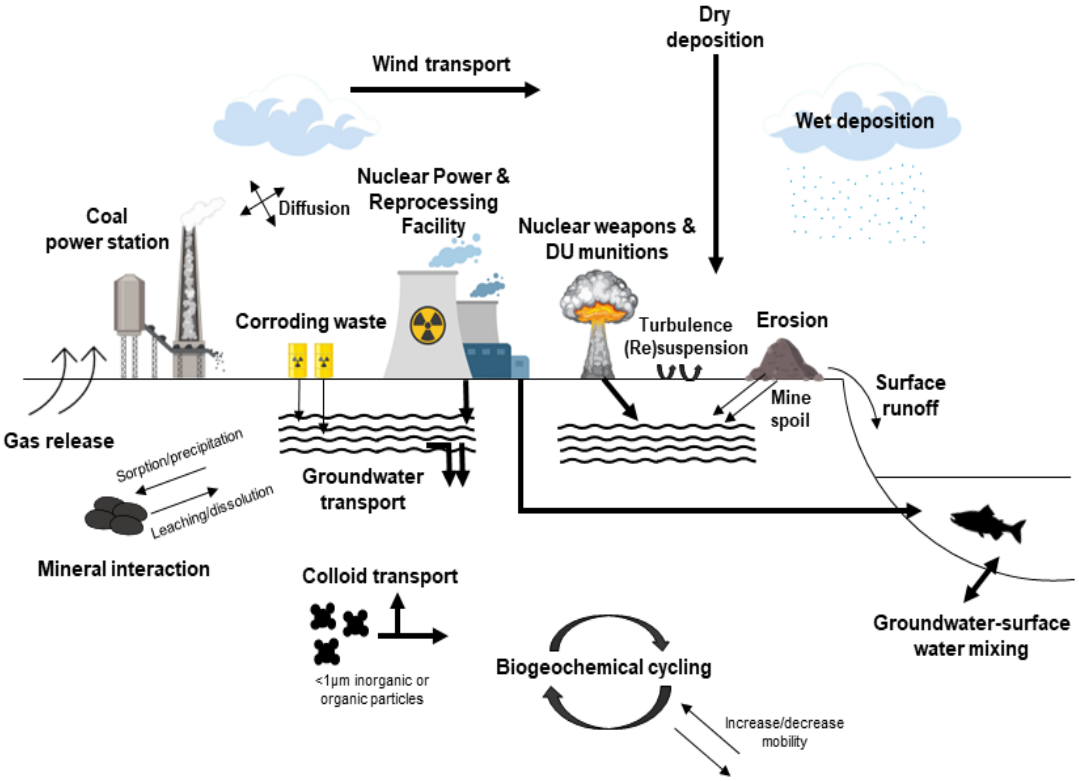

Figure 6. The primary sources of radionuclides in the environment and the fundamental processes that control their mobility in the environment (based on Renshaw et al., 2011).

1.3.1 Nuclear Weapons Testing

The nuclear arms race that emerged with the onset of the Atomic Age following World War II led to widespread radioactive contamination across numerous locations globally. Key nations, such as the United States, the USSR, the United Kingdom, France, and China, became nuclear powers between 1945 and 1962 due to the interplay of Cold War dynamics and the absence of a comprehensive international disarmament initiative (Bergkvist and Ferm, 2000; Katz, 2008; Schenck and Youmans, 2012). The inaugural nuclear weapon test occurred on July 16, 1945, in the Alamogordo Desert, New Mexico, USA. Subsequently, over 2,000 nuclear tests were conducted by various countries worldwide between 1945 and 2023. The precise number is challenging to ascertain as some tests were covertly conducted, and not all nations have publicly divulged information regarding their nuclear testing programs. After the test ban agreement in 1963, atmospheric and surface testing of nuclear weapons largely ceased, giving way to the adoption of underground detonations as the primary testing method (Prăvălie, 2014).

Furthermore, signing the Comprehensive Nuclear-Test-Ban Treaty (CTBT) in 1996 did not completely halt nuclear testing. India, Pakistan (Livingston and Povinec, 2000), and, more recently, the Democratic People's Republic of Korea have conducted nuclear tests, with the latter testing five nuclear missiles between 2006 and 2016 (Gaebler et al., 2019). The fallout from historical atmospheric nuclear tests remains the primary source of radionuclide input from the stratosphere to the Earth's surface, including global ocean surface waters (Livingston and Povinec, 2000). Moreover, nuclear tests were historically carried out on Mururoa and Fangataufa Atolls in French Polynesia, where the French conducted their first nuclear weapon test in 1966. Subsequently, 210 nuclear tests were conducted until 1996 (IAEA, 1998). The primary source of contamination to the marine environment in these locations was the release of plutonium buried in lagoon sediments resulting from the tests (Livingston and Povinec, 2000).

Nuclear weapon tests have released significant quantities of radioactive materials into the atmosphere, including ^{241}Am. It is worth noting that approximately 90% of all nuclear tests were conducted in the northern hemisphere, primarily by countries such as the USA, USSR/Russia, and China. In contrast, only 10% of tests occurred in the

southern hemisphere by nations like France and the United Kingdom. Consequently, the northern hemisphere tends to be more contaminated than the southern hemisphere due to the substantial amounts of radioactive isotopes released into the atmosphere during these tests (UNSCEAR, 1993). Emitting large quantities of radioactive material directly into the environment during atmospheric nuclear weapons use has led to the highest overall exposure from artificial radiation sources (UNSCEAR, 2000). The reports published by UNSCEAR, particularly the comprehensive assessments from 1982 and 1993, remain highly regarded as complete and up-to-date analyses of the cumulative dose to the global population (UNSCEAR, 1982; UNSCEAR, 1993; UNSCEAR, 2000). Radioactive isotopes such as ^{137}Cs, ^{90}Sr, $^{239+240}$Pu, ^{241}Am, and ^{131}I, commonly found at various nuclear test sites worldwide, have had a significant environmental impact and pose a radiation risk to human beings. During the atmospheric nuclear weapon testing, about 142 PBq of ^{241}Pu and 13 PBq of ^{241}Am were released into the environment (Browne et al., 1986). It was estimated that the total deposition of ^{241}Pu for the northern hemisphere was approximately 108 PBq to a reference date of 1965 (UNSCEAR, 2000). These isotopes are noteworthy due to their substantial environmental impact and potential for irradiating the human body.

1.3.2 Nuclear Accidents

In addition to nuclear weapon tests, nuclear power plant accidents contribute to the higher radioactivity observed in the northern hemisphere. Notable examples of such accidents include Three Mile Island in the USA (1979), Chernobyl in the Soviet Union (1986), and Fukushima in Japan (2011) (Grandin et al., 2011; Högberg, 2013). These incidents resulted in the significant release of radionuclides into the atmosphere, with ^{137}Cs and ^{131}I among the most prominent (UNSCEAR, 1988; IAEA, 2012). The Chernobyl disaster was the largest radiation event in the history of the nuclear power industry, rated as a major accident, with a maximum grade of 7 on the International Nuclear and Radiological Event Scale (INES), introduced in 1990 by the International Atomic Energy Agency (IAEA) to enable rapid communication of safety-relevant information in the event of nuclear accidents. The Fukushima Daiichi nuclear disaster was also estimated at 7 on the INES scale, but it was calculated that the Chernobyl accident, as the amount of isotopes released, was 15 times greater (Imanaka et al., 2015; Mattsson et al., 2018).

Among these accidents, the Chernobyl Nuclear Power Plant disaster is particularly relevant due to its impact on the Baltic Sea environment (Imanaka et al., 2015). The Chernobyl NPP, located 120 km north of Kyiv, the capital of Ukraine, housed Unit 4, a graphite-moderated channel-type boiling water reactor known as RBMK. This Soviet-designed reactor had a thermal power output of 3200 MW and was commissioned in 1984. Its core consisted of 1660 fuel channels with zirconium alloy tubes surrounded by graphite, each containing a fuel element cooled by water pumped upward through the channel (Högberg, 2013). Tragically, during a test program on April 25-26, 1986, operators conducted improper actions, causing the reactor to become unstable and exceed safety limits at low power. An attempt to shut down the reactor led to a violent power spike, resulting in an uncontrolled chain reaction and the destruction of numerous fuel channels. The core cavity was over-pressurized by escaping steam and gases, causing the 1000-ton lid to lift and overturn, displacing the control rods from the core. An additional explosion occurred, possibly due to the disappearance of the control rods and the presence of hydrogen. The reactor's destruction resulted in evaporated fuel and fuel fragments ejected into the atmosphere. A fire ignited in the remaining graphite, burning for approximately ten days and releasing further radioactive material (INSAG 1986; INSAG 1992). The Chernobyl Nuclear Power Plant disaster is the most serious radiation exposure incident in history. It resulted in the deaths of 30 workers in a matter of days or weeks, and more than a hundred other people suffered radiation-related injuries. This catastrophic event prompted the immediate evacuation of some 116,000 people from around the reactor in 1986. Subsequently, some 220,000 people from Belarus, the Russian Federation, and Ukraine were permanently displaced after 1986. The incident caused significant social and psychological shocks in the lives of those directly affected and led to significant economic losses throughout the region. Vast areas in three countries were contaminated, and deposition of released radionuclides was detectable in all countries of the Northern Hemisphere. The consequences of the Chernobyl disaster were far-reaching, leaving a lasting impact on the affected countries and beyond (UNESCAR, 2000).

The release of radionuclides from the Chernobyl accident, including ^{137}Cs, ^{90}Sr, and Pu, amounted to reported total activities of 85 PBq, 10 PBq, and 0.055 PBq, respectively (De Cort et al. 1998; WHO, 2010). The contamination caused by radio-cesium from Chernobyl was mainly confined to the Baltic Sea (Aarkrog, 2005). ^{241}Am

released in nuclear accidents, like the accident at Chernobyl, stays in the lower atmosphere and begins to settle to the Earth near the site from which it was released. Larger particles settle out more quickly and over a smaller area; smaller particles may remain in the atmosphere for several months and travel far from where they were released. Precipitation removes particles from the air more rapidly. The original release of ^{241}Pu from the Chernobyl nuclear disaster was approximately 2.6 PBq, and the release of ^{241}Am was estimated to be around 2 TBq (UNSCEAR, 2000; Kashparov et al., 2003a).

Another significant incident occurred at the Fukushima Daiichi Nuclear Power Plant in 2011 following the Tohoku earthquake and the tsunami. The loss of power and subsequent overheating led to the release of radionuclides into the Pacific Ocean. The total release of ^{137}Cs from Fukushima was comparatively smaller than that from Chernobyl and has been estimated to be similar in magnitude to the discharge from the Sellafield nuclear reprocessing facility (~15–16 PBq) (Buesseler et al., 2017). Consequently, the impact of the released radioactive effluent on terrestrial and marine populations has gained renewed attention (Kinoshita et al., 2011; Castrillejo et al., 2015). The Fukushima Daiichi Nuclear Power Plant (FDNPP) incident underscores the critical importance of unintentional releases to the marine environment, the resulting radioecological impacts, and the need to improve the reliability of predicting human and wildlife exposure (Hinton et al., 2013).

1.3.3 Radioactive Waste

The production of electricity, like any other industry, generates waste that needs to be managed responsibly to protect public health and minimize environmental impact. Spent nuclear fuel, an essential component of radioactive waste, is generated during nuclear power generation. It consists of spent fuel rods whose performance has declined after nuclear reactions. Spent nuclear fuel, rich in highly radioactive fission products, transuranic elements, and uranium residues, requires meticulous handling and long-term storage (Deng et al., 2020). Nearly all radioactive waste is controlled and contained, with some requiring deep burial. Unlike other thermal power generation technologies, nuclear energy utilizes regulated waste that poses no harm to the environment. Nuclear power generates a relatively small amount of waste compared to other thermal power generation systems (Brunnengräber and Di Nucci, 2019).

The ^{241}Am, a byproduct of nuclear reactor operations, poses a challenge due to its long half-life and the difficulty separating it from recyclable waste. It accounts for most of the heat generated in nuclear waste (Dares et al., 2015).

1.3.4 Nuclear Reprocessing Plants

A small amount of the radioactive discharges from Sellafield, a nuclear fuel reprocessing plant, situated in west Cumbria, on the west coast of England and discharges into the Irish Sea, and from La Hague, located on the northwest coast of France and discharging into the English Channel, are carried into the Baltic Sea via the inflow of saline water through the Danish Straits. The transport times for these radioactive particles are around 4–5 years for discharges into the Irish Sea from Sellafield and about two years for discharges into the English Channel from La Hague, according to Nies et al. (1995). Based on model calculations, only about 4% of the discharges from Sellafield and 8% from La Hague reach the Skagerrak. Most radioactivity returns to the Skagerrak due to the efficient mixing of water masses in the Kattegat and the Belt Sea, and only about 1% of the discharges enter the Baltic Sea (Nielsen et al. 1995). Americium is intentionally added to some fuel types for specific applications. For example, ^{241}Am can be added to mixed oxide (MOX) fuel, which contains a mixture of uranium and plutonium oxides, to increase the thermal output of the fuel and to reduce the risk of nuclear proliferation (Yoshimochi et al., 2004). Nuclear fuel reprocessing includes recovering fissile material (enriched uranium and plutonium) and separating waste from "spent" (used) fuel rods from nuclear reactors. Fuel rods are stored for a while to allow radionuclides with short half-lives to decay and dissolve throughout the process, and the resulting solution is chemically cleaned and divided into wastes with various compositions and activities. Regular environmental releases from the facilities occur under controlled circumstances and are restricted to discharge totals set by the supervising authorities of each country. The amount and kind of fuel processed and advancements in reprocessing technologies have all impacted how the discharges have changed (Kershaw and Baxter 1995). Americium is a significant element in nuclear fuel reprocessing, particularly in separating plutonium from spent nuclear fuel. Since much of the plutonium has been stored for a long time, the ^{241}Pu that was once contained within it has beta-decayed into the isotopically pure ^{241}Am. Americium has several isotopes, but the two most paramount for nuclear fuel reprocessing are ^{241}Am and ^{243}Am. The spent fuel contains a mixture of ^{241}Am and

^{243}Am, the ratio of which varies depending on the amount of burn-up of the fuel in the reactor; for example, from 96:4 for 5 GWd/teU (Magnox reactor) to 70:30 for 40 GWd/teU (PWR reactor) (Brown et al., 2018).

1.3.5 Ingrowth of ^{241}Am from ^{241}Pu

Since ^{241}Am is the decay daughter of beta-radioactive, relatively short-lived plutonium ^{241}Pu ($T_{1/2}$ = 14.35 years), its environmental concentration will rise with time. In this way, ^{241}Am is introduced indirectly into the environment. The ^{241}Am highest activity is predicted to be around 3.2 PBq, expected in the middle of the 21st century (Bunzl and Kracke, 1988; Muravitsky et al., 2005; Clark et al., 2010) (Fig. 7).

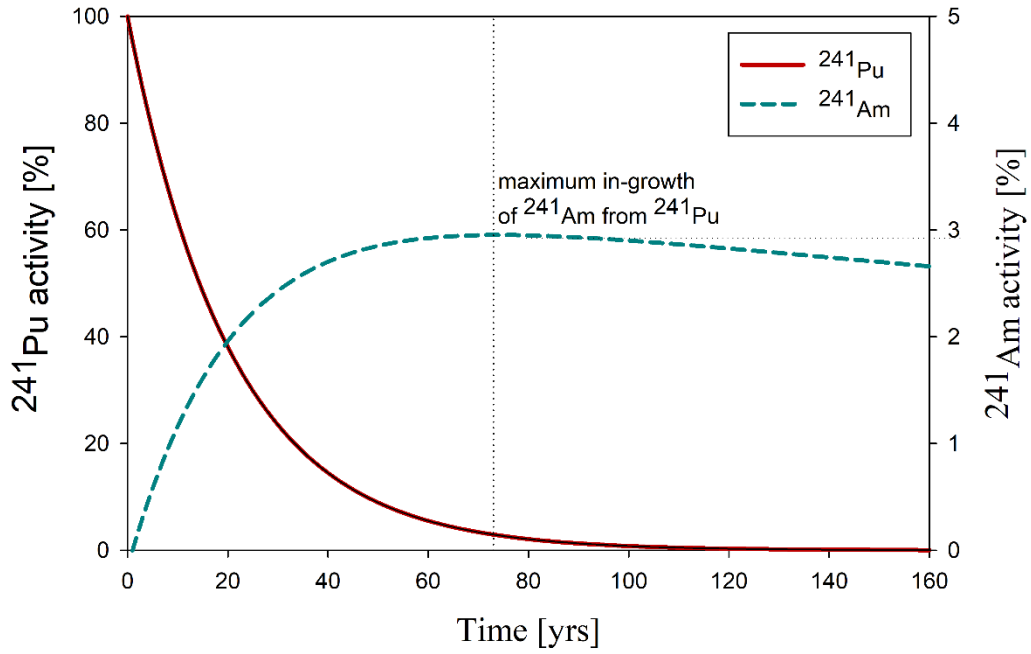

Figure 7. In-growth of ^{241}Am from ^{241}Pu as a function of time

Understanding the in-growth of ^{241}Am is essential for accurately assessing its presence and quantifying its concentration in various materials and environmental compounds. The in-growth of ^{241}Am occurs when the concentration of ^{241}Pu decreases over time due to decay, and the concentration of ^{241}Am increases. Over time, the concentration of ^{241}Am will approach a steady state, where the rate of decay of ^{241}Pu equals the rate of in-growth of ^{241}Am. The half-life of ^{241}Pu is approximately 14.33 years. After five half-lives (72 years), the concentration of ^{241}Pu would have reduced to about 3% of its original value. At this point, the concentration of ^{241}Am will have

reached a steady state, where the production rate from the decay of ^{241}Pu matches the rate of decay of ^{241}Am. Therefore, after around 73 years, the maximum in-growth of ^{241}Am from ^{241}Pu is generally achieved, as the concentration of ^{241}Pu has significantly declined due to radioactive decay, and the concentration of ^{241}Am has reached a steady state. The exact time this maximum will occur will depend on the initial concentration of ^{241}Pu and the isotope's half-life.

The theoretical quantity of the daughter nuclide produced during the radioactive decay of the parent nuclide can be calculated using the Bateman equation (Eq. 1) (Bateman, 1910; Centar, 2006). The expression for the activity of the daughter sample A_d as a function of time (Levin, 2004):

$$A_d(t) = A_p(0)\frac{\lambda_d}{\lambda_d - \lambda_p}\left(e^{-\lambda_p t} - e^{-\lambda_d t}\right) + A_d(0)e^{-\lambda_d t} \qquad \text{(Eq. 1)}$$

Where:

A_d, A_p are the activities of the daughter and parent, respectively;

λ_d, λ_p are the decay constants of daughter and parent nuclides, respectively;

$A_d(0)$ and $A_p(0)$ are the daughter and parent sample activities at time t = 0, respectively;

t is the elapsed time.

1.3.6 Sources of Americium in the Baltic Sea

The ^{241}Am activity concentrations in the Baltic Sea sediments range from 0.08 to 4.80 Bq·kg^{-1} d.w. (Ilus et al., 2007; Runde, 2010). Americium isotopes in the Baltic Sea can be attributed to various sources. Between 1999 and 2006, no significant incidents could have substantially increased the levels of artificial radioactivity in the sediments of the Baltic Sea. However, the concentration of ^{241}Am in its major components is not well-documented, with limited information available for bottom sediments in the Baltic Proper and the Gulf of Bothnia, but a lack of data for the southern Baltic Sea (Lujaniene et al., 2014; Olszewski et al., 2018; Ilus et al., 2007). The Baltic Sea connects the

territories of nine densely industrialized countries with a total population of approximately 85 million people (Lundberg, 2005). Within the boundaries of the Baltic Sea catchment area, there are almost 600 local wastewater treatment plants in towns with populations of more than 10,000 inhabitants and more than 2,000 wastewater treatment plants in smaller cities. In addition, the area has 200 large industrial plants, 1,085 smaller factories, and more than 200 large fish farms. Most industrial pollution comes from various sources, including 95 paper mills, 25 metal ore mines, beneficiation plants, 23 chemical plants, 22 non-ferrous metallurgy plants, leather and textile factories, and petrochemical plants (HELCOM, 2004). The quality status of the Baltic Sea is influenced by several factors resulting from land use and hydrological conditions in different geographical and climatic zones. Several countries around the Baltic Sea have nuclear power plants. The Baltic Sea drainage basin and the location of nuclear reactors and dumping sites for radioactive waste in the area are shown in Figure 8.

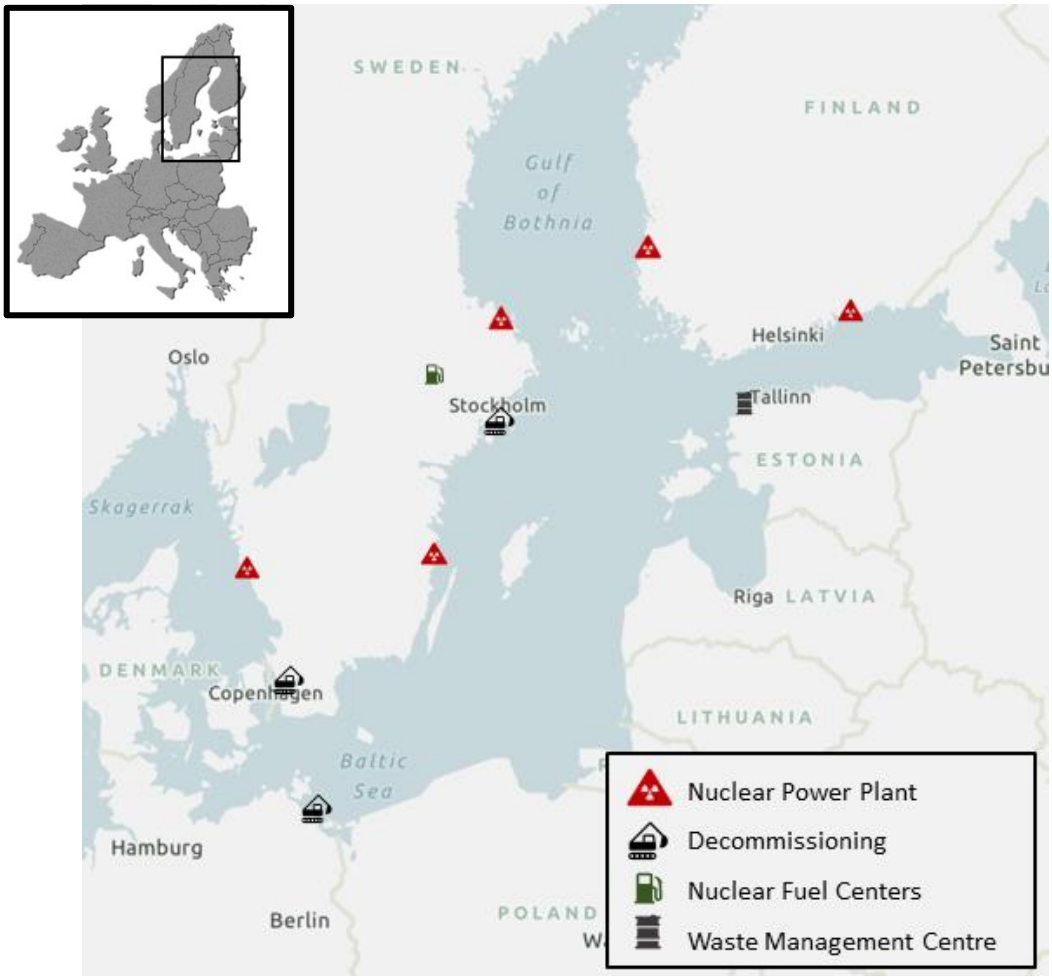

Figure 8. The Baltic Sea drainage basin and location of nuclear reactors and dumping sites for radioactive waste in the area (outline of Baltic Sea from HELCOM website maps.helcom.fi/website/mapservice/)

As ^{241}Am is the decay product of the beta-radioactive isotope ^{241}Pu, its concentration in the environment increases over time. The activities of $^{239+240}$Pu in the Baltic Sea sediments ranged from 0.01 to 14.1 Bq·kg^{-1} dry weight, while ^{238}Pu activities ranged from 0.006 to 0.48 Bq·kg^{-1}. The total inventory of $^{239+240}$Pu in the Baltic Sea was estimated to be approximately 15.3 TBq, primarily originating from global fallout. However, some amounts of ^{238}Pu and ^{241}Pu from the fallout of the Chernobyl accident were also detected, indicated by activity ratios of ^{238}Pu/$^{239+240}$Pu and ^{241}Pu/$^{239+240}$Pu, as well as excess amounts of ^{241}Pu (Ikäheimonen, 2003). Reported concentrations of ^{241}Am between 1999 and 2006 ranged from 0.08 to 4.80 Bq·kg^{-1} dry weight (HELCOM, 2009).

The occurrence of artificial radioactive substances in the Baltic Sea can be attributed to four main factors. Firstly, atmospheric nuclear weapons tests conducted by the United States and the Soviet Union between 1950 and 1980, with the 1960s being the peak period, resulted in widespread radioactive fallout across the northern hemisphere, including the Baltic Sea region. Secondly, the Chernobyl Nuclear Power Plant accident 1986 resulted in significant contamination in the vicinity of the plant and widespread fallout over the Baltic Sea. Chernobyl-derived radionuclides released during the accident spread across Europe, with a substantial amount reaching the Baltic Sea (Żarnowiecki, 1988). The event notably increased radioactivity levels in the region, particularly around the Bothnian Sea and the eastern Gulf of Finland. From the perspective of human life and the functioning of terrestrial and aquatic ecosystems, the most significant radionuclides are medium- and long-lived radioactive isotopes, especially alpha-emitters like ^{238}Pu, ^{239}Pu, ^{240}Pu, ^{241}Pu, and nuclear fuel fission products such as ^{137}Cs and ^{90}Sr (Aarkrog, 1991). The deposition patterns of volatile elements such as isotopes of ^{137}Cs differed from those of heavier refractory elements like transuranic nuclides, including ^{241}Am, ^{238}Pu, ^{239}Pu, ^{240}Pu, and ^{241}Pu (Boulyga et al., 2003; Kashparov et al., 2003a; Reponen et al., 1993). The concentration of transuranic isotopes in the Chernobyl fallout was atypical for global atmospheric fallout due to the high burnup of reactor fuel. Approximately 20 kg of plutonium isotopes (^{238}Pu, ^{239}Pu, ^{240}Pu, ^{241}Pu) were released in the accident, including 13 TBq of ^{239}Pu and 4.8×10^{12} Bq of ^{241}Am (WHO, 1989; Aarkrog, 1991; Mietelski and Wąs, 1995; Kashparov et al., 2003a). In the Baltic Sea, the total amount of Chernobyl-derived ^{137}Cs was estimated at 4700 TBq, surpassing the global fallout from nuclear weapons tests, which measured

900 TBq (HELCOM, 1995). Various studies conducted in the region reported wide ranges of activity ratios for transuranic elements following the Chernobyl accident (Ikäheimonen and Saxen, 2002; Sinkko et al., 1987), indicating complex dynamics in the distribution and behaviour of these radionuclides. Numerous laboratories in the Baltic States have conducted measurements on aerosol and sediment samples, revealing high concentrations of radionuclide activity from the Chernobyl accident, along with the presence of "hot" particles (Lujanas et al., 1994; Pöllänen et al., 1997; Lujanienė et al., 2006; 2009). Holm, in 1995, reported that less than 10% of the total released plutonium during the Chernobyl accident entered the Baltic Sea, highlighting the regional impact and distribution of radioactive contaminants in aquatic environments. Thirdly, radioactive substances discharged into the sea by the Sellafield facility in the U.K. and the La Hague facility in France have also contributed to radioactivity in the Baltic Sea, transported by sea currents from the North Sea. It should be emphasized that the highest release of ^{241}Am from the nuclear reprocessing plant at Sellafield occurred between 1971 and 1975, reaching its peak discharge of 118 TBq in 1974. Subsequently, following this initial peak, the release of ^{241}Am from Sellafield decreased to approximately 8 TBq per year from 1978 to 1981. From 2005 to 2009, the discharge further diminished to about 0.04 TBq annually (Hunt et al., 2013). The environmental impact of the Fukushima accident on the Baltic Sea was deemed insignificant. Measurements of radionuclide activity concentrations originating from the Fukushima accident in the air showed significantly lower levels in European countries bordering the Baltic Sea compared to the aftermath of the Chernobyl accident (Lujanienė et al., 2012b; Masson et al., 2011). Lastly, authorized discharges of radioactivity during the routine operation of nuclear installations, such as nuclear power plants and research reactors, in the Baltic Sea region have added to the presence of artificial radioactive substances in the sea (UNSCEAR, 2000; Zaborska et al., 2014). The activity ratios of ^{238}Pu/$^{239+240}$Pu, ranging from 0.016 to 0.47, correspond to different sources of plutonium, including weapon-grade plutonium, nuclear test fallout, releases from nuclear fuel reprocessing plants, and Chernobyl fallout.

Similarly, the activity ratios of ^{241}Pu/$^{239+240}$Pu, ranging from 4 to 86, indicate various sources, with nuclear test fallout being a significant contributor. According to Holm (1995), nuclear test fallout is the primary source of plutonium in the Baltic Sea, although other sources have also been identified. Numerous studies have emphasized

the significance of river inflow in the contamination of the Baltic Sea (Saxén and Ilus, 2001; Saniewski and Zalewska, 2018). Researchers have estimated the influx of Pu isotopes from rivers with varying results. For instance, Bergström and Carlsson (1994) suggested that 2 GBq of $^{239+240}$Pu is contributed annually by 500 km^3 of freshwater.

Similarly, Skwarzec et al. (2011) reported an annual input of 10.3 MBq of ^{238}Pu and 89.0 MBq of $^{239+240}$Pu from the Vistula River into the southern Baltic Sea. Moreover, measurements conducted in Polish river waters revealed that the Vistula and Odra rivers, as well as the Pomeranian Rivers to a lesser extent, annually introduce 2.42 MBq of ^{241}Pu into the southern Baltic Sea (Strumińska-Parulska and Skwarzec, 2013). These findings highlight the substantial contribution of river inflow to the presence of Pu isotopes in the Baltic Sea.

1.4 Processes and Factors Affecting ^{241}Am Transport in Aquatic Ecosystem

Understanding the potential ecological effects associated with the presence of ^{241}Am in the marine ecosystem requires an in-depth understanding of the dynamics of radionuclide transport and fate in the environment. Once radionuclides entered the water via wet/dry atmospheric deposition and direct discharges, a number of physical and biogeochemical processes developed. These processes included:

- Oceanic advection and dispersion, which facilitated the transport and dilution of radionuclides.
- Various exchange mechanisms between seawater and suspended particulate matter, such as sorption and ion exchange.
- Accumulation of radionuclides in sediments through sorption, particle scavenging, and deposition.
- Biological uptake and turnover of radionuclides by marine biota, including uptake from seawater, food/sediment consumption, depopulation, and transfer through the food chain.
- Remobilization of radionuclides found in sediments through desorption, sediment resuspension, or biological activity.

This comprehensive understanding is critical to assessing the broader implications of ^{241}Am in the marine environment (Livingston and Povinec, 2002; Lujanienė et al., 2012a; Vives and Batlle et al., 2008). Figure 9 conceptualizes the critical processes involved in the transport and fate of ^{241}Am in the marine environment.

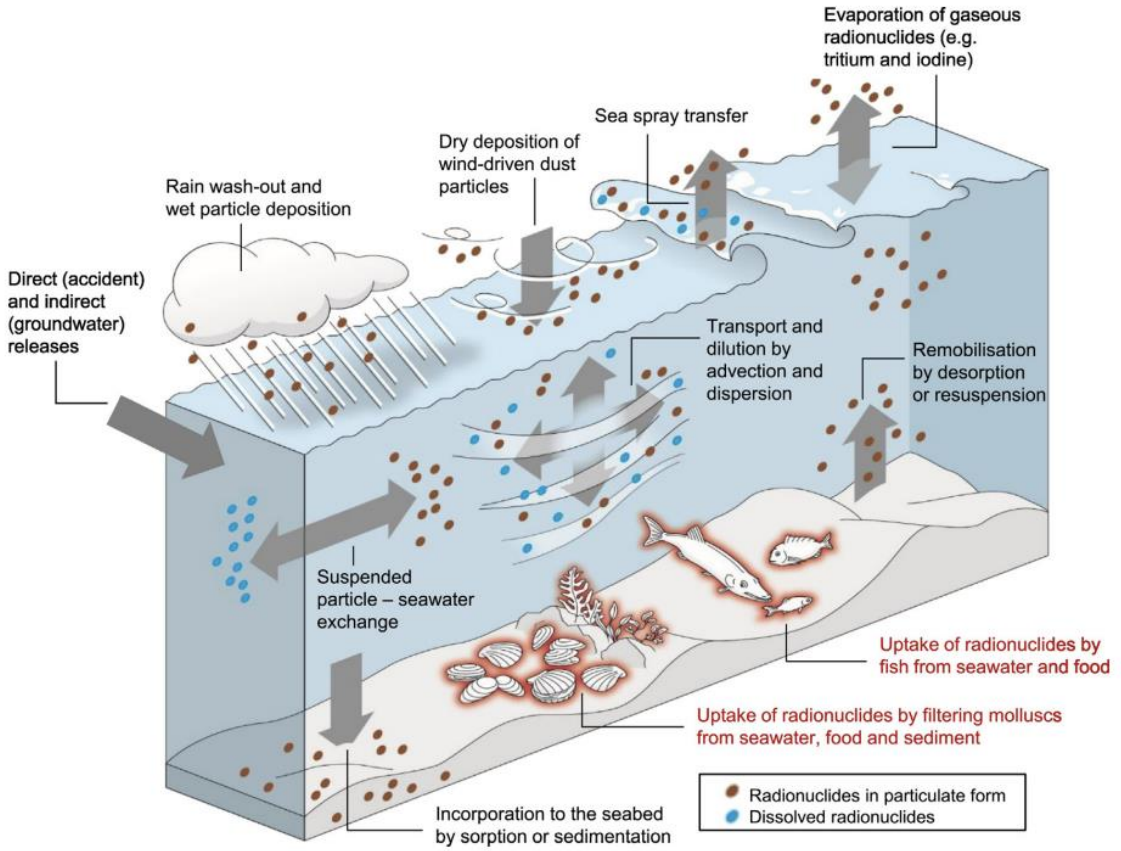

Figure 9. The fate of radionuclides in the marine environment, including the principal processes of dry and wet deposition, advection and dispersion, particulate transfer, sedimentation, seabed remobilization, and biological uptake (Batlle et al., 2018)

Fine-grained sediment particles possess chemically active surfaces with surface sites typically carrying negative charges. As a result, ions with opposing charges in the surrounding solution are attracted to these surfaces. This characteristic makes sediments an essential sink for radionuclides like uranium, plutonium, americium, or curium, as they can adhere to sediment or mineral grain surfaces. Studies by McKay and Walker in 1990 and Choppin et al. in 1995 have highlighted the significance of this process. The extent to which ions are attracted to binding sites on sediment surfaces depends on various factors, including environmental acidity or alkalinity, the sediment's mineralogical composition, and the presence of organic matter (Evans, 1989). The mobility of sediment plays a pivotal role in the deposition and retention of radionuclides

within a particular area. It can occur through direct transport or resuspension processes, which control how radionuclides are distributed and held within the sediment (Ray et al., 2020).

The behavior and mobility of radionuclides are closely related to their chemical speciation, affecting properties such as solubility and reactivity with surfaces (Salbu, 2009). Chemical speciation, in turn, is highly dependent on biogeochemical conditions, including factors such as pH, Eh (redox potential), the presence of complexants, and the nature of mineral surfaces in the system (Fig. 10). The interaction of these factors plays a key role in the partitioning of radionuclides between the solid and solution phases (Renshaw et al., 2007; Warren and Haack, 2001).

Processes such as sorption and (co)precipitation can impede radionuclide migration, acting as retarding mechanisms. On the other hand, dissolution, complexation, and colloid formation can enhance migration by keeping radionuclides in the solution phase.

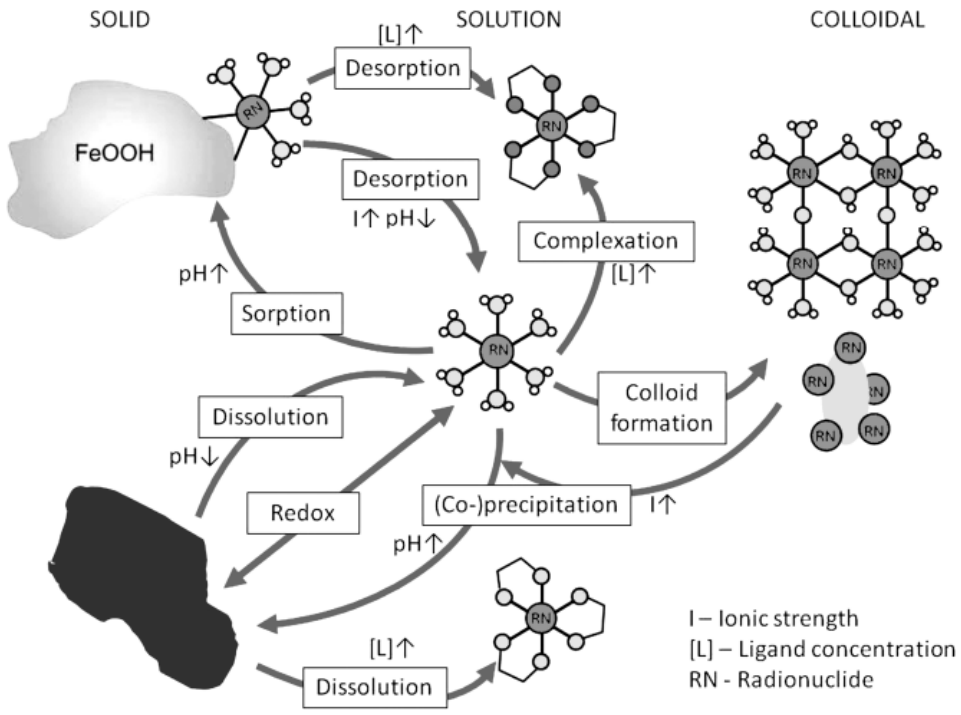

Figure 10. A summary of the key geochemical processes controlling radionuclide speciation and some of the factors influencing these processes (Renshaw et al., 2011)

In seawater, ^{241}Am tends to be scavenged by adsorption onto settling particles. This process is facilitated by its relatively high distribution coefficient (*Kd*), which is approximately ten times larger than that of $^{239+240}$Pu (Kershaw et al., 1986; Martin and Thomas, 1990; Mitchell et al., 1991; Molero et al., 1995).

Studies have shown that a significant fraction of ^{241}Am in seawater exists in particulate form. For instance, approximately 21% of ^{241}Am in surface waters is collected by filters with a pore size of 0.45 μm, indicating its association with particles even in surface waters (Fowler et al., 1983). Furthermore, even at depths of 100 m and 750 m, the same filter collects 10% of ^{241}Am, suggesting its affinity for particulate matter throughout the water column. This behavior of ^{241}Am in seawater, where a substantial fraction is associated with particles, contributes to its longer residence times than more soluble species like ^{137}Cs. The higher *Kd* value of ^{241}Am allows it to readily adsorb onto suspended particles, leading to its removal from the water column and eventual accumulation in sediments. Therefore, ^{241}Am is a valuable tracer for understanding marine environment particle dynamics and sedimentation processes.

1.5 Bioaccumulation and Biomagnification of ^{241}Am

Bioaccumulation and biomagnification, two processes resulting in the accumulation of toxins, metals, or radionuclides in living organisms, operate differently. Bioaccumulation entails the gradual buildup of a substance within an individual organism over time. In contrast, biomagnification involves the concentration of a compound in the tissues of organisms as it ascends the food chain. Ultimately, the primary repository for americium isotopes is the soil or sediment. Plants can absorb some ^{241}Am from the soil, but the uptake is minimal. Fish can take in ^{241}Am, yet accumulation in their flesh is negligible. Shellfish, like shrimp or mussels, predominantly contain ^{241}Am in their shells rather than the edible portions of the organism (DOE, 1996).

Aquatic organisms demonstrate bioaccumulation of americium through various means, including uptake from water or ingestion of sediment or organisms lower in the food chain. Crustaceans and mollusks passively absorb americium onto their exoskeletons when in contact with water (Fisher et al. 1983). However, when ingested

through suspended diatoms or other food sources, americium tends to pass through the digestive system and is subsequently eliminated. In marine organisms, the digestive gland, gill, and exoskeleton are the primary target organs and tissues for americium bioaccumulation (Chassard-Bouchaud 1996). Mussels, for instance, absorb americium primarily from seawater rather than ingested sediment, with the uptake associated with the shell from water and soft tissue from food (Fisher et al. 1996). Benthic organisms exhibit variable uptake and retention of americium. Factors such as feeding habits, physiological differences, and environmental conditions contribute to this variability. Filter feeders, like tunicates, can clear particles containing ^{241}Am from seawater and accumulate small amounts in internal tissue. Mucous feeding guilds, such as crinoids, do not efficiently trap americium, suggesting complexation or adsorption mechanisms. Bioaccumulation in aquatic organisms can depend on factors such as temperature, time after intake, season of the year, and water quality. For example, temperature influences initial uptake in the brittle star (*Ophiothrix fragilis*), but depuration is not temperature-dependent (Hutchins et al. 1996). The freshwater snail (*Lymnaea stagnalis*) exhibits higher ^{241}Am uptakes in acidic water and during certain seasons (Thiels et al. 1984). Microorganisms, including algae, plankton, and bacteria, influence americium uptake. Bioconcentration by bacteria involves adsorption onto cell surfaces rather than actual biological uptake (Horikoshi et al., 1981).

1.6 Health Risks Associated with Radiation

Exposure to radioactivity is commonly associated with various health risks, including cancer, developmental effects such as mental retardation, and non-genetic effects (UNSCEAR, 1982). Skin cancer, leukemia, and lung cancer are among the types of cancer that can be linked to exposure to radionuclides. It is well known that exposure to ionizing radiation is a significant risk factor for cancer. Estimating the specific risk of cancer after radiation exposure is problematic due to regulatory uncertainty and public concern. One of the reasons for this uncertainty is that risk estimates are often applied to populations that differ from the populations on which the estimates are based initially. The potential for adverse health effects to humans exposed to americium depends on the amount of americium isotopes (^{241}Am and ^{243}Am) present in the body and the radiation dose and dose rate each produces. The radiation dose from these radionuclides can be

classified as either external (if the source is outside the body) or internal (if the source is inside). The external dose from americium radionuclides may be attributed to the gamma radiation. Alpha particle decay emits alpha radiation, which cannot penetrate the outer layers of the skin, and a variety of low energy gamma rays, which penetrate the skin, although rarely in sufficient quantity to exceed a regulatory limit. At very high doses of americium, there is an increased risk for gamma radiation to cause dermal and subdermal effects such as erythema, ulceration, or even tissue necrosis (ATSDR, 2004).

The UNSCEAR, along with the International Atomic Energy Agency (IAEA) and the Nuclear Regulatory Commission (NRC), have established limits based on hypothetical data derived from responses of the affected population following the Chernobyl accident. According to the no-threshold hypothesis, the observed effects of radiation increase at high doses, but the effects at low doses are uncertain. The principle of As Low As Reasonably Achievable (ALARA) should always be followed to minimize radiation exposure. Historical records have shown that doses exceeding 25–50 rems can harm human health.

1.7 Geochronological Methods

Geochronology is the science of determining the age of rocks, fossils, sediments, and the Earth itself. It plays a key role in retrieving all historical aspects of earth science. Geochronology is an indispensable tool for calculating sediment deposition rates and determining the age of the source rocks from which sedimentary detritus is derived. A wide range of geochronological tools and methods can be used to date geological materials. Geological processes ranging from billions of years to short-lived anthropogenic events can be dated by selecting an appropriate radiometric system based on the nature of the mineral or rock and its presumed age (Cuney, 2021).

Radioisotope geochronology is based on the law of natural disintegration of elements and disequilibrium that arises in natural radionuclide decay series. Naturally occurring ^{210}Pb is commonly used to date bottom sediments (Bricker-Urso et al. 1989; Cundy and Croudace 1996; Bellucci et al. 2007; Kolker et al. 2009). In this thesis, the ^{210}Pb method was used for sediment cores from three locations in the Baltic Sea. Generally, ^{210}Pb dates are confirmed using ^{137}Cs profiles when the ^{137}Cs profiles are

sufficiently intact (Appleby and Oldfield, 1983). The method was validated by the activity peak of ^{137}Cs, which in the Baltic Sea originates mainly from the fallout of the Chernobyl accident in 1986.

1.7.1 ^{241}Am as a Time-Marker for Sediment Dating

Similarly to ^{137}Cs, ^{241}Am can be found in sediment profiles and used for dating purposes. The basic premise of this method is that the level of ^{241}Am in fresh remains after nuclear weapons testing is essentially negligible and that its presence in older sediments is due to an increase in ^{241}Pu from weapon fallout releases. Reconstruction data on cumulative ^{241}Pu and ^{241}Am inventories for the Northern Hemisphere since 1954 reveal a clear peak in 1963, accounting for about 20% of the inventory (Appleby et al., 1991, Corcho-Alvarado et al., 2014).

Ages determined using ^{241}Am align well with those obtained through ^{137}Cs in young Holocene sediments from the coastal Caribbean Sea (Corcho-Alvarado et al., 2014), coastal lagoons, and near-shore sediments in Australia and New Zealand (Everett et al., 2008; Hancock et al., 2011), as well as deep-sea sediments (>3000 m) in the Northwest Pacific Ocean (Lee et al., 2005). The utilization of ^{241}Am has been coupled with ^{210}Pb and ^{137}Cs to determine the age of a peat core extracted from the Southern Indian Ocean. The estimated peat accumulation rate was 0.75 mm·year^{-1} over 157 years (Lee et al., 2005). Applying the same methods, the ages of coastal sediments in East Taiwan were determined, successfully identifying three earthquakes, including the 2003 Taitung earthquake (M 6.8), the 1951 Chengkong earthquake (M 7.1), and the 1935 Lutao earthquake (M 7.0), respectively (Dezileau et al., 2016). Furthermore, ^{241}Am has served as a valuable temporal marker for assessing global anthropogenic radionuclide fallout in deep sediments (Díaz-Asencio et al., 2020).

Nevertheless, ^{241}Am proves to be a superior timing indicator for marine environments across a broad range of pH values. It indicates much lower mobility than ^{137}Cs and renders it valuable for dating sediments from the early 1960s onward, particularly when the ^{137}Cs signal has significantly faded. The half-life of ^{241}Am ensures that it remains detectable in sediments for several centuries, while ^{137}Cs disappear

during this period. Its low concentration is the main challenge in using ^{241}Am as a time marker.

1.7.2 Radiolead Method

^{210}Pb geochronology is widely used in environmental investigations to determine the ages of sediment layers. Assessments of material fluxes to the seafloor and environmental pollution studies are typical applications (Benninger et al. 1975). ^{210}Pb geochronology is a standard tool in sedimentological studies that aims to determine the absolute ages of modern sediments (up to 100 years). It is supplied in shallow ocean areas by *in situ* disintegration of ^{222}Rn ($T_{1/2}$ =3.8 days) from dissolved ^{226}Ra in seawater and atmospheric deposition of ^{210}Pb to sea surfaces. Since lead, including ^{210}Pb, is a reactive particle, it readily binds to sinking particles in the ocean (Cochran, 1982). As the bottom sediments also contain ^{210}Pb from ^{226}Ra *in situ* decay (supported ^{210}Pb), the additional ^{210}Pb is referred to as excess or unsupported ^{210}Pb (^{210}Pbex) (Fig. 10). Since deposition, ^{210}Pbex activity has decreased while $^{210}Pb_{supp}$ activity has remained constant (Zaborska et al., 2007). Based on the down-core activities of $^{210}Pb_{ex}$, a ^{210}Pb-chronology for a sediment core is determined (total minus supported).

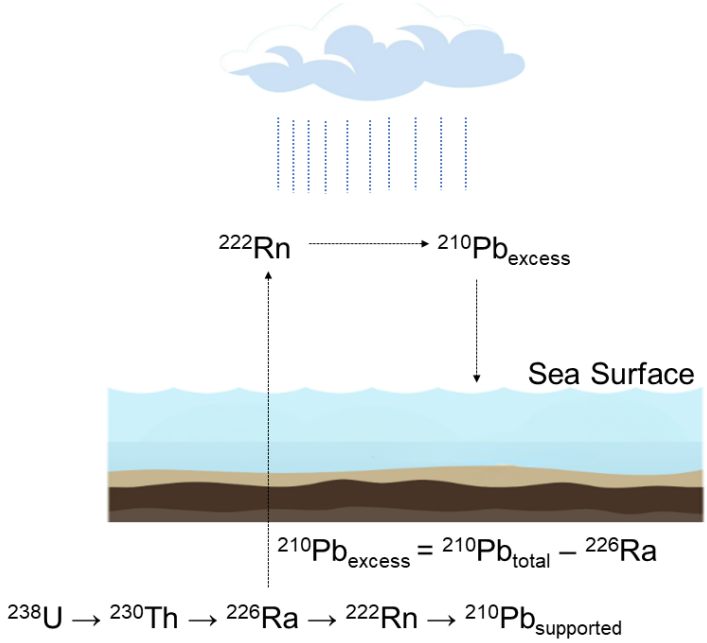

Figure 10. Origin of geogenic ^{210}Pb and fallout ^{210}Pb (based on Mabit et al., 2014)

This work used gamma spectrometry with direct ^{210}Pb measurement to determine the total activity of ^{210}Pb in sediment samples (^{210}Pb emits a 46.5 keV gamma photon). $^{210}Pb_{supp}$ by gamma spectrometry is achieved by measuring the activity of other daughter products of ^{226}Ra (^{214}Bi, ^{214}Pb) simultaneously with a total of ^{210}Pb on each sediment depth interval. The difference between total and $^{210}Pb_{supp}$ activity is used to calculate $^{210}Pb_{ex.}$ In the case of sedimentary column dating, the $^{210}Pb_{ex}$ is used to determine the age-depth relationship in the sediment using conventional dating models. The method is based on the fact that a layer at the water-sediment interface with an activity A_0 must be buried at a certain depth in the sediment after a certain time.

1.7.2.1 Constant Flux Constant Sedimentation Rate (CF:CS) model

The Constant Flux Constant Sedimentation Rate (CF:CS) model – assumes the excess ^{210}Pb flux is constant and there must be no redistribution of the particles after their deposition (Goldberg, 1963; Krishnaswamy et al., 1971). Sediment accumulation rates were estimated from the profile of $^{210}Pb_{ex}$ activity concentration versus porosity-corrected sediment depth [cm] and mass sediment depth, which was calculated using sediment porosity. The sediment porosity was computed using measured water content, an average grain density of 2.20 $g \cdot cm^{-3}$, and a mean density of pore water (the mean density of sea water) equal to 1.00 $g \cdot cm^{-3}$ (Damrat et al., 2013).

The CF:CS model is based on the following equation (Eq. 2):

$$A = A_0 \times e^{-\lambda \frac{z}{w}} \qquad \text{(Eq. 2)}$$

Where:

A – $^{210}Pb_{ex}$ activity in excess with depth [$Bq \cdot kg^{-1}$]

A_0 – $^{210}Pb_{ex}$ activity of the surface layer (t=0) [$Bq \cdot kg^{-1}$]

z – depth of the sedimentary core [cm]

w – sedimentation rate [$cm \cdot year^{-1}$]

λ - is the ^{210}Pb disintegration constant (λ = 0.03114 per year)

While the CF:CS model is a valuable tool for estimating sedimentation rates, it does have some limitations. For example, it assumes that the sedimentation rate has been constant over time, which may not always be accurate. Additionally, variations in the sedimentation flux can affect the model's accuracy, particularly in areas with high sedimentation rates.

1.7.2.2 Constant Rate of Supply (CRS) model

The CRS model is the most widely used ^{210}Pb-based radiometric dating model for recent sediments. In many cases, the CRS model has been verified based on independent chronostratigraphic markers (^{137}Cs and ^{241}Am peaks) (Abril, 2019). The CRS model (Goldberg, 1963; Appleby and Oldfield, 1978) assumes that the influx of ^{210}Pb to the sediment surface is constant and that the concentration of ^{210}Pb in the sediment varies inversely proportional to the sediment accumulation rate. This model assumes that the seston does not sweep more ^{210}Pb from the water column as the sedimentation rate increases and that higher sediment accumulation rates dilute ^{210}Pb sedimenting at a constant rate. It is based on comparing the inventory of $^{210}Pb_{ex}$ below a given depth with the overall inventory of $^{210}Pb_{ex}$ in the sediment core in the sediment core. According to the CRS model, the site-specific sediment MAR, SAR, and layer age (*ti*) at depth can be estimated from the slope of Eq. (3), Eq. (4), and Eq. (5):

$$\text{MAR (g·cm}^{-2}\text{·year}^{-1}) = A_i/C_i \times \frac{1}{\lambda} \quad \text{(Eq. 3)}$$

$$\text{SAR (cm·year}^{-1}) = MAR \times \rho \quad \text{(Eq. 4)}$$

$$t_i = \frac{1}{\lambda} ln \frac{A_0}{A_i} \quad \text{(Eq. 5)}$$

Where:

A_i – the accumulated $^{210}Pb_{ex}$ deposit below layer (*i*);

C_i – the $^{210}Pb_{ex}$ concentration in layer (*i*);

ρ – the mean dry bulk density of a certain layer.

The models discussed here share the primary assumption of an undisturbed temporal structure in the sediment core, in which ^{210}Pb incorporation occurs in a natural sequence unaffected by subsequent redistribution processes. However, they differ in terms of the ^{210}Pb fraction studied and its expected decay function, resulting in different age models (Table 5). The choice of model not only affects age estimates for individual sediment layers and has significant implications for the derived sediment mass accumulation rates. This is crucial for assessing potential changes in accumulation rates over the past decades, which is a key but unresolved problem in modern limnology. The variability introduced by different models complicates the interpretation of data from sediment cores and underscores the need for careful consideration in selecting the appropriate model for accurate age estimation and subsequent environmental analysis.

Table 9. Summary of dating models highlighting key assumptions of each of the two dating models used

Model	Assumption
Constant flux constant sedimentation model (CFCS)	Assumes a constant sedimentation rate along the entire core
	Activity of unsupported ^{210}Pb is expected to decay as a function of the cumulative dry mass of the sediment in the core
Constant rate of supply model (CRS)	Assumes a constant fallout of ^{210}Pb from the atmosphere, yielding a constant rate of supply of unsupported ^{210}Pb to the sediment surface
	Unsupported ^{210}Pb of the initial activity (at time zero) will be inversely proportional to the mass accumulation rate, such that increases in burial driven by sediment erosion or autochthonous production result in the dilution of unsupported ^{210}Pb

1.7.3 Cesium Method

Cesium ^{137}Cs ($T_{1/2}$ = 30.17 y) is an artificial radionuclide that appeared in the environment as a consequence of nuclear tests conducted in the 1950s, 1960s, the Chernobyl Nuclear Power Plant accident in 1986, and recently the accident in the Fukushima Dai-Ichi NPP in 2011. Cesium has spread globally and has been deposited on the surface. Terrestrial and atmospheric nuclear weapons tests were carried out from 1952 to 1981, with the highest intensity in 1958–1965. Cesium generated from these explosions was ejected into the stratosphere and thus spread globally. Significant spatial variation in its deposition occurred only at the scale of climatic regions and latitudinal zones, influenced by large-scale atmospheric circulation and differences in precipitation

regimes. A reactor accident at the Chernobyl power plant in Ukraine in 1986 resulted in the deposition of 70 to 100 PBq of ^{137}Cs (Cambray et al., 1987; OECD, 1995; Playford et al., 1990; RADNET, 1996).

After the Chernobyl fallout was deposited on the surface of the Baltic Sea, nuclides from the fresh fallout sank rapidly through the water layers. Further factors influenced radionuclide concentrations, including ocean currents, mixing of water masses, river discharges from drainage areas, sinking in the water column, and deposition on the bottom (Ilus et al., 1998).

The amount of cesium from nuclear explosions is less in the Southern Hemisphere than in the Northern Hemisphere, and equatorial areas received much less cesium than areas in the higher latitudes of Europe and North America (Larsen, 1985). Total cesium precipitation in North America and Europe ranged from 2,000 to 4,000 $Bq \cdot m^{-2}$, while lower values, e.g., 420 $Bq \cdot m^{-2}$, 270 $Bq \cdot m^{-2}$, and 252 $Bq \cdot m^{-2}$ were recorded in Australia, New Zealand, and Zimbabwe, respectively (Hewitt, 1996; He and Walling, 1997). Low cesium levels are associated with areas of reduced radioactive fallout impact.

Historical events (such as represented by the ^{137}Cs time-marks) can then be used to constrain the probability distributions of sediment ages (Waugh et al., 1998). In 2001, Smith introduced a protocol for research journals outlining criteria for accepting papers relying on ^{210}Pb dating to establish sediment core geochronology. The protocol emphasizes the need for validation by at least one independent tracer that offers an unequivocal time-stratigraphic horizon (Smith, 2001).

Accordingly, the simultaneous examination of man-made fallout radionuclides, such as ^{137}Cs, $^{239+240}$Pu, or ^{241}Am, is deemed crucial. These radionuclides, exhibiting a well-defined peak in atmospheric deposition around 1963, serve as valuable additional tests for ^{210}Pb chronology. Numerous applications involving artificial fallout radionuclides often link 1963 to the sediment layer, displaying a peak activity. Similar approaches with other time markers have also been employed in various studies (von Gunten et al., 1987; Waugh et al., 1998; Santschi et al., 2001).

^{137}Cs dating is used to confirm sediment accumulation rates in the recent cores. The distribution of radiocesium in the southern Baltic Sea was investigated to validate ^{210}Pb dating (Suplińska and Pietrzak-Flis, 2008).

1.8 Alpha Spectrometry for ^{241}Am Measurement

Alpha spectrometry is a highly sensitive method for detecting ^{241}Am. Complete separation of ^{241}Am from the sample matrix is crucial for obtaining thin alpha sources, especially in samples with trivalent lanthanides and ^{210}Pb interference. Excess lanthanides can degrade alpha spectra, and ^{210}Pb, through its granddaughter ^{210}Po, interferes with measuring ^{243}Am, a performance marker for americium separation. The similarity in chemical behavior between americium and curium can result in curium peaks in the ^{241}Am alpha spectra. The isotopes of ^{242}Cm and ^{244}Cm do not affect the determination of ^{241}Am because the alpha peaks of ^{241}Am, ^{244}Cm, and ^{242}Cm are easily distinguishable in alpha spectrometry.

Alpha spectrometry is a long-established method for measuring ^{241}Am, offering a limit of detection (LOD) of 0.2–0.4 mBq/sample with a 2-day measurement time. However, it is time-consuming, taking several days to weeks for samples with low ^{241}Am levels. LOD can be improved by increasing the sample size, counting time, and chemical yield. Because of these drawbacks, in recent years, mass spectrometry has increasingly replaced by alpha spectrometry.

Alpha decay is a process of atomic nucleus decay, resulting in the emission of an alpha particle (helium nucleus), and it is an example of the most common cluster decay involving the expulsion of a cluster (group) of nucleons from the primary nucleus. Alpha decay occurs due to the quantum tunneling phenomenon, which involves the penetration of the potential barrier, and both nuclear and electromagnetic interactions are implicated in the process (Choppin et al., 2002).

The emission of an alpha particle is a prevalent decay channel for nuclei with a high atomic number ($Z > 83$). The scheme of this transformation can be expressed according to the Soddy-Fajans rule. After the decay, the mass number (A) and the atomic number (Z) of the new nucleus are lower by four and two, respectively (Eq. 6) (Ojovan et al., 2019):

$$^{A}_{Z}X \rightarrow {}^{A-4}_{Z-2}Y + {}^{4}_{2}He \qquad \text{(Eq. 6)}$$

Due to the principles of energy conservation and momentum, the distribution of energy (the difference in energy between the initial and final states) among the

secondary nuclei is strictly defined. Consequently, the emitted particle is monoenergetic, and the radiation spectrum is linear (Magill and Galy, 2005). The kinetic energy of the alpha particle (E_α) can be calculated from (Eq. 7):

$$E_\alpha = Q\left(1 - \frac{1}{1+\frac{m_Y}{m_\alpha}}\right) \qquad \text{(Eq. 7)}$$

Where Q is the disintegration energy, m_Y is the mass of the daughter nuclide Y, and m_α is the mass of the alpha particle (α).

Typically, alpha particles have energies in a narrow range, between 4 MeV and 8 MeV. If the alpha energy exceeds these values, the nuclides' half-lives become too short for the radionuclides to be easily detected or so long that they can be considered practically stable. Both cases require special skills and highly sophisticated analytical techniques (Vajda et al., 2012).

1.8.1 Alpha-particle Spectrometry

Radiometric techniques determine radionuclide activity by detecting and measuring decay processes. In the context of this research, alpha-spectrometry using semiconductor detectors was utilized to measure the investigated americium isotopes.

Radioactive elements, like americium, can be quantified in units of mass (grams), but they are typically measured based on their radioactivity, expressed in curies or becquerels. The curie (Ci) and becquerel (Bq) indicate the rate at which a radioactive material decays per second. Specifically, one becquerel represents one atom transforming every second, while one curie corresponds to 37 billion atoms transforming per second (Lieser, 2008).

The radiometric technique of alpha-ray spectrometry is widely used in various scientific fields. The known radionuclides release alpha particles with energies that range between a narrow area of 2 and 8 MeV (Vajda, 2012). High-energy resolution spectrometers are necessary to analyze mixtures of alpha-emitting radionuclides. An advantage of using alpha-spectrometry is obtaining acceptable counting statistics for even low activity or low yield samples by increasing the counting time.

The main drawback of alpha spectrometry is the requirement of efficient chemical separation of the element of interest from the sample matrix to reduce interferences of other alpha-emitting isotopes, particularly the uranium and thorium decay chains (Kim et al., 2008; Warwick et al., 2001). The most significant advantages and disadvantages of alpha spectrometry are shown in Table 6.

Table 10. Advantages and disadvantages of alpha spectrometry (Vajda et al., 2020)

Advantages	**Disadvantages**
detection of short-living isotopes	^{241}Am has to be separated from matrices and interfering radionuclides (very similar alpha-energy emissions)
the high sensitivity due to the low background	time-consuming (from days to weeks, depending on the involved Am activity)
simplicity	huge amount of acids
high selectivity for alpha particles against other types of radiation	the thin counting source is needed for the prevention of self-absorption of alpha particles to the sample
relatively low cost of the equipment	the basic spectral interferences: ^{241}Am, which completely overlaps with the ^{238}Pu

The main features of alpha particle spectra depend on the type and quality of the detector and electronic units, the geometrical arrangement, and the quality of the alpha source.

In standard analytical procedures, alpha peaks are distinguished by their Full Width at Half Maximum (FWHM) values, which are easily determined by measuring the peak width in keV at half of the peak height from the spectrum. The FWHM values associated with alpha peaks tend to exceed the detector's specified limits. For PIPSi detectors, typical FWHM values range from 17 to 19 keV for detectors with active areas of 300 mm² and 30 to 37 keV for those with 1200 mm² active areas (Steinbauer et al., 1994). These parameters encompass the geometric configuration of the source and the detector, as well as the specific properties of the alpha source. Each of these factors contributes to peak broadening during the measurement process (Amoudry, 1990; Vajda, 2012). The impact of the geometric arrangement on energy resolution is shown in Figure 11.

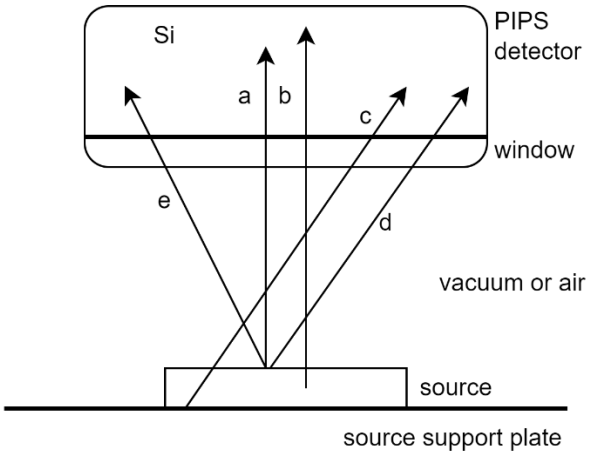

Figure 11. Paths of alpha particles in source-detector system (Vajda, 2012)

Alpha particles emitted by radionuclides within the source material can follow different paths before reaching the Si detector. Some may deposit energy in the source material (particles b and c). In contrast, all particles (a, e, and d) will deposit energy in the air gap between the source and the detector, as well as in the detector window. The former process is termed self-absorption, while the latter represents external absorption. The impact of air absorption can be negligible under high vacuum conditions in the detector chamber. However, maintaining limited air pressure is often preferred to shield the detector from recoil particles. Contributions to total absorption from processes like "self-absorption" in the source, absorption in the detector window, and absorption in other materials vary. Each process reduces the total energy deposited in the Si detector, resulting in a range and energy straggling of monoenergetic alpha particles. The lengths of the arrows in the Si material denote the paths of alpha particles and the energy deposited by each particle in the detector's active volume. Variations in individual energy depositions contribute to peak broadening. Absorption and self-absorption exert different effects on the alpha spectrum. If absorption dominates energy losses (thin source but thick absorber), the spectrum shifts to lower energies due to alpha particles losing energy outside the detector. The phenomenon results in peak broadening due to variations in energy loss angles and a decreased number of charge carriers produced in the detector. In contrast, when self-absorption is significant, as in the case of thick sources, peak broadening occurs without a shift in the spectrum because particles from the source's surface layer can reach the detector without losing energy through self-absorption (Vajda, 2012).

A final source of low mass is necessary to minimize the attenuation of alpha particles during counting, especially as americium is chemically similar to other components of environmental samples, such as Al^{3+}, rare earths, and some transition elements (Livens and Singleton, 1989; Warwick et al., 2001). Figure 12 displays the alpha energies of various interfering radionuclides. Using a low-mass final source reduces the impact of chemical interferences, allowing for more accurate and precise alpha particle counting in environmental samples containing americium and other similar elements. This approach helps to distinguish the alpha emissions from americium from those of interfering radionuclides, ensuring reliable alpha spectrometry results.

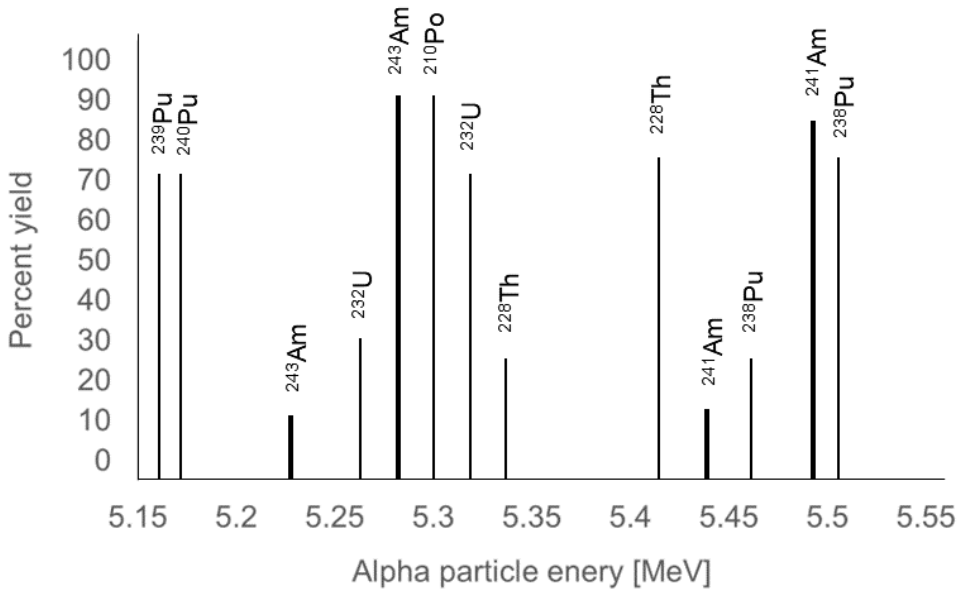

Figure 12. Alpha energies of the interfering radionuclides

2. CHARACTERISTICS OF THE STUDY AREA

2.1 Overview of the study area

The Baltic Sea, situated in northern Europe, is bordered to the south by Russia, Estonia, Latvia, Lithuania, Poland, Germany, and Denmark, while its northern boundary is defined by the Scandinavian Peninsula, encompassing Finland and Sweden. The Baltic Sea is one of the largest brackish seas in the world, with 415.24 km^2 (including the Danish Straits and Kattegat) of shallow inland water with an average depth of 52 m (Emelyanov, 1995). Its catchment area is four times the size of the entire sea and is in northern Europe. Oxygenated and salty water can enter the Baltic Sea's deepest regions through the Kattegat and Skagerrak straits, which connect the Baltic Sea to the North Sea. As a result, despite the continuous intake of fresh water from the numerous rivers within its catchment region, the waters of the Baltic preserve their marine character. If the Baltic were cut off from the ocean, it would become a lake since much more freshwater flows into it than evaporates (Snoeijs-Leijonmalm and Andrén, 2017).

The Baltic Sea can be divided morphologically into four smaller areas, three of which are significant basins: the Bothnian Basin, the Gotland Basin, which includes the Gdańsk Basin, and the Bornholm Basin (Majewski, 1987). The Belt Sea is the remaining fourth area. In more than a century of research focusing on the Baltic Sea (Elmgren, 2001), extensive studies have been conducted in regions including the Bornholm, Gdańsk, and Gotland Basins. The following regions of the described areas were the research sites given in the following chapters of this work: the Bornholm Basin (78M), the Gdańsk Basin (P1), and the Gotland Basin (BY15). Their exact locations are shown in Figure 13.

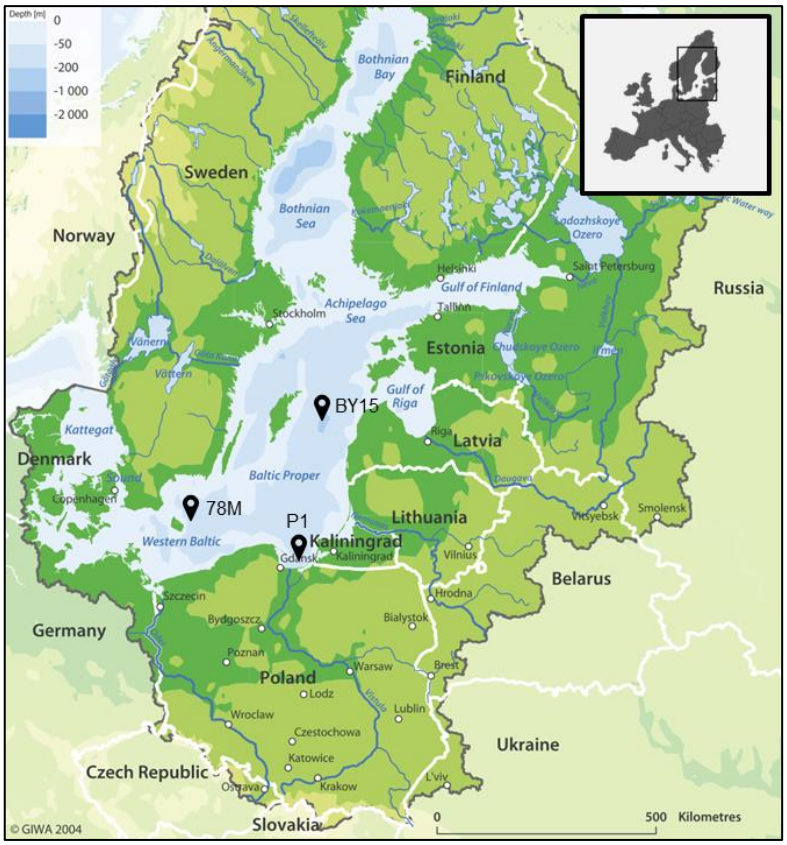

Figure 13. Map of the Baltic Sea and the sampling area; P1 – Gdańsk Basin; 78M – Bornholm Basin; BY15 – Gotland Basin (based on HELCOM, 2006).

2.1.1. The geological history of the Baltic landscape

The unique morphology of the Baltic Sea can be traced back to quaternary glaciations. During this period, glacial erosion shaped the crystalline Precambrian rocks of the Fennoscandian Shield, forming the basin that now cradles the Baltic Sea (Seppälä, 2005). Meanwhile, the lowlands of the European Plain were covered by glacial sediments. As the Scandinavian Ice Sheet began its retreat approximately 12,600 years ago, it left behind a proglacial lake sustained by the melting ice—this body of water was known as the Baltic Ice Lake. Varved clays, deposited on the lake floor due to seasonal fluctuations in sediment load from melting ice, serve as evidence of this ancient water body (Marks et al., 2022). Around 10,300 years ago, as the Baltic Ice Lake connected with the global ocean, it transitioned into the brackish Yoldia Sea, named after the marine bivalve Yoldia Arctica (now Portlandia Arctica) that thrived in its waters. However, roughly 9,500 years ago, postglacial isostatic uplift exceeded the eustatic sea level rise, leading to the closure of the central Swedish strait once again. This event transformed the sea into a freshwater lake inhabited by various species, such

as the gastropod Ancylus fluviatilis (Emeis et al., 2002; Vuorinen, 2018). Over the ensuing millennia, saltwater incursions from the Kattegat gradually increased the lake's salinity, evolving it into the brackish Ancylus Lake. Erosion and rising eustatic sea levels eventually submerged the Danish Straits permanently, triggering a rapid 20-meter rise in sea level within a few centuries—an event known as the Littorina Transgression. The resulting Littorina Sea became so saline that it supported marine life, including the gastropod Littorina litorea, around 7,500 years ago. Approximately 4,000 years ago, ongoing isostatic uplift led to decreased water exchange with the North Sea, lowering the Baltic Sea's salinity (Bunke, 2017; Vuorinen, 2018).

2.1.2. Water supply and exchange

The Baltic Sea presents two prominent hydrographical characteristics. Its water renewal process is sluggish, primarily dependent on the influx of saline Baltic waters (average flux = 634 $km^3 \cdot y^{-1}$) and freshwater input (average flux = 454 $km^3 \cdot y^{-1}$) from numerous rivers within its expansive catchment area. The ten largest rivers (according to their drainage area) that discharge into the Baltic Sea are summarized in Table 7. However, the relatively restrained inflow of saline waters compared to the vast water volume of the Baltic Sea (21,200 km^3) results in an extended residence time for the saline water, estimated at around 20 years (Franck et al., 1987; Leppäranta and Myrberg, 2009; Winsor et al., 2001). The inflow of fresh oxygenated ocean water is relatively small, mostly only 900 km^3, so only 4% of the seawater volume of the Baltic Sea is exchanged (Majewski, 1987; Uścinowicz, 2014). Secondly, the Baltic Sea exhibits a highly stratified structure. It features a horizontal salinity gradient that diminishes from 15–35 PSU in the transition zone between the North Sea and the Baltic Sea to 6–14 PSU in the southern and middle Baltic regions and drops to below 6 PSU in the northern Baltic region. During winter, a permanent halocline is evident at depths of 40–80 meters, while in summer, a seasonal thermocline emerges alongside a three-layer structure: a warm and fresher upper layer, a saltier cold intermediate layer, and the saltiest and warmer deep layer. These vertical density gradients between layers play a pivotal role in vertical fluxes and the overall functionality of the sea, effectively isolating saline and deoxygenated deep waters from fresh and oxygenated surface waters (BACC II Author Team, 2015).

Table 11. The ten largest rivers (according to drainage area) feed into the Baltic Sea region (The BACC Author Team, 2015; Kulinski and Pempkowiak, 2011). The Göta River drains into the Kattegat, sometimes included in the Baltic Sea region.

River	**Country**	**Drainage area [km^2]**	**Mean annual discharge [m3·s^{-1}]**	**% of total river inflow to the Baltic Sea**	**Runoff L·km^{-2}·s^{-1}**
Neva	RUS/FIN	281 000	2460	17.6	8.8
Vistula	POL/UKR/BY/SLK	194 400	1065	7.6	5.5
Odra	POL/GER/CZR	118 900	573	4.1	4.8
Nemunas	BY/LIT/RUS	98 200	632	4.5	6.4
Daugauva	BY/LV/LIT/EST/RUS	87 900	659	4.7	7.5
Narva	EST/RUS	56 200	403	2.9	7.2
Kemi	FIN	51 400	562	4.0	11.0
Göta	SWE	50 100	574	4.1	11.5
Torne	SWE/FIN	40 100	392	2.8	9.8
Kymi	FIN	37 200	338	2.4	9.1
Total		**1 015 400**	**7658**	**55**	**8.2**

2.1.3. Geological Composition and Sedimentation Dynamics: Key Factors Influencing Pollution Management in the Baltic Sea

In general, the distribution of average contents of C_{org} in the Baltic sediments of different grain sizes follows the rule of the pelitic fraction—the more pelite (fraction <0.01 mm) the sediments contain, the higher their C_{org} content. Previous examinations of the Baltic Sea's geology have been undertaken (Emelyanov, 2014; Gudelis and Litvin, 1976). Carbonaceous (sapropelic) mud tends to accumulate in the basin deeps. Numerous researchers have delved into the characterization of this mud, and maps detailing the distribution of organic carbon (C_{org}) in the Baltic Sea have been compiled by scholars (Emelyanov, 1995, 2012; Leipe et al., 2010). The geological composition of the Baltic Sea plays a crucial role in pollution management. Its clay-rich materials, similar to those used in soil decontamination and remediation, have exceptional sorption capacities. These clays effectively bind organic and inorganic contaminants, facilitating reversible and irreversible processes and even catalyzing specific chemical reactions (Darmawan and Wada, 2002; Shahidi et al., 2015). Various factors, including riverine inputs, hydrodynamic processes, and anthropogenic activities, influence sedimentation processes in the Baltic Sea. Approximately one-third of the Baltic seabed is characterized by sediment accumulation, with sedimentary processes varying widely across the region, from shallow coastal areas to deep basins and from sedimentary to crystalline rock regions (Kaskela et al., 2012; Kaskela and Kotilainen, 2017). Radionuclides within the Baltic Sea undergo transportation between water and sediment phases through physical, chemical, and biological mechanisms, with variations in redox conditions affecting their mobility (Kaskela and Kotilainen, 2017).

Accordingly, the geophysical properties of the Baltic Sea enhance the absorption of organic and inorganic pollutants. It serves as a reservoir for water-soluble and water-insoluble pollutants discharged by numerous industrial plants along its shores (Rana et al., 2021). The functioning of the Baltic Sea hinges significantly on the mechanisms driving strong vertical stratification within its waters. This structure arises from the interplay between freshwater inflow from the drainage area and the exchange of water and salt through the Danish straits, resulting in a pronounced halocline across most parts of the sea (Leppäranta and Myrberg, 2009). This halocline, typically located at depths of around 60–80 meters in the central Baltic Proper and serving as the primary

pycnocline, is a crucial conduit for internal waves, facilitating wave energy transfer between different sea regions. Its position indirectly impacts the dynamics of intermediate-depth layers by altering the properties of internal waves (Talipova et al., 1998), triggering regions of wave breaking and intense mixing, and potentially causing resuspension of bottom sediments (Friedrichs and Wright, 1995). Over recent decades, the vertical structure of water masses in the Baltic Sea, including the main halocline and pycnocline depths, has significantly changed (Väli et al., 2013). These alterations in vertical stratification can profoundly influence the sea's dynamics by modifying the conditions for generating and propagating internal waves. Shifts in the depth of the pycnocline can relocate the typical areas affected by internal-wave-induced hydrodynamic loads (Kurkina et al., 2011), with far-reaching implications for large-scale infrastructure on the seabed and the overall Baltic Sea ecosystem (Meier et al., 2011; Väli et al., 2013). Due to the slow exchange of water and relatively rapid sedimentation rates (Ilus et al., 2000), all radionuclides have a prolonged residence time in the water of the Baltic Sea.

2.1.4. Surface Water Circulation and Sedimentary Dynamics: Implications for Sediment Transport and Distribution in the Baltic Sea

The surface water circulation in the Baltic Sea forms distinct circulation cells for each basin (Central Baltic, Bothnian Sea, and Bothnian Bay). Water movement occurs counterclockwise within these cells, influencing sedimentation processes and settling suspended materials and pollutants (Håkanson, 1991). Surface water movement arises from the rotation of the Earth, resulting in the Coriolis force, which deflects the direction of water flow to the right in the northern hemisphere. From the Danish straits, water movement proceeds northward along the southern and western coasts. The Bothnian Bay's transport turns southward along the Swedish coast (Masłowski and Walczowski 2001). Within individual cells, surface currents form outer eddies, which weaken towards the center of each basin. Marine currents in the Baltic Sea are generally stable, but in different seasons, they may locally flow in many different directions (Håkanson, 1991).

The directions of water velocity vectors in the Baltic Sea throughout the year are similar, but their values are highly variable. The most significant differences occur along the eastern shores of the Baltic, where they slow down and change direction

(Osiński, 2007). The strongest currents occur in winter, while the weakest occur in summer. The stronger currents during winter may result in enhanced sediment transport, leading to increased sedimentation rates in certain areas. Conversely, weaker currents during summer months may lead to reduced sediment transport and deposition. The strongest currents are found in the surface layer, with velocity decreasing with depth. The surface water circulation patterns in the Baltic Sea significantly influence sedimentation processes. The counterclockwise circulation within distinct circulation cells affects the movement and distribution of sediment particles suspended in the water column. As water flows within these cells, it carries suspended sediments along its path, transporting them from one area to another (Håkanson, 1991). Sedimentation and resuspension of sediments in marine environments are fundamental to shaping the seafloor environment and crucial to several fields. For example, understanding the location and rate of sediment accumulation is essential for monitoring pollution and understanding erosion and sediment deposition changes. Sedimentary processes in the Baltic Sea have been widely studied, and in general, one-third of the Baltic seabed is considered an area of sediment accumulation (Kaskela et al., 2012). However, the seabed of the Baltic Sea is very heterogeneous in places. High local variability in sedimentation can occur in shallow coastal areas and deep basins. Seafloor heterogeneity generally increases in the Baltic Sea from south to north, from open sea to archipelagos, and sedimentary to crystalline rocks (Kaskela and Kotilainen, 2017).

2.1.5. Human-Induced Pressures and Environmental Challenges in the Baltic Sea

Introducing organic pollutants and nutrients into the Baltic Sea poses significant threats to its oxygen-sensitive ecosystems. These pollutants contribute to algal blooms' proliferation, elevating the water column's organic matter levels. Consequently, this surge in organic matter triggers deoxygenation processes, forming hypoxic and anoxic zones (Murray et al., 2019). Eutrophication, as known, imposes constraints on oxygen-dependent benthic ecosystems, ultimately fostering the emergence of dead zones across the marine environment. Furthermore, alterations in redox conditions have implications for the solubility and mineralization of metals in bottom waters and sediments (Szymczak-Żyła et al., 2019).

Consequently, the transition from oxygenated to anoxic conditions could potentially heighten the bioavailability of metals in soluble forms, facilitating their uptake and accumulation within organisms (Hendożko et al., 2010; Polak-Juszczak, 2012). In addition to metals, these environmental shifts may also impact the behavior and fate of radionuclides in the Baltic Sea. Changes in redox conditions and the availability of organic matter can influence the mobility and bioaccumulation of radionuclides, potentially exacerbating their presence and effects within marine ecosystems.

The Baltic Sea faces significant environmental pressures stemming from human activities. With a catchment area inhabited by 85 million people, the sea receives substantial discharges of hazardous substances and nutrients, contributing to its status as one of the world's most heavily polluted seas, marked by contamination, eutrophication, and hypoxia expansion (HELCOM, 2018). Hazardous substances enter the Baltic Sea through various pathways, including point sources like wastewater treatment plants, diffuse sources such as agriculture and leaching from waste deposits, atmospheric deposition from urban and industrial combustion, and inputs from rivers and the North Sea. These substances encompass artificial organic chemicals (e.g., polybrominated diphenyl ethers and tributyltin), heavy metals (e.g., mercury and lead), plastic litters, and radionuclides (e.g., ^{137}Cs). Many of these pollutants are non-degradable and accumulate in the aquatic food web, posing long-term threats to the ecosystem (HELCOM, 2018; Szefer, 2002). Eutrophication, induced by excess nitrogen and phosphorus compounds since the 1940s, remains a persistent challenge in the Baltic Sea. Despite significant reductions in nutrient loadings since the 1980s, over 97% of the sea's surface area is still assessed as eutrophied. Eutrophication leads to heightened primary production and frequent algae blooms, deteriorating water clarity, exacerbating hypoxia in bottom waters, and ultimately diminishing marine biodiversity. Hypoxia, inherent in some deep sub-basins of the Baltic Sea due to its highly stratified structure, is further exacerbated by excessive nutrient loadings from human activities. Renewal of hypoxic (sometimes anoxic) bottom waters primarily relies on oxic saline inflows from the North Sea. However, the frequency of these Baltic inflow events has been low in recent decades, with only slight increases observed since 2014. Nevertheless, the efficacy of these inflows in improving hypoxia status remains uncertain, as they also intensify stratification, propagate nutrient-rich waters to adjacent areas, and enhance

phosphorus release from sediments, collectively contributing to hypoxia expansion in the Baltic Sea (Carstensen et al., 2014; Conley et al., 2009; HELCOM, 2018; Meier et al., 2018).

Each selected study area is characterized by high anthropopressure affecting the water column and the seabed. The primary sources of human impact on the environment in these regions, in the case of the Gdańsk and Bornholm Basins, are the presence of the most significant Baltic fishing grounds and sea routes, as well as areas where chemical munitions produced during World War II were dumped. Examples of anthropogenic impact on the seabed in the mentioned regions include the presence of various types of waste on the seabed's surface in the form of wrecks, used deck equipment, and conventional and chemical munitions, as well as furrows created on the seabed by fishing vessels using demersal equipment during trawling operations. It is worth noting that the Bornholm and Gotland Basins hold significant recognition as officially designated areas for storing Chemical Warfare Agents (CWA) in the Baltic Sea. The primary CWA disposal site, often called the "primary dump," is in the Bornholm Basin. The northern region of this location is currently indicated on maritime charts as a "greater explosives dump" (Bełdowski et al., 2016).

2.2. Bornholm Basin

The Bornholm Basin has substantial depths ranging from 92 to 96 meters (Missiaen and Noppe, 2009). It is the largest dump site located east of Bornholm Island within the Danish extended economic zone. Notably, this region serves as a conduit for oxygenated ocean water from the North Sea, allowing it to flow into the Baltic Sea (Czub et al., 2018).

A distinct and noteworthy characteristic of the Bornholm Basin is the formation of a permanent halocline, observed at a depth of approximately 50 meters (Rak and Wieczorek, 2012). Above this halocline, surface waters maintain salinity levels of around 7 PSU; below it, salinity can increase up to 21 PSU during the inflow of the North Sea water (Czub et al., 2018).

The seafloor landscape of the Bornholm Basin has a relatively even topography, interspersed with depressions believed to have formed due to past chemical munition

disposal. Geophysical surveys conducted in 2006 and 2007 indicated the presence of buried objects and gas-releasing sediments that impact the marine substrate (Missiaen and Noppe, 2009). Beneath the seafloor, a layer of loosely compacted marine mud extends from 0 to 6 meters (Christoffersen et al., 2007). Notably, the erosion of these sediments is observed due to bottom currents, influenced by hydrodynamic processes from wind and storms, with average speeds of around 2.14 cm·s¹, similar to those observed in the Gdańsk area (Czub et al., 2018).

Furthermore, the Bornholm Basin features a permanent halocline spanning 50 to 75 meters, delineating less-saline surface waters (7─8 PSU) from more saline bottom waters (10─18 PSU) (Møller and Hansen, 1994). This salinity stratification adds complexity to the dynamics of the Bornholm Basin and its role within the basin.

The bottom of the Bornholm Basin comprises silty and clay sediments (Bulczak et al., 2016), contributing to the unique composition of this underwater landscape. The intricate interplay of various factors in this region highlights the importance of continued research and understanding to safeguard the delicate balance of this marine environment.

2.3. Gdańsk Basin

The Gdańsk Basin's deepest section is known as the Gdańsk Depp, which forms an extensive depression from southwest to northeast. It reaches a maximum depth of 108 meters (Uścinowicz, 1997). This part of the Baltic Sea's seabed is characterized by flat formations that gradually recede to create a depression extending from the southwest to the northeast. This region's marine substrate primarily comprises silts and mixed sediments (Mojski et al., 1995).

At the bottom of the Gdańsk Basin area are bacterial and fungal moulds that can survive under anaerobic conditions. These conditions are almost constant in this region, with only occasional influxes of oxygenated water from the North Sea (Czub et al., 2018). The speed of bottom currents in the Gdańsk Basin area can reach up to 5 $cm \cdot s^{-1}$ (Cieslikiewicz et al., 2017). However, due to various anthropogenic impacts, the Gdańsk Basin is exposed to significant stress on its seabed. Notably, the area hosts the largest uncontrolled chemical weapons storage facility in the Baltic Sea, contributing to

increased levels of arsenic in local sediments, an essential ingredient in toxic compounds used for chemical bombs (Bełdowski et al., 2016). The Gdansk Basin is a focal point of heavy metal and radionuclide contamination (Szmytkiewicz and Zalewska, 2014; Zaborska et al., 2017). Industrial activity in the Polish region and potentially from the Russian enclave (Kaliningrad Oblast) has contributed to the peak levels of contamination observed over the past 30 years. The coastline of the Gulf of Gdansk, extending more than 200 km from Poland toward Germany, bears the brunt of this pollution (Bindler et al., 2009).

Many deep basins, including the Gotland Basin and Gdańsk Basin, are persistently hypoxic (Conley et al., 2009). Sediments within the Gdańsk Basin primarily consist of clay and silt, with sand and gravel deposits observed in shallower areas (Uścinowicz, 1998). In the deeper waters of the Gdańsk Basin, medium and fine silts are commonly encountered beneath the pycnocline (around 60 meters), and they extensively cover the seafloor (Jankowska and Łęczyński, 1993; Uścinowicz et al., 2011). The pollution trend in the Gdansk Basin underscores the long-term impact of industrial activities along rivers and estuaries, with significant consequences for marine biodiversity and ecosystem health in the southern Baltic.

2.4. Gotland Basin

The Gotland Basin is the largest basin within the Baltic Sea, accounting for 39% of the total water volume. It spans an area of 151,920 km^2. The mean depth of the Gotland Sea (71 m) is larger than the mean depth of the entire Baltic Sea. The Gotland Basin, located within this basin, holds the record for the deepest point in the area, reaching 249 meters (Leppäranta and Myrberg, 2009). This part of the Baltic Sea plays a crucial role in the distribution and fate of environmental pollutants, including radionuclides. The region, governed by a circulation center around the island of Gotland, serves as a dispersal channel for substances from various sources, including anthropogenic activities along the southwestern, southern, southeastern, and eastern coasts and rivers (Diaz and Rosenberg, 2008). Strong vertical stratification results in bottom waters experiencing stagnant periods, during which oxygen levels drop to low levels or become undetectable.

Consequently, sulfide often accumulates in the deepest parts of the Gotland Basin. The bottom water at BY15 has been predominantly anoxic and euxinic over the past decades (Fonselius and Valderrama, 2003). Circulation dynamics, characterized by slow water movement and an average residence time of 22 years, contribute to increased retention and sedimentation of pollutants, including radionuclides (Fonselius, 1970; Fonselius and Valderrama, 2003). Particularly in the deep regions of the central Baltic Sea, biotic transformations of radionuclides occur, affecting their dissolution and sedimentation processes (Nealson et al., 2002; Thamdrupet al., 1994). While radionuclide levels rose steadily until the late 1990s, concentrations have remained relatively stable (Apler and Josefsson, 2016; Hallberg, 1991). The central Baltic Sea has three sections with different redox potentials, affecting radionuclide residency and transformation. One region shows an oxidizing potential, leading to precipitation reactions of most divalent radionuclides.

In contrast, a second region with a reducing potential facilitates the resuspension and reduction of precipitated radionuclides, keeping them in circulation (Hallberg, 1991). The third region with mixed redox chemistry prolongs suspension periods, also for some radionuclides. Situated along the eastern coast of Sweden, the island of Gotland is the largest in the Baltic Sea. The sediments found in the Gotland Basin consist mainly of silty clay, occasionally interspersed with deposits of sand and gravel (Bulczak et al. 2016).

When examining the topography of the Gotland Basin, features were observed that lie between the basin fill characteristics of the Bornholm Basin and the conformable deposition pattern typically seen in the North Central Baltic Basin (Winterhalter, 1992).

A significant aspect within the marine mud sequence, spanning a thickness of 4.5 meters, is the presence of distinct layers. These layers can be categorized into darker laminated and lighter, more uniform sequences. The darker laminated sequences are associated with prolonged periods marked by anoxic conditions in the lowermost layers of water. Anoxic conditions are when dissolved oxygen is depleted in the water, leading to distinct chemical and sedimentary processes. These conditions likely contributed to our unique layering pattern in the mud sequence (Kowalewska et al., 1999).

At station BY-15, located at a depth of 228 meters in the Gotland Basin, the sediment exhibits a notably delicate texture, with the surface layers containing a substantial amount of water. Consequently, there exists a considerable likelihood that the upper sediment layers may experience disruption, mixing, or even displacement during the sampling process.

2.5. Research Material

Sediments are paramount in environmental and radioactivity monitoring in the Baltic Sea. Numerous radionuclides tend to attach to sediment particles, which results in their accumulation in bottom sediments. Therefore, it becomes pretty simple to analyze them from sediment samples. At a suitable monitoring station and under favorable circumstances, sediment layers have accumulated suspended matter and radionuclides continuously for extended periods. It allows for examining the history and total quantities of specific radionuclides in sediments.

Samples were collected during research cruises on the r/v '*Oceania*.' Sediments for the ^{241}Am study were collected at the Gotland and the Gdańsk Basin in April 2010, and the Bornholm Basin, the Gotland Basin, and the Gdańsk Basin in 2019. The locations of the sampling areas from 2019 are presented in Table 8. The locations selected for the study are characterized by silt-clay sediments, specifically, the Baltic olive-grey mud, composed primarily of particles smaller than 0.063 mm. The sea floor in these regions experiences frequent oxygen deficiency and anaerobic conditions, leading to laminated deposits lacking bioturbation structures that reflect the annual sedimentary cycle. The accumulation rate of the silt-clay sediment can range from 0.5 to 2 mm per year, with considerable variation (Uścinowicz, 2011).

Table 12. Sampling locations

Sample ID	Site description	Date	Latitude	Longitude	Depth [m]	Textural group
78M	Bornholm Basin	12.05.2019	55º19’ N	15º42’ E	86	Sandy muds
P1	Gdańsk Basin	17.05.2019	54º49’ N	19º19’ E	102	Muddy sands
BY15	Gotland Basin	11.05.2019	57º20’ N	20º03’ E	228	Muddy sands

3. AIMS AND SCOPE OF WORK

This thesis aimed to improve the knowledge of ^{241}Am activity concentrations in the bottom sediments of the southern Baltic Sea, namely the Bornholm Basin, the Gdańsk Basin, and the Gotland Basin. The work concentrated on understanding the behaviour and distribution of ^{241}Am in the bottom sediments of the southern Baltic Sea to contribute to the broader knowledge of radioisotope contamination, sediment dynamics, and potential environmental risks in this specific marine environment. The study might assess the potential impact of radioactive contamination on the ecosystem and marine life in the southern Baltic Sea due to the presence of ^{241}Am in the sediments. The research could help to identify potential sources of ^{241}Am contamination in the Baltic Sea, including nuclear facilities, historical discharges, or atmospheric fallout from nuclear events.

The research problem was divided into three questions:

1. What are the spatial and temporal patterns of ^{241}Am accumulation and distribution in the bottom sediments of the southern Baltic Sea?

2. How do these patterns relate to sediment dynamics, local sources of contamination, and potential risks to the marine ecosystem and human health?

3. Should ^{241}Am be an alternative for validation in future sediment dating studies?

4. CHARACTERISATION AND APPLICATION OF A SEQUENTIAL PROCEDURE FOR ^{241}Am DETERMINATION IN MARINE SEDIMENT

4.1 Sample Pre-treatment

The sediment cores analyzed in the study were collected from the southern Baltic Sea in 2010 and 2019. Cores from 2010 were taken aboard research cruises on the r/v '*Oceania*' by dr. Agata Zaborska from the Institute of Oceanology Polish Academy of Science. The analyzed sediments from 2019 were also collected during research cruises on the r/v '*Oceania*' (Fig. 14.) with a GEMAX gravity corer (Fig. 15.), ideally suited for the undisturbed sampling of soft mud for environmental monitoring purposes. GEMAX is a gravity corer with 2 parallel Plexiglas coring tubes with the closing mechanism of 2 lateral rudder closers. The tube length is 79 cm, and the inner diameter of the tubes 2 x 90 mm. Rubber valves with a plastic (polyamide) flange at the top of each barrel help retain the sediment sample during the initial drawdown from the seafloor. They are designed to restrict water flow through the barrels during lowering, thus ensuring good sediment penetration (Winterhalter, 2001).

Undisturbed, high-quality samples are significant in sedimentation rate studies. Loss of soft surface sediments during sampling can significantly affect results, at least if the calculations are based on ^{241}Am and ^{137}Cs. Sediment sampling is undoubtedly one of the most challenging tasks in aquatic environment studies. The main reason is that the upper last layers of sediment are usually very soft and vulnerable to resuspension. The crew's inability to observe the sampling device's activities during sediment penetration adds to the complexity of the task (Ilus, 1998). The extruder unit permits precise slicing of the sediment core for detailed analysis to obtain clean, untouched samples. The core layers were cut on the board of the ship into 10 mm (0─10 cm section) and 20 mm (10─30 cm section) layers, then deep-frozen and transported to the Laboratory of Toxicology and Radiation Protection at the Department of Environmental Chemistry and Radiochemistry, Faculty of Chemistry, University of Gdańsk. The sediments of the organisms' remains needed to be cleaned. The primary objective of pre-treating a

sample is to acquire a homogeneous solution devoid of insoluble residues that may obstruct the subsequent chemical processing or hold onto the analyte.

Figure 14. *OCEANIA* Research vessel

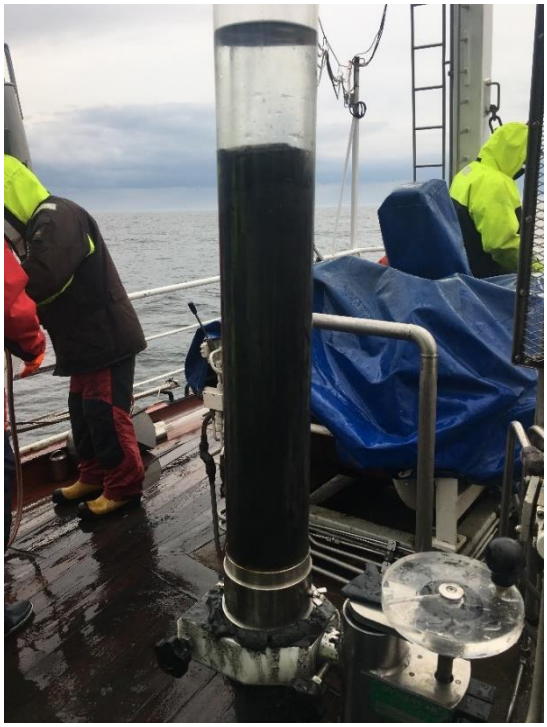

Figure 15. Plexiglas coring tube from GEMAX gravity corer

Additionally, the solution should be free of organic material that could form complexes with the analyte or reagents and contain the analyte with minimal losses. In the case of soil, sediment, and other mineral samples, pre-treatment generally entails oven-drying, homogenization, and sieving (if necessary), followed by removing organic material via ashing and subsequent wet chemical destruction. In the laboratory, dry bulk density (DBD) was measured by determining the weight after drying (60°C) of a known volume of wet sediment. The sediment porosity contents also were determined using wet and dry sediment weights. A RadWag laboratory balance was used for this purpose, providing mass measurements with an accuracy of 0.001 g. The results of the dry mass measurements are summarized in Table 9. Each sample name from sampling in 2019 includes the station code and depth number. Names of samples from 2010 are G.G. – Gdańsk Basin and Got – Gotland Basin. Sample weights varied, ranging from 0.79 g to 18.0 g.

Table 13. Mass and porosity of the samples

Lp.	Sample ID	Layer [cm]	Dry mass [g]	Porosity
1	78M-1	0–1	2.23	0.97
2	78M-2	1–2	4.10	0.92
3	78M-3	2–3	4.41	0.92
4	78M-4	3–4	7.24	0.90
5	78M-5	4–5	13.3	0.94
6	78M-6	5–6	7.87	0.89
7	78M-7	6–7	6.77	0.89
8	78M-8	7–8	8.53	0.90
9	78M-9	8–9	8.25	0.97
10	78M-10	9–10	8.43	0.94
11	78M-12	10–12	17.7	0.90
12	78M-14	12–14	16.1	0.84
13	78M-16	14–16	17.6	0.87
14	78M-18	16–18	16.3	0.91
15	78M-20	18–20	15.4	0.88
16	78M-22	20–22	12.5	0.96
17	78M-24	22–24	13.2	0.88
18	78M-26	24–26	18.0	0.90
19	78M-28	26–28	14.2	0.91
20	78M-30	28–30	12.4	0.88
21	BY15-1	0–1	2.67	0.97
22	BY15-2	1–2	3.16	0.97
23	BY15-3	2–3	5.04	0.95
24	BY15-4	3–4	8.04	0.94
25	BY15-5	4–5	6.53	0.94
26	BY15-6	5–6	7.72	0.93
27	BY15-7	6–7	8.42	0.94
28	BY15-8	7–8	11.4	0.91
29	BY15-9	8–9	7.39	0.93
30	BY15-10	9–10	7.52	0.90
31	BY15-12	10–12	13.4	0.90
32	BY15-14	12–14	15.1	0.90
33	BY15-16	14–16	12.5	0.91
34	BY15-18	16–18	14.3	0.89
35	BY15-29	18–20	14.8	0.90
36	BY15-22	20–22	15.1	0.89

Table 14. continued

37	BY15-24	22–24	10.5	0.92
38	BY15-26	24–26	16.1	0.93
39	BY15-28	26–28	13.1	0.91
40	BY15-30	28–30	14.9	0.91
41	P1-1	0–1	0.79	0.99
42	P1-2	1–2	1.30	0.97
43	P1-3	2–3	2.64	0.99
44	P1-4	3–4	1.20	0.96
45	P1-5	4–5	2.45	0.96
46	P1-6	5–6	2.32	0.96
47	P1-7	6–7	2.64	0.93
48	P1-8	7–8	5.14	0.92
49	P1-9	8–9	3.76	0.98
50	P1-10	9–10	6.96	0.96
51	P1-12	10–12	10.8	0.86
52	P1-14	12–14	6.36	0.93
53	P1-16	14–16	14.3	0.88
54	P1-18	16–18	8.83	0.89
55	P1-20	18–20	9.78	0.92
56	P1-22	20–22	11.6	0.96
57	P1-24	22–24	10.1	0.90
58	P1-26	24–26	14.0	0.96
59	P1-28	26–28	12.6	0.94
60	P1-30	28–30	13.2	0.94
61	Got-1	0–1	4.52	0.99
62	Got-2	1–2	7.39	0.97
63	Got-3	2–3	2.66	0.99
64	Got-4	3–4	12.4	0.96
65	Got-5	4–5	9.74	0.96
66	Got-6	5–6	11.6	0.96
67	Got-7	6–7	9.59	0.93
68	Got-8	7–8	10.8	0.92
69	Got-9	8–9	9.77	0.98
70	Got-10	9–10	9.71	0.96
71	Got-12	10–12	10.1	0.86
72	Got-14	12–14	8.68	0.93
73	Got-16	14–16	10.4	0.88

Table 15. continued

74	Got-18	16─18	12.0	0.89
75	Got-20	18─20	11.4	0.92
76	Got-22	20─22	5.24	0.96
77	Got-24	22─24	8.07	0.90
78	Got-29	24─29	11.0	0.96
79	GG-1	0─1	4.52	0.99
80	GG-2	1─2	7.39	0.97
81	GG-3	2─3	2.66	0.99
82	GG-11	10─11	12.4	0.96
83	GG-13	12─13	9.74	0.96
84	GG-19	17─19	11.6	0.96
85	GG-20	19─20	9.59	0.93
86	GG-29	27─29	10.8	0.92
87	GG-31	29─31	9.77	0.98

The first chemical treatment step was the addition of internal radioactive tracers with comparable physicochemical properties to the radionuclides under study. The tracer was an isotope that emitted alpha particles and energy significantly equal to that of the isotope under analysis and had similar physicochemical properties to the radionuclide under study, which was present in the environment at undetectable levels or was completely absent (Brown and Firestone, 1986). The 100 µl of ^{243}Am (NPL, Teddington, U.K.), with an activity of 94.60±3.42 Bq·mL, was used as a tracer. The activity of the tracer injected into the sample was matched as far as possible to the activity level of the isotopes under study. Only then can proper spectral analysis and quantitative evaluation be performed.

4.2 Sample Decomposition

Mineralization is a process used in analytical chemistry to decompose complex organic and inorganic materials into simpler forms, such as elemental metals, salts, or oxides. One standard mineralization method is nitric acid, a strong oxidant that can decompose many organic and inorganic materials into elementary forms (Balaram and Subramanyam, 2022).

In the initial stage of the process, 10 cm^3 of 65% HNO_3 is utilized. The sample is exposed to the acid, and this mixture can sit undisturbed for around three days. During this period, the liquid portion of the mixture begins to evaporate, gradually leading to the formation of a dried residue. This process might need to be repeated twice or thrice until the resulting residue achieves the desired lightness. After the acid evaporation step, the sample enters the final mineralization phase. This phase involves the use of 3 ml of 30% H_2O_2. Through a controlled chemical reaction, the remaining components of the sample are broken down and mineralized, transforming them into the desired form for subsequent analysis. Finally, the solution was filtered into glass beakers through a 9 cm GF/A filter paper supported on a Whatman 540 filter (Jakopič et al., 2007).

4.3 Preconcentration of Am by Oxalate Precipitation

Actinides are known to co-precipitate with calcium oxalate while iron remains in the solution. Environmental and geological samples contain significant iron (Lehto and Hou, 2010). The co-precipitation of americium with calcium oxalate is affected significantly by the concentration of iron present in the solution because iron reacts with oxalic acid forming a soluble complex $Fe^{3+} + 3C_2O_4^{2-} \leftrightarrow [Fe(C_2O_4)_3]^{3-}$, so the iron remained in solution as oxalate complexes while the actinides were co-precipitated (Moreno et al.,1997; Ristic et al., 2002).

Dry residue from the sample decomposition was dissolved in 3M HNO_3, heated, and oxalic acid ($C_2H_2O_4 \cdot 2H_2O$) was added. The pH of the solution was then adjusted to 5.5─6.0 using a 25% ammonia solution, and the sample was mixed using a magnetic stirrer-equipped plate (Moreno et al., 1997; Ristic et al., 2002). The solution was left overnight, and the oxalate precipitate was centrifuged and washed several times with distilled water. What remained in the filtrate were mainly non-covalent alkaline earth metals and the americium radioisotope under study in the residue. The precipitate, used for further analysis, was separated from the filtrate (Figure 16). The filtrate was stored in plastic bottles in case of improper co-precipitation with calcium oxalates. Oxalate precipitates are easily decomposed by ashing or wet chemical oxidation (Yamato, 1982). The oxalate precipitate was destroyed by concentrated HNO_3 and hydrogen peroxide (H_2O_2) and evaporated to dryness. The residue was dissolved in 2M HNO_3,

and approximately 1 g of hydroxylamine hydrochloride ($NH_2OH \cdot HCl$) was added to the solution, which was then gently heated for about 15 minutes to reduce plutonium to Pu(III). Sodium nitrite (over 2 g) was added to stabilize the conversion of Pu(III) to Pu(IV) after cooling (Moreno et al., 1997).

Figure 16. Precipitate and filtrate after oxalate precipitation

The americium separation and purification and the alpha spectrometric measurements were performed at the University of Gdańsk (Gdańsk, Poland) and the Jožef Stefan Institute (Ljubljana, Slovenia).

4.4 Anion Exchange Chromatography

Ion exchange is a procedure where mobile ions in an external solution are swapped with ions held by electrostatic forces within a solid matrix (Haddad, 2005). When the functional groups carry a negative charge, this swapping process will encompass cations; conversely, if they carry a positive charge, it will involve anions. By leveraging the property that, under specific conditions, ion exchange materials exhibit a stronger attraction to particular ionic species than others, it becomes possible to separate these species. Ion exchange (AG 1×8, Cl^- form, 50─100 mesh, Triskem, France) is one of the most common and effective treatment methods for separating and purifying radionuclides (Mushtaq, 2004). Cation-exchange resins show strong trivalent americium and curium adsorption from diluted nitric acid solutions (Lehto and Harjula, 1999).

The solution was converted to 8M with conc. HNO_3, and next loaded onto an anion exchange column (AG 1x8, 50─100 mesh, resin height approx. 7 cm) shown in Figure 17. The column was conditioned with 8M HNO_3. The sample passed through and was washed with 90 mL 8M HNO_3 at a 1 mL min^{-1} flow rate. This fraction was collected in the beaker and used to analyze americium radionuclides. The presented method also showed how to obtain pure fractions of other actinides. The column was washed with 100 mL 9M HCl to elute thorium. Plutonium was eluted with a 70 mL 9M HCl solution with 2 mL NH_4I. Ions of iodine reduce Pu(IV) to Pu(III), and then Pu(III) is not absorbed on the column and elutes. The eluents were evaporated until dry (Holm and Ballestra, 1989; Skwarzec, 2010).

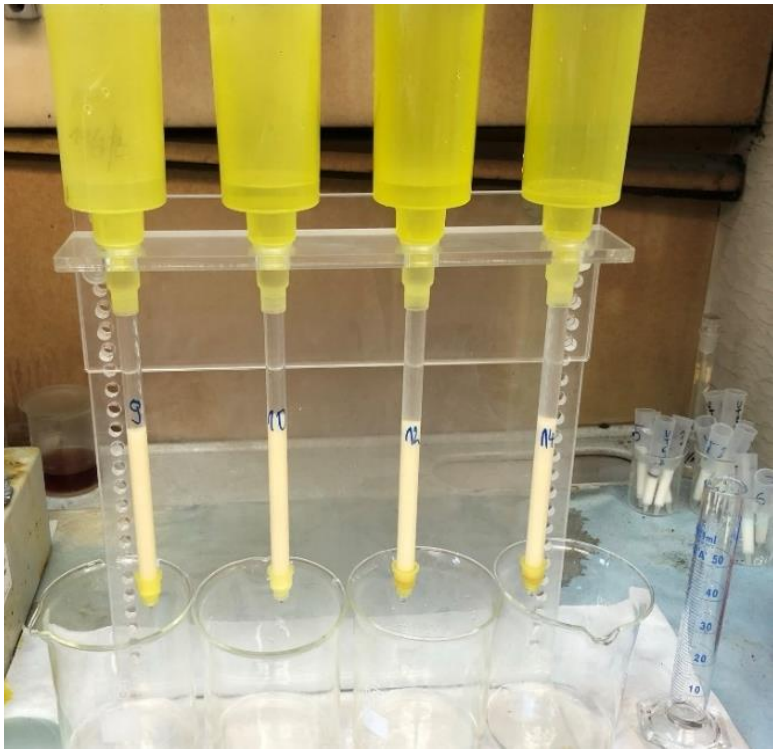

Figure 17. Ion exchange columns

4.5 Extraction Chromatography

Extraction chromatography is a technique that combines the selectivity of solvent extraction with the ease of use of column chromatography. The efficiency of extraction in this process can be influenced by various factors, including the chemical and physical characteristics of the metal analyte, the counter ion of the analyte, and the matrix components (Qi, 2018). Consequently, an extraction chromatography system can be

adjusted selectively to extract a specific analyte to a desired extent based on the composition of the mobile phase. This feature makes extraction chromatography highly valuable for the targeted separation of specific analytes. However, it also necessitates comprehensively characterizing the cations and anions in the sample matrix. The evaluation of the effectiveness of extraction chromatographic separations heavily relies on the determination of element uptake on a specific resin through batch extraction studies. This work used selective chromatographic extraction resins (Triskem International, Bruz, France). Two types of resin were used: UTEVA resin for separating the Am-Pu fraction from the U-Th fraction and TRU resin for obtaining clear Am fractions (Fig. 18) (Zhang et al., 2022).

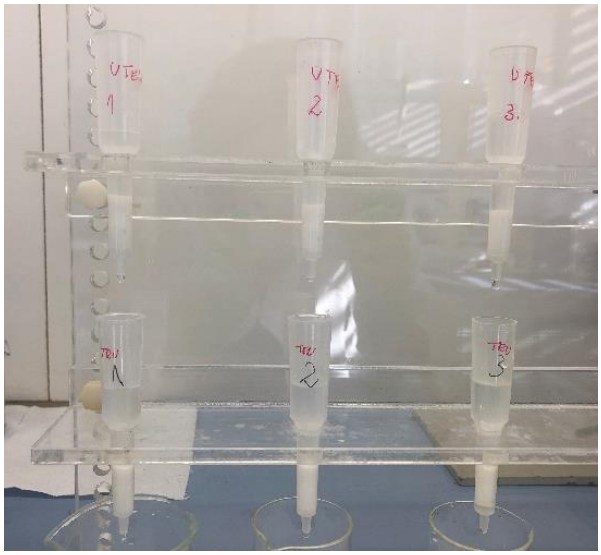

Figure 18. Tandem column arrangement of the UTEVA/TRU resins

UTEVA resin (Uranium and TEtraValents Actinides) separates uranium and tetravalent actinides like Np, Th, and Pu. The extractant coated on the inert support is the dipentyl pentylphosphonate. The ability of the resin to retain uranium(VI), thorium(IV), neptunium(IV), and plutonium (IV) relies on the concentration of nitrate in the solution; higher nitrate concentrations lead to better actinide absorption. In contrast, in diverse biological or environmental samples, phosphates can adversely affect absorption, as phosphate anions can readily outcompete tetravalent actinides, impeding the absorption of neptunium or thorium into the resin (Horwitz et al., 1993).

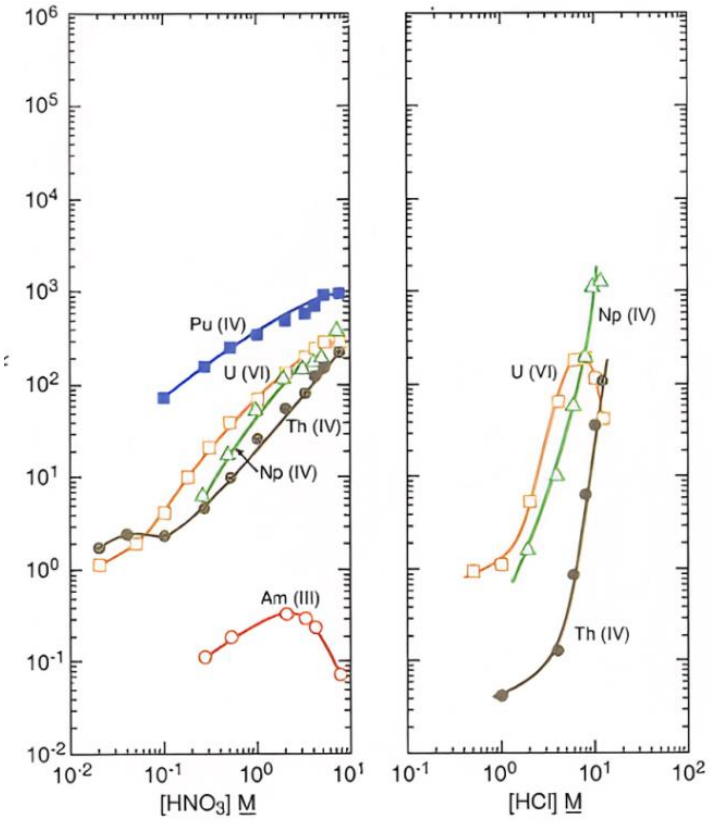

Figure 19. Capacity factors k' for various actinides on UTEVA resin concerning the acid concentration (23–25°C) (www.eichrom.com)

Figure 19 demonstrates the comparable uptake of tetravalent actinides and uranium from nitric acid. These elements exhibit robust retention (k'>100) when exposed to nitric acid concentrations above 5M. Also, since UTEVA resin does not have an affinity for trivalent metals, Pu(IV) can be separated from Am(III). Notably, it should be emphasized that americium (Am) does not exhibit any retention regardless of the nitric acid concentration. This observation holds significance in the development of analytical separation schemes.

TRU resin extractant system is octyl phenyl-N,N-di-isobutylcarbamoylmethylphosphine oxide dissolved in tri-n-butyl phosphate (TBP). TRU resin is used to extract and separate TRansUranium elements, including americium. Figure 20 shows the elution profiles of various radionuclides in HNO_3 and HCl solutions. It can be seen that the transuranic elements show a strong binding affinity to the resin, significantly as the concentration of HNO_3 increases. In HCl media, Am(III) is not retained on TRU Resin (Horwitz et al., 1993).

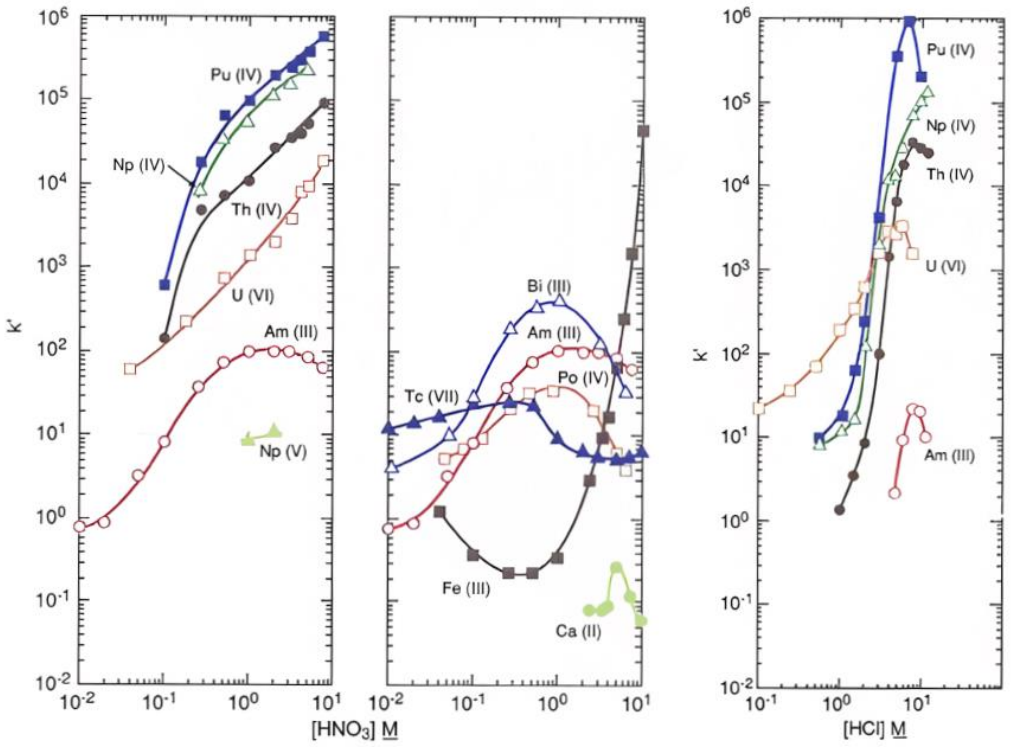

Figure 20. Capacity factors k' for various actinides on TRU resin concerning the acid concentration (23–25°C) (www.eichrom.com)

After separation on AG resin, the americium fraction was evaporated to dryness. Sequential separation of uranium and americium fraction from the sample solution was performed using a combination of two extraction chromatographic resins. UTEVA and TRU Resin cartridges with funnels (Polypropylene + Polyethylene – PP+PE) were placed in tandem (Fig. 18). Combined procedures are often used for the chemical separation of a single element to obtain high decontamination rates for a single element or the simultaneous determination of several elements (Vajda et al., 2012). Five ml of 2M HNO_3 was passed through the cartridges to equilibrate the resin. Samples were passed through the cartridges, UTEVA first, followed by TRU. The cartridges were then rinsed with 30 ml of 2M HNO_3. Afterward, the UTEVA and TRU columns were separated and treated independently (Thakkar, 2002).

The TRU column was washed with 5 mL of 2M HNO_3/0.1M $NaNO_2$ (plutonium was oxidized to Pu(IV)). Sodium nitrite was used only to oxidize Pu(III) to Pu(IV) to afford Pu and Am separation. This fraction was discarded. The column was converted to the chloride system using 5 mL of 9M HCl; Am was eluted using 60 mL of 4M HCl and kept for microprecipitation (Jakopič et al., 2007). Am(III) in the HCl system is not

retained on the TRU Resin. In some instances, small amounts of Th could have passed through UTEVA resin and subsequently been absorbed into TRU Resin.

4.6 Source Preparation

After the chemical separation from the sample matrix, the analytes must be transformed into a thin, flat, and uniform source suitable for alpha-spectrometric analysis. For a high-quality source, certain key characteristics are essential. Firstly, the alpha particles should experience minimal and consistent energy loss while exiting the source to minimize energy straggling. Secondly, the geometry of the source-detector arrangement should ensure a high counting efficiency, which remains consistent across different sources. Additionally, the deposited activity should be relatively homogeneous throughout the deposit, and the source itself should be robust, easy to handle, and store (Vajda et al., 2012). To separate the ^{241}Am peaks from the ^{243}Am peaks without any overlapping, it is necessary to have high-quality sources as the energy difference between them is relatively small (200 keV). Microprecipitation is an alternative to electrodeposition for alpha spectrometry source preparation. Sometimes, microprecipitation produces a thick alpha-counting target, causing peak broadening in the spectrum, as this method is not specific to the target radionuclides and can result in the co-precipitation of other elements. Microprecipitation offers sufficient alpha peak resolution for most analytical applications, and tri- and tetravalent actinides can be co-precipitated from a solution with lanthanide fluorides, e.g., with NdF_3 or CeF_3 (Hindmann, 1983; Nilsson et al., 2001). Direct precipitation reduces the time needed to prepare an alpha spectrometry source from 2 hours to 60 minutes and eliminates several evaporations and digesting steps typically necessary for electrodeposition. Besides, it removes the problem of corrosive acid fumes released through the vents of the lab fume hood.

In the study, neodymium fluoride micro-precipitation was used to obtain americium targets. The solutions eluted from the columns in each method were evaporated to dryness and fumed with 2 mL of concentrated HNO_3 to degrade any organic compounds (resin) that might have been present in the eluent. The solution was transferred to a polypropylene centrifuge tube with 15 mL of 1M HNO_3, 100 μL of the

stock solution containing 50 µg $Nd^{3+,}$ and 5 mL of 40% hydrofluoric acid added. After shaking, the sample was left for 30 min in an ice bath (Fig. 21). The achieved neodymium fluoride suspension with americium radioisotopes was filtered through a 25 mm diameter 0.1 µm Resolve Filters™ (RF-100-25PP01, Eichrom, Lisle, USA) pre-wetted with 80% ethanol (C_2H_5OH) solution, deionized water and conditioned with 5 mL of neodymium substrate solution. The centrifuge tubes were washed with 5 mL of 0.58M hydrofluoric acid solution, twice with deionized water and twice with 80% ethanol. The filters were dried under a heat lamp for 3–5 minutes, glued to a planchet, and measured by alpha spectrometry (Fig. 22) (Mietelski et al., 2000; Moore, 1963). The whole analytical procedure is shown in Figure 23.

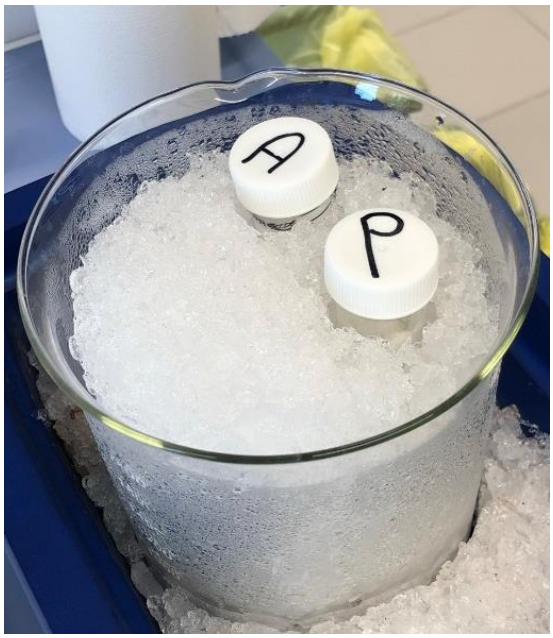

Figure 21. Ice bath in the microprecipitation process

Figure 22. Source of ^{241}Am for Alpha Particle Spectrometry

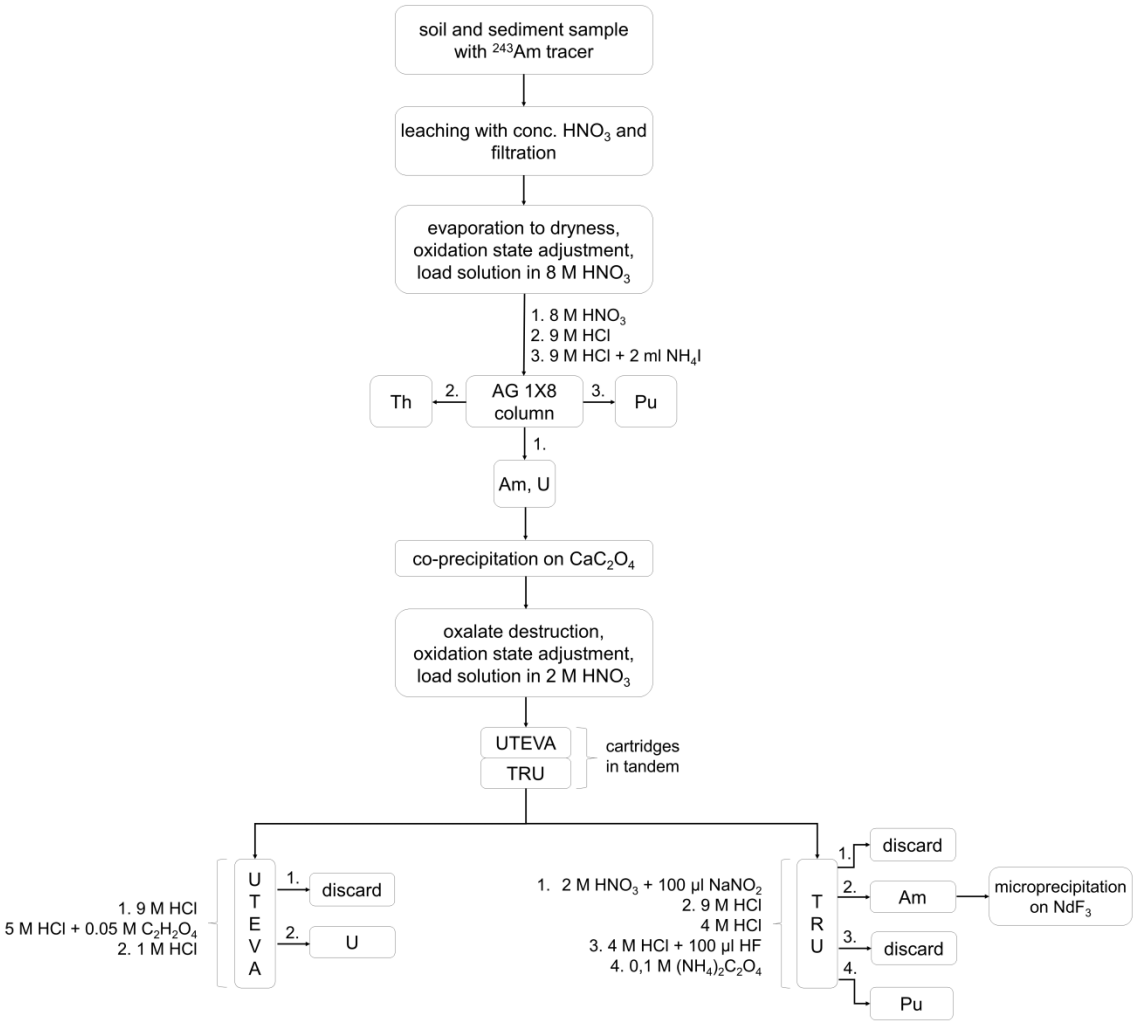

Figure 23. Flow diagram of general steps of the total analytical process

4.7 The Efficiency of the Radiochemical Procedure

Based on the nuclear radiation spectra obtained, the chemical yield of the sequential radiochemical procedure was calculated for each sample and the americium elements studied. The alpha spectrometer efficiency and energy calibration were done using the Isotrak™ certified (Eckert and Ziegler Isotope Products) calibrated solid mixed nuclide source of ^{237}Np, ^{241}Am, and ^{244}Cm (Table 10).

Table 16. Characteristics of the calibrated solid mixed nuclide source

Product code	Isotope	Activity on date 2004 (k = 2) [Bq]
QCRB4021	^{241}Am	100 ± 3
	^{244}Cm	72 ± 3
	^{237}Np	175

The source is a stainless steel disc with radionuclides deposited in the center of a surface. A series of measurements were conducted using the standard source to determine the efficiency and resolution parameters of the two detectors in the system. Each measurement lasted 100 seconds and covered all feasible distances between the detectors and the source within the counting chambers. The efficiency of each detector was determined from the spectra by dividing the measured counts per second by the known number of alpha decays per second for each detector-source distance. Likewise, the detector's energy resolution was assessed by calculating the full width at Half Maximum (FWHM) of the peaks observed.

Regular monitoring of instrument performance involves counting check sources. These check sources consist of alpha-emitting radionuclides, and they serve to verify the energy, Full FWHM, and efficiency calibration of the detector or alpha spectrometer. The check source is counted under fixed conditions, similar to how samples are handled. The key parameters to assess the system's stability are the peak location, FWHM, and counting efficiency of a specific radionuclide in the check source. In alpha spectrometry, the detector's energy resolution performance is traditionally expressed as the FWHM in keV at the 5486 keV peak of ^{241}Am. In alpha spectrometry, peaks are usually not symmetric (not Gaussian-shaped). The asymmetry appears as a low-energy side tailing that can be better characterized by the full width at one-tenth of the peak maximum (FWTM).

Figure 24 presents an illustrative example of the alpha particle spectrum obtained from the certified standard source. The peaks generated by the well-known alpha particles emitted by ^{237}Np, ^{241}Am, and ^{244}Cm at energies of 4.79, 5.49, and 5.81 MeV, respectively, are visible for evaluating the efficiency and energy resolution of the alpha spectroscopy system at that particular configuration.

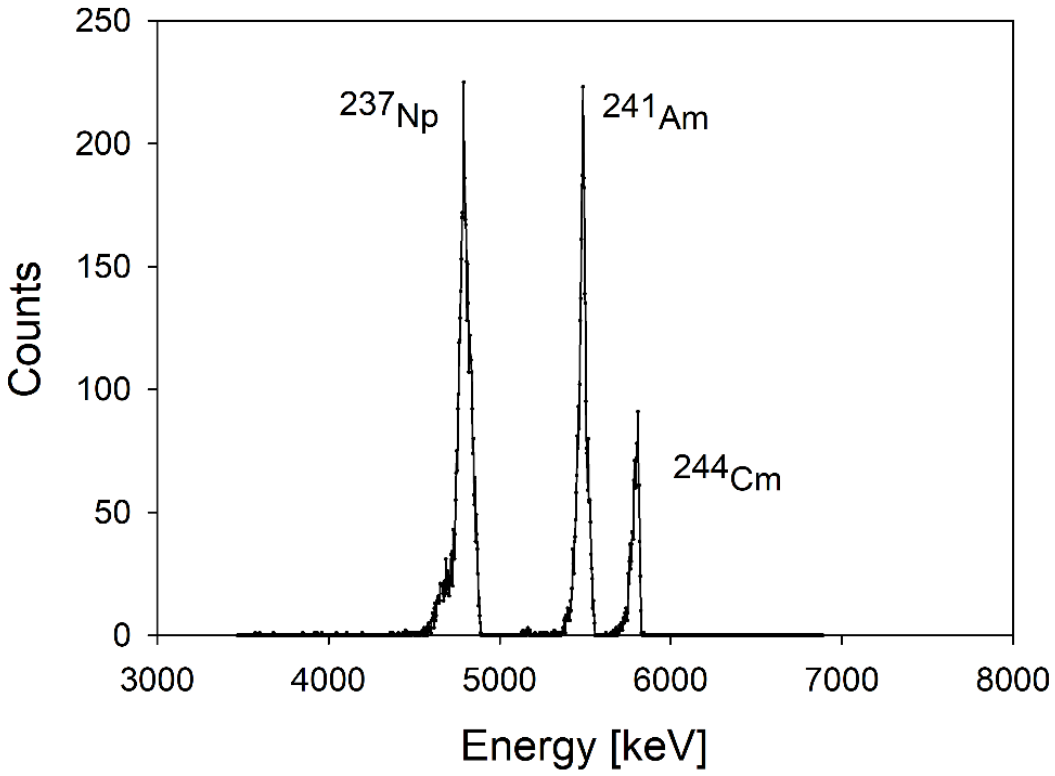

Figure 24. Alpha spectrum of a commercially available calibration source containing ^{237}Np, ^{241}Am, and ^{244}Cm

4.8 Analysis of Americium Isotopes by α-particle Spectrometry

Isotope activities were measured using an alpha spectrometer (Alpha Analyst S470, Canberra, USA) (Fig. 25) equipped with Passivated Implanted Planar Silicon (PIPS) semiconductor detectors. More information about Alpha-particle Spectrometry is in Chapter 1.

The sample sources were placed in a vacuum chamber. The detector voltage was then set. Environmental samples with low activity are usually_counted over several days, so the counting time was 3 to 5 days. The basic parameters of the equipment were detector efficiencies of 33–35%, an active surface of 450 mm^2, a resolution of 17–18 keV, and an energy range of 3.0–7.5 MeV. The software used to analyze the spectra was Genie2K.

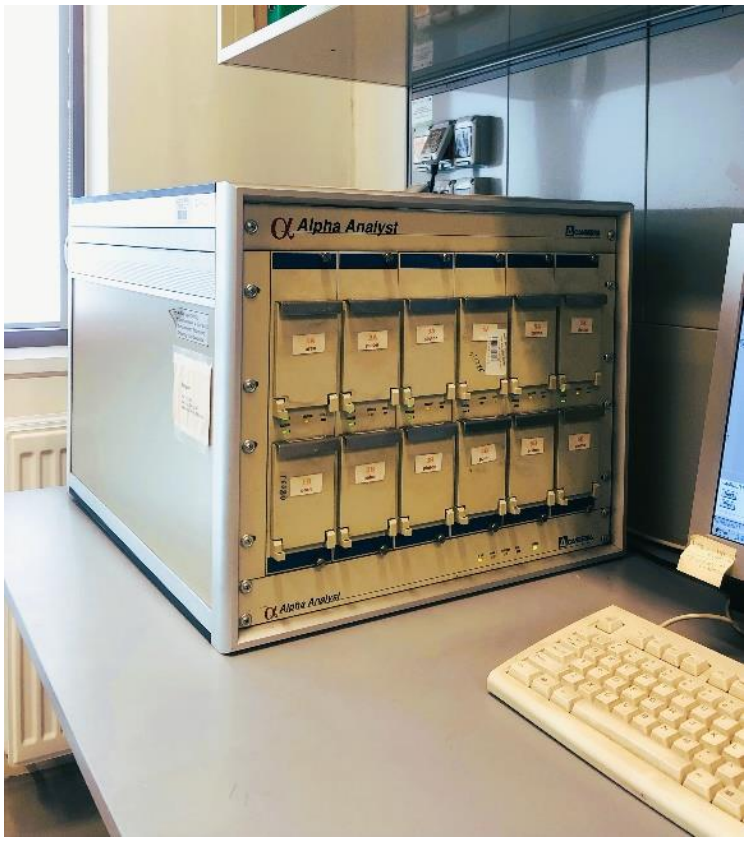

Figure 25. Alpha spectrometer at the University of Gdańsk

For nuclear analytical approaches, ensuring accuracy and reliability involves implementing quality assurance and control measures to evaluate and quantify sources of uncertainty. These methods are typically regarded as relative rather than absolute analytical techniques. Consequently, measurement protocols necessitate calibration using suitable standards, and the outcomes must undergo validation to guarantee consistency and comparability. Uncertainty linked to calibration primarily stems from the reference materials used, the appropriateness of the calibration curve fitting, or the scaling factor applied (Neacsu, 2020). One of the spectra is displayed in Figure 26:

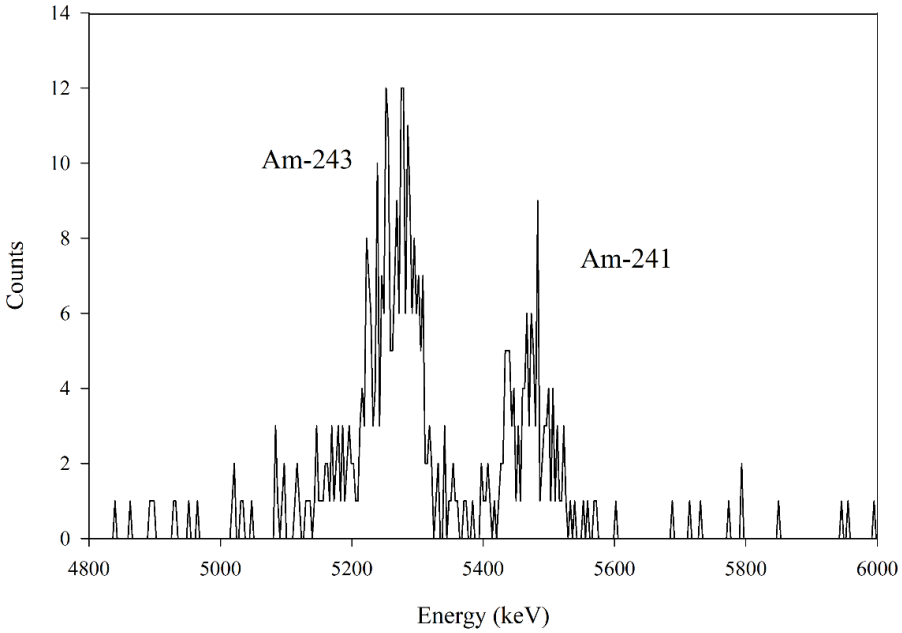

Figure 26. Alpha spectrum of americium isotopes

The peaks of ^{241}Am (5486 keV, 85.2% abundance; 5443 keV, 12.8% abundance) and ^{243}Am (5277 keV, 88% abundance; 5486 keV, 10.6% abundance) were partially overlapping because of the minimal energy difference.

4.9 Analysis of ^{210}Pb and ^{137}Cs Isotopes by γ-spectrometry

The direct measurements of ^{210}Pb and ^{137}Cs with gamma spectrometry were done at the Technical University of Denmark (Roskilde, Denmark) and the Institute of Oceanology Polish Academy of Sciences (Sopot, Poland) using gamma-ray spectrometry with planar HPGe (high-purity germanium) detectors (Mirion, Canberra, USA). All detectors were placed in a 10-cm low background lead shield with a 2–3 mm copper or cadmium sheet inside. The relative efficiency of the detector ranged from 35–50%. The energy calibration is done using a multi-nuclides calibration point source. The sources contained ^{241}Am, ^{137}Cs, and ^{60}Co, covering the environmental samples' main energy window. Detector efficiencies were calibrated using a standardized mixture of radionuclides (Eckert and Ziegler Isotope Products GmbH, Braunschweig, Germany). This source covered an energy range between 46 and 1835 keV and contained ^{210}Pb, ^{241}Am, ^{109}Cd, ^{57}Co, ^{123m}Te, ^{51}Cr, ^{113}Sn, ^{85}Sr, ^{137}Cs, ^{60}Co and ^{88}Y. The efficiency curve

was prepared for different sample geometries and corrected using the efficiency transfer technique. The efficiency transfer and coincidence summing corrections are calculated using EFFTRAN software.

After homogenization, the samples were packed in low-density plastic Petri dishes (sealed using teflon tape) with known geometry. The weight and height of the samples were measured. The activities of ^{210}Pb and ^{137}Cs were determined using characteristic emission peaks at 46.5 and 662 keV, respectively. $^{210}Pb_{supp}$ (^{226}Ra) was determined by measurement of ^{214}Pb (at 295 and 352 keV) and ^{214}Bi (at 609 keV). The $^{210}Pb_{ex}$ activity was determined by subtracting $^{210}Pb_{supp}$ (average of ^{214}Pb and ^{214}Bi activities) from the total ^{210}Pb for each depth interval. Corrections were made for the effect of self-absorption of low-energy γ-rays within the sample. However, the weights of these samples were relatively low. The samples were measured until they reached a statistical uncertainty of less than 5% for the ^{137}Cs peak with a limit of 4 days maximum. For ^{210}Pb quantification, an additional measurement was carried out. After the standard sample measurement, a ^{210}Pb point source was placed on the top of the sample container and measured to get at least 1% statistical uncertainty in the ^{210}Pb peak (after deducting the sample contribution in this peak). This additional measurement allows the correction of the ^{210}Pb self-attenuation in the sample. The background was measured for at least one week. The data analysis was done using the in-house developed software GENTRAN. The software is a graphical user interface that interacts with Mirion Genie 2000 and EFFTRAN.

5. DATA ANALYSIS

The technique used to determine analyte activity relies on the known activity of the tracer introduced into the sample. This method, known as isotope dilution alpha spectrometry, offers the distinct advantage of an inherent correction for chemical losses. This correction is achieved by assuming that analyte losses are equivalent to tracer losses. This assumption is true because the tracer and analyte are the same element and have identical chemical forms (Vajda et al., 2012).

5.1 Radiochemical Recovery

The certified radiochemical tracer, ^{243}Am, was added to estimate the recovery (efficiency of the radiochemical sample preparation method for removing americium from a biological matrix). The amount of tracer was carefully considered in relation to the average activity concentration of americium in the sample. Detection efficiency is not needed directly to calculate activity concentration in alpha spectrometry. However, it allows for calculating chemical recovery based on the added tracer's activity and the net counts in the corresponding peak. The recovery of americium was calculated using Equation 8 (Kanisch, 2004).

$$R = \frac{N_t}{A_t \times t \times m_t \times \varepsilon_{det}} \quad \text{(Eq. 8)}$$

Where:

R is chemical recovery;

A_t is the activity concentration of ^{243}Am (Bq·kg^{-1});

N_t is the net peak area of ^{243}Am;

m_t is the mass of ^{243}Am (kg);

ε_{det} is the detector efficiency;

t is the time of measurement (s).

The detection efficiency is determined from the activity of a calibration source and the net count rate measured in the same geometry as the sample (Vajda et al., 2012). The average recovery in this work generally ranged from 59–84% (average value 74%).

5.2 Minimum Detectable Activity (MDA)

Minimum detectable activity (MDAs) were around 0.1 mBq for ^{241}Am. MDA was calculated from the measurement of a blank vial under the same conditions as the samples using the formula given by Currie (Currie, 1968) using the following Eq. (9) and varied from 0.1 to 0.9 mBq for the chamber.

MDA can be derived from the measurement using Equation:

$$MDA = \frac{2.71+4.65\sqrt{N_b}}{t\ \varepsilon_{det}\ R} \quad \text{(Eq. 9)}$$

Where:

N_b is net background counts;

ε_{det} is the efficiency of the alpha detector;

R is the radiochemical yield (recovery);

t is the counting time.

5.3 Activity Concentration

The alpha spectrometry sources are counted in the spectrometer for a suitable duration. The activity is determined by integrating the analyte's and the tracer's counts in the corresponding peaks in the same spectrum. The computation of the results, along with the uncertainty budget, decision threshold, detection limit, and confidence limits, is thoroughly explained in multiple standards, including ISO 11929-7 and ISO/DIS 18589-4. Analysis of the energy spectrum obtained from the measurement allows us to determine the activity concentrations of alpha-emitting isotopes in the test material. The

activity concentration of the analyte (A_1, $Bq \cdot kg^{-1}$) at the separation time can be calculated by Equation 10. The background count rate is subtracted from each measurement of the count rate.

$$A_1 = \frac{N_{241_{Am}} \times A_t}{N_t \times m_s} \times m_t \times f_T \quad \text{(Eq. 10)}$$

Where:

A_1 is the activity concentration of the ^{241}Am in the sample on the date of chemical separation ($Bq \cdot kg^{-1}$);

$N_{241_{Am}}$ is the net peak area of ^{241}Am;

N_t is the net peak area of ^{243}Am (tracer);

A_t is the activity concentration of the tracer solution ($Bq \cdot kg^{-1}$);

m_s is the sample mass (kg);

m_t is the tracer mass (kg);

f_T is decay correction factor calculated as following Equation 11:

$$f_T = e^{-\lambda_t \times t_t} \quad \text{(Eq. 11)}$$

Where:

λ_t is the decay constant of the tracer ($years^{-1}$)

t_t is the elapsed time between the reference date of the tracer and the separation time (years).

Finally, the massic activity of the analyte in the sample is calculated back to the date of sample collection (A_0) by Equation 12:

$$A_0 = A_1 \times e^{\lambda_A t_1} \quad \text{(Eq. 12)}$$

Where:

λ_A is the decay constant of the analyte ($years^{-1}$)

t_1 is time interval between the sampling date and the separation time (years).

5.4 Uncertainty Analysis

The IAEA Guide provides the structure for quantifying uncertainty for specific nuclear analytical methods is shown in Fig 27:

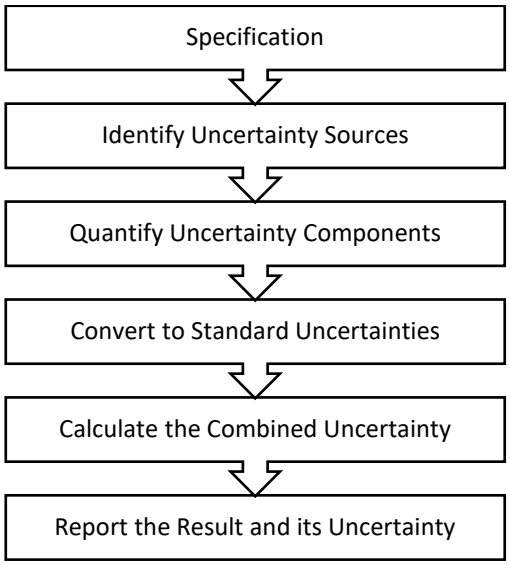

Figure 27. Approach and structure of the specific guidance for quantifying uncertainty

A measurement is not fully characterized solely by stating the value of the measurement. It becomes complete only when accompanied by the expression of its associated uncertainty. The uncertainty serves as a quantitative indicator of the quality of measurement results. This aspect is crucial for comparing measurements or measurement systems with each other or standards and drawing valid conclusions about test hypotheses. In essence, including uncertainty provides a comprehensive understanding of the reliability and precision of the reported measurement value.

Identifying the uncertainty components is necessary to properly assess the values of total uncertainty of ^{241}Am activity concentrations in environmental samples. Each radioisotope's relatively low activity levels are affected by relatively high uncertainty. The uncertainty of the ^{241}Am activity concentrations in environmental samples is generally less than 30%. The procedure for evaluating the level of uncertainty in a ^{241}Am activity concentration result is described below. The calculation of the combined

standard uncertainty can be carried out following the ISO Guide for the Expression of Uncertainty in Measurement (1995) or according to the IAEA publication on the Quantification of Uncertainty in Nuclear Analytical Measurements (IAEA, 2004). First, the individual uncertainties of the input parameters are calculated or estimated, and then the uncertainty of the activity concentration $u(a_0)$ is calculated according to the uncertainty propagation law.

The uncertainty associated with the mass of the sample was estimated using data from the laboratory balance manufacturer's recommendations. Equation X was used from the GUM approach (ISO, 2000). If it is assumed that the balance with 0.001 g of uncertainty is used for weighing the sample and the linearity distribution is assumed to show a rectangular distribution, the standard uncertainty in weighing the sample mass can be calculated by the following Equation 13:

$$u(m_s) = \frac{0.001}{\sqrt{3}} = 0.00058 \qquad \text{(Eq. 13)}$$

Uncertainty in the mass of the tracer solution is calculated similarly.

The uncertainty of the detector efficiency $u(\varepsilon_{det})$ was estimated from a series of repeated observations by calculating the standard deviation of the mean.

The uncertainty of the chemical recovery $u(R)$ consists of the uncertainty of the tracer activity contribution $u(A_t)$, the peak area of americium tracer $u(N_t)$, the mass of the americium tracer added to the sample $u(m_t)$, and the detector efficiency $u(\varepsilon_{det})$. The uncertainty of the chemical recovery is calculated from Equation 14 (Vreček and Benedik, 2003)

$$u(R) = \sqrt{\left(\frac{u(m_t)}{m_t}\right)^2 + \left(\frac{u(\varepsilon_{det})}{\varepsilon_{det}}\right)^2 + \left(\frac{u(A_t)}{A_t}\right)^2 + \left(\frac{u(N_t)}{N_t}\right)^2} \qquad \text{(Eq. 14)}$$

In standard spectrometry practice, the counting rates are usually very low; hence, the uncertainty of the measuring time is negligible.

The uncertainty of the tracer activity $u(A_t)$ was taken from the certificate. The uncertainty of the peak area $u(N_t)$ was calculated as the square root of the peak area $u(N_t) = \sqrt{N_t}$.

The uncertainty of the decay correction factor (IAEA, 2004) was calculated from Eq. 15.

$$u(f_t) = f_T \times t_t \times u(\lambda_t) \quad \text{(Eq. 15)}$$

In determining ^{241}Am (a_i), the combined overall uncertainty (ISO, 1993) is calculated from Eq. 16.

$$u(a_1) = \sqrt{\sum_i \left(\frac{\partial a_i}{\partial x_i}\right)^2 \times u(x_i)^2} \quad \text{(Eq. 16)}$$

Where x_i is the individual parameter of the result a_1.

5.5 Quality Assurance and Control on ^{241}Am Analyses

Following the ISO, validation refers to establishing analytical necessities and verifying that the evaluated method can perform adequately based on the application's demands (ISO, 1993). Method validation, on the other hand, entails developing an analytical method that is deemed acceptable for its intended use. A quality assurance (QA) procedure is necessary to achieve high effectiveness and reliability in analytical chemistry (Taylor, 2018). Reference materials (RM) are intended for calibrating analytical methods and validating measurement results in nuclear safeguards and environmental monitoring (Budd et al., 2018). The International Vocabulary of Metrology (VIM) defines RM as a "material, sufficiently homogeneous and stable regarding one or more specified properties, which has been established to be fit for its intended use in measurement or examination" (BiPM, 2012). The main steps to the production of RM are planning, defining the source of material, preparation, stability studies, homogeneity testing, and determining the content of main components and certifications (Quevauviller et al., 1999; Walker and Lumley, 1999).

If the RM contains isotopes of americium and plutonium, the activity concentration values of ^{241}Am should be corrected for the increase from ^{241}Pu (Fitzgerald et al., 2015). However, not every RM provides a ^{241}Pu value. Reliable comparisons of such data present an excellent challenge for researchers. Due to the low energy of the beta radiation emitted by ^{241}Pu, direct measurement of this radiation is

associated with some obstacles (Moreno et al., 1997). Accordingly, it requires a suitably sensitive beta radiation detector, usually in a spectrometric system. Sample preparation involves separating the radioisotope under analysis in pure form to reduce to a minimum the radiation from other beta-emitting radionuclides contained in the sample (Kaihola, 2000; Mietelski et al., 1999; Piekarz and Komosa, 2014). All these obstacles may cause a lack of information regarding ^{241}Pu in reference material. The International Atomic Energy Agency (IAEA) and the National Institute of Standards and Technology (NIST) produce the most popular reference materials.

During this doctoral research, the effect of ^{241}Pu decay on the activity concentration of the ^{241}Am isotope in reference materials was also studied. Isotopes of americium and plutonium are present in reference materials; therefore, ^{241}Am activity concentration values should be corrected by its increase from ^{241}Pu. However, most reference materials do not have an approved or certified ^{241}Pu value. Reference material without information about ^{241}Pu is not good enough for ^{241}Am analysis. For reliable determination of ^{241}Am in reference materials, the concentration of ^{241}Pu should be known. To ensure compatibility, it is recommended that measurement results of ^{241}Am be supplied alongside the corresponding measurement date. In order to ensure reliable quality assurance of ^{241}Am determination, it is crucial to have information regarding the concentration of ^{241}Pu while selecting suitable reference material. The presence of ^{241}Pu can be presented on the official certificate sheet or determined by calculations if the concentrations of ^{241}Am are known from two separate dates. This condition limits the number of considerable RMs, as seen in Tables 11 and 12. NIST RMs cannot be selected due to the lack of information on ^{241}Pu. Therefore, choosing the RMs from the officially published catalog provided by the IAEA (analytical-reference-materials.iaea.org/radionuclides) is advisable. Specific laboratories may possess older reference materials containing ^{241}Pu, such as IAEA-300, IAEA-367, and IAEA-368. The issue with these RMS is that they only provide information values about the ^{241}Pu, which leads to an increase in uncertainty during the correction of ^{241}Am. Considering this, the most preferred RMs are the IAEA-384 and IAEA-385. For both, the ^{241}Pu is communicated as an information value. However, it can be calculated as a recommended value because the concentration of ^{241}Am is published on two separate dates: first as a recommended value and then as a certified value. IAEA-447 may also be used, although it has only information values for ^{241}Am and ^{241}Pu.

Table 17. List of available reference materials produced by IAEA for analysis of ^{241}Am radionuclides in the soil and sediment (extended uncertainty at k=2)

Reference material	Description	Reference day	^{241}Am [Bq·kg^{-1}]	^{241}Pu [Bq·kg^{-1}]	Ratio ^{241}Pu/^{241}Am	$^{239+240}$Pu [Bq·kg^{-1}]
IAEA-Soil-6	soil from Austria	30.01.1983	0.48±0.10	-	-	1.04 (0.962–1.11)
IAEA-135	sediment from the Irish Sea	01.01.1992	318** (310–325)	-	-	213* (205–225.8)
IAEA-300	sediment from the Baltic Sea	01.01.1993	1.38* (1.2–1.5)	20.3±4.8****	14.7	3.55* (3.44–3.65)
IAEA-326	soil from Russia	31.12.1994	0.19** (0.16–0.22)	-	-	0.50* (0.48–0.52)
IAEA-327	soil from Russia	31.12.1994	0.22** (0.19–0.25)	-	-	0.58* (0.56–0.60)
IAEA-367	sediment from Enewetak Atoll	01.01.1990	26.4** (24–27.7)	170** (154–190)	6.4	38* (34.4–39.8)
IAEA-368	sediment from Mururoa Atoll	01.01.1990	1.3** (1.2–1.5)	17.1±1.4**** 70±20****	13.2 53.8	31* (29–34)
IAEA-375	soil from Russia	31.12.1991	0.13** (0.11–0.15)	-	-	0.30** (0.26–0.34)
IAEA-384	sediment from Fangatuafa Atoll	01.08.1996 0.1.01.2019	7.1* (6.7–7.6) 9.3±1.0***	66** (48–188) 22±15**	9.3 2.4	108* (105–110) 118±5.8***
IAEA-385	sediment from the Irish Sea	01.01.1996	3.90*** (3.60–4.10)	28–144****	7.2–36.9	2.98* (2.81–3.13)
IAEA-412	sediment from the Pacific Ocean	01.01.2019	0.3±0.1**	-	-	0.611±0.028***
IAEA-447	moss-soil	01.05.2011	2.3± 0.2**	4.6± 0.6**	2	5.3±0.2**
IAEA-465	sediment from the Baltic Sea	01.01.2020	0.99±0.15***	-	-	2.17±0.16
IAEA-478	Agricultural soil (spiked sample)	01.01.2018	53.1±0.7***	-	-	-

* Recommended **Information value ***Certified value ****only a few measurements of the radionuclide have been reported

Table 18. List of available standard reference materials from NIST for analysis of ^{241}Am radionuclides in the soil and sediment (extended uncertainty at k=2)

SRM number	Description	Reference day	^{241}Am* [Bq·kg^{-1}]	^{241}Pu [Bq·kg^{-1}]	Ratio ^{241}Pu/^{241}Am	$^{239+240}$Pu [Bq·kg^{-1}]
4350B	Columbia River Sediment	09.09.1981	0.15±0.04**	-	-	0.508±0.003**
4353A	RF Soil II	01.04.1998	2.5* (0.6–5.4)	-	-	16.8±1.8**
4354	Freshwater Lake Sediment	14.12.1986	1.1** (0.77–1.99)	-	-	4.0** (3.72–4.72)
4355	Peruvian Soil	01.06.1982	0.004±0.001**	-	-	0.0075±0.0021**
4357	Ocean Sediment	16.02.1994	10* (7–18)	-	-	10.4±0.2**

*Uncertified value **Certified value

The reference materials had the appropriate certificates and were selected so that the isotopes labeled in them were the same as those labeled during the author's study and, as far as possible, were characterized by a similar matrix to the analyzed research material research material. These were the following attested (nucleus.iaea.org) materials: IAEA-384 and IAEA-385 (Tab. 13). All the measured results agreed very well with the expected values. IAEA-384 is contaminated sediment collected at Fangataufa Lagoon (French Polynesia) in July 1996. The reference date for decay correction for ^{241}Am is 01.08.1996. In 2019, IAEA-384 was changed into certified reference materials (CRM), and the reference date for decay correction for ^{241}Am is 01.01.2019. IAEA-385 is sediment from the Irish Sea collected in July 1995. The reference date for decay correction for ^{241}Am is 01.01.1996. For recovery determination, 20 µl of ^{243}Am tracer (NPL, Teddington, UK) with an activity concentration of 94.6±3.42 Bq·kg^{-1} was used.

Table 19. Activity concentrations in Bq·kg^{-1} dry weight for ^{241}Am radioisotope in IAEA references materials (decay ^{241}Pu corrected value and extended uncertainty at k=2)

	Measured value [Bq·kg^{-1}]	**Reference recommended value**	**Confidence interval**
IAEA-384	7.16±0.70 Bq·kg^{-1} Measurement date: 07.07.2022	7.1* Reference date: 1.08.1996	(6.7–7.6)
	8.73±0.77 Bq·kg^{-1} Measurement date: 07.07.2022	9.3** Reference date: 1.01.2019	(8.3–10.3)
IAEA-385	3.86±0.29 Bq·kg^{-1} Measurement date: 09.07.2022	3.9** Reference date: 1.01.1996	(3.60–4.10)

*recommended value **certified value

Using the provided values of ^{241}Pu activity concentrations, considering both ^{241}Am activity increase from ^{241}Pu decay and ^{241}Am decay as itself, calculated values of ^{241}Am in IAEA-384 and IAEA-385 agreed with the reference value provided by the International Atomic Energy Agency (IAEA).

Following the recommendations for assessing laboratory performance, the Z-score methodology has been used to evaluate results. The Am analysis results for

IAEA-384 and IAEA-385 were evaluated in terms of Z-test based on IAEA/AQ/11 (IAEA, 2009) Eq. 17:

$$\mathrm{Z-score} = \frac{\mathrm{Value_{reported}} - \mathrm{Value_{target}}}{S_b} \qquad \text{(Eq. 17)}$$

where: "$Value_{reported}$" is the obtained result using the separation procedure, "$Value_{target}$" is the reference value in the standard or reference sample, and S_b is the target standard deviation. If |Z-score| $\leq$ 2, the reported value will be considered satisfactory; it would be questionable if |Z-score| $\leq$ 3; and unsatisfactory if |Z-score| $\geq$ 3.

All Z-score values for ^{241}Am radionuclides were acceptable and ranged between 0 and 2.

The International Atomic Energy Agency (IAEA) certificate sheets present three reference values: certified, recommended, and information. Certified value, assigned to a property of a reference material accompanied by an uncertainty statement and a statement of metrological traceability, is identified as such in the reference material certificate (ISO, 2000). The recommended values are consensus values derived from intercomparison evaluations. While they are generally reliable, they may not possess the same level of certainty as certified values. These values are obtained through a collective agreement among experts. Information values are provided when assigning a certified or recommended value is impossible, usually due to insufficient accepted intercomparison results. These values are also obtained through a consensus among experts. However, they did not meet the criteria to qualify as recommended values. Information values may come with confidence intervals, standard errors, or ranges of accepted results to indicate the variability or uncertainty associated with them (IAEA, 1998). In summary, the certified value possesses the highest credibility, whereas the information value is comparatively less reliable.

6. RESULT AND DISCUSSION

6.1 Assessment of Age-Depth Relationships

This study aims to comprehensively investigate the spatial and temporal patterns of ^{241}Am accumulation and distribution within the bottom sediments of the southern Baltic Sea. To achieve this aim, it is imperative to perform sediment dating to establish chronological records of sediment deposition and understand the temporal dynamics of ^{241}Am accumulation within the southern Baltic Sea's bottom sediments. This dating process will provide a critical context for interpreting the spatial and temporal patterns of ^{241}Am distribution in the study area. All sediment samples collected in 2019 were used in sediment geochronology.

6.1.1 Sediment Accumulation Rates

The essential parameters, including total ^{210}Pb, supported ^{210}Pb, excess ^{210}Pb, and porosity, were presented in Table 14. These parameters are crucial for sediment dating, as they provide insights into the sediment's history, the chronological records of deposition, and environmental changes in the studied area.

Table 20. Activities of ^{210}Pb total, supported, excess, and porosity concerning the depth of the sediment cores 78M, BY15, and P1 (extended uncertainty at k=2); NA – not available

Layer [cm]	**Porosity**	**Total ^{210}Pb**	**^{210}Pb$_{supported}$**	**^{210}Pb$_{excess}$**
		Bq·kg^{-1} (extended uncertainty at k=2)		
78M – Bornholm Basin				
0–1	0.97	287±23	NA	NA
1–2	0.92	201±12	47.3±3.1	154±12
2–3	0.92	150±12	44.0±3.3	106±12
3–4	0.90	146±10	48.8±2.9	97.6±10.2
4–5	0.94	107±7	50.6±2.8	56.2±8.0
5–6	0.89	102±7	60.3±3.3	41.7±7.7
6–7	0.89	91.9±7.8	52.5±3.0	39.4±8.4
7–8	0.90	104±7	55.8±3.1	48.3±7.8
8–9	0.97	95.8±8.5	54.9±3.1	40.8±9.1
9–10	0.94	103±6	58.8±3.1	44.2±6.9
10–12	0.90	92.7±6.2	57.4±3.1	35.3±7.0

Table 21. continued

12–14	0.84	101±7	64.3±3.5	37.0±7.7
14–16	0.87	90.1±5.6	60.2±3.2	29.9±6.5
16–18	0.91	79.5±5.3	66.2±3.6	13.3±6.4
18–20	0.88	80.8±4.8	58.3±3.0	22.6±5.6
20–22	0.96	76.6±5.1	60.6±3.2	16.0±6.0
22–24	0.88	78.3±5.2	60.7±3.3	17.6±6.1
24–26	0.90	71.5±4.4	30.2±1.6	41.3±4.6
26–28	0.91	59.0±4.1	61.9±3.2	>0
28–30	0.88	71.9±4.8	60.4±3.2	11.5±5.7
BY15 – Gotland Basin				
0–1	0.97	552±31	70.9±4.5	481±31
1–2	0.97	325±20	70.5±4.5	255±19
2–3	0.95	205±14	74.2±4.3	130±13
3–4	0.94	158±11	84.1±4.6	73.6±9.9
4–5	0.94	141±9	74.0±4.0	66.5±8.2
5–6	0.93	102±6	72.3±3.9	29.3±4.8
6–7	0.94	125±8	87.3±4.7	37.7±6.4
7–8	0.91	137±8	102.4±5.4	34.2±6.4
8–9	0.93	119±7	93.2±4.9	25.6±5.5
9–10	0.90	127±8	50.1±2.7	76.9±7.4
10–12	0.90	117±8	103±5	13.4±5.6
12–14	0.90	121±7	108±6	12.7±4.4
14–16	0.91	110±7	105±5	5.31±3.91
16–18	0.89	108±7	106±6	1.97±3.91
18–20	0.90	109±7	107±6	1.82±3.35
20–22	0.89	115±7	51.3±2.7	64.1±6.2
22–24	0.92	115±7	98.4±5.1	16.6±4.9
24–26	0.93	109±7	99.1±5.2	9.76±4.00
26–28	0.91	111±7	103±5	8.42±4.16
28–30	0.91	111±7	52.9±2.8	58.0±6.0
P1 – Gdańsk Basin				
0–1	0.99	616±50	18.6±7.8	597±51
1–2	0.97	510±26	NA	NA
2–3	0.99	653±38	7.46±1.23	645±38
3–4	0.96	751±50	13.7±2.8	738±50
4–5	0.96	535±32	24.7±3.3	510±32
5–6	0.96	701±44	9.91±1.75	691±44
6–7	0.93	340±27	10.4±1.4	390±27
7–8	0.92	271±19	26.3±3.0	245±20
8–9	0.98	278±15	23.2±2.3	254±16

Table 22. continued

9–10	0.96	257±18	22.2±2.6	235±18
10–12	0.86	161±10	25.4±2.1	135±10
12–14	0.93	158±11	12.0±1.4	146±11
14–16	0.88	164±9	24.8±2.0	139±10
16–18	0.89	219±14	26.4±2.6	192±15
18–20	0.92	137±10	24.1±2.1	113±10
20–22	0.96	145±9	27.1±2.2	118±9
22–24	0.90	181±10	27.2±2.2	154±11
24–26	0.96	121±8	12.6±1.2	108±8
26–28	0.94	110±7	29.2±2.34	80.4±7.5
28–30	0.94	88.7±5.9	29.9±2.38	58.8±6.3

The data shows that the sediment layers from the Bornholm Basin varied in porosity, ranging from 0.84 to 0.97. The porosity of the sediment from the Gotland Basin remains relatively constant throughout the core, with an average of 0.93. The average porosity in the sediment from the Gdańsk Basin is 0.94. Sediment accumulation rates are determined from profiles of excess versus porosity-corrected sediment depth.

Bulk density is the mass of dry soil per unit volume, typically expressed as $g \cdot cm^{-3}$. The proportion of mineral versus organic particles, to a large extent, determines bulk density. Organic soils have much lower bulk density compared to mineral soils. Bulk density of sediment typically increases with depth (Dadey et al. 1992, Munsiri et al. 1995). The dry bulk density for analyzed sediments is shown in Figure 28.

Activity concentrations of ^{210}Pb strongly differed in the subregions. In order to determine the age and intensity of sediment accumulation, it is necessary to separate the allochthonous part of ^{210}Pb. The excess ^{210}Pb activity concentrations were defined as a difference between the total ^{210}Pb activity concentrations and the average of ^{214}Pb and ^{214}Bi activity concentrations. Estimating the accumulation rate in this study was mathematically forced, considering the exponential decrease of $^{210}Pb_{ex}$ activity observed in the profiles.

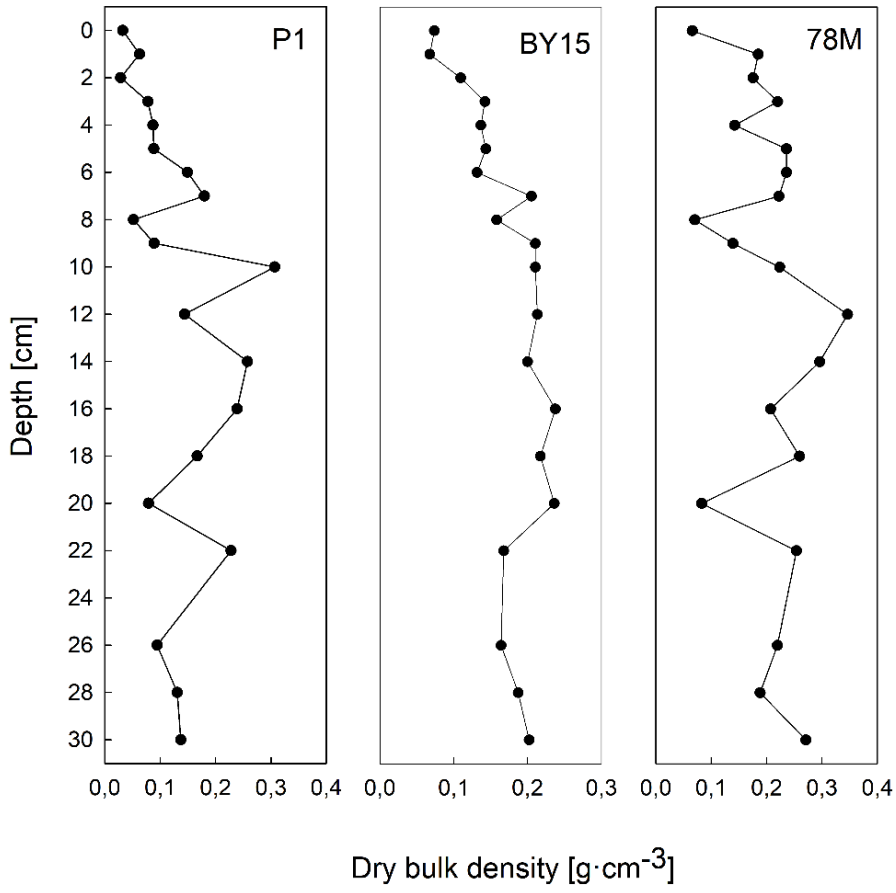

Figure 28. Depth profiles for dry bulk density

In the upper layer, 0–1 cm of the sediments, activity concentrations of total ^{210}Pb decreased from about 287±23.3 Bq·kg^{-1} to about 59.0±4.1 Bq·kg^{-1} (layer 26–28) in the Basin of Bornholm. Excess ^{210}Pb activity concentrations decreased from 481±31 to 1.82±3.35.Bq·kg^{-1}. The maximum activity concentrations of ^{210}Pb were not found in the surface sediment layer but in layers 3–4 in the Gdańsk Basin (751±50 Bq·kg^{-1}) and decreased rapidly to 88.7±5.9 Bq·kg^{-1} at 30 cm depth of the sediment. Excess ^{210}Pb activity concentrations varied from 738±50 to 58.8±6.3 Bq·kg^{-1}. In the Gotland Basin, activity concentrations of ^{210}Pb varied from 109±7 Bq·kg^{-1} in the 24–26 sediment layer to 552±31 Bq·kg^{-1} in the surface layer, while excess ^{210}Pb activity concentrations varied from 738±50 to 58.8±6.3 Bq·kg^{-1}.

Individual sediment layers were assigned ages based on the CF:CS model, with the dating range limited to the depth corresponding to the isotope measurements at levels guaranteeing measurement with a certain accuracy. Using the results obtained by applying the CF:CS model, the date and age of the subsample were calculated based on

the depth of the sediment core (Table 15). The date is derived by subtracting the age of the corresponding layer from the date of sampling (2019). The age uncertainties calculated from the ^{210}Pb-derived sediment accumulation rates are challenging to estimate. Qualitatively, any age estimated from these rates carries an uncertainty. The data were analyzed using the *serac* package (Bruel and Sabatier, 2020) using R version 4.1.3.

Table 23 Sediment accumulation rates and mass accumulation rates calculated from radiolead-dated cores from the Baltic Sea, CS:CF model (extended uncertainty at k=2)

	SAR [mm·year^{-1}]	**R^2**	**MAR [g·m^{-2}·year^{-1}]**	**R^2**
BY15	1.153±0.102	0.908	210±20	0.882
78M	1.071±0.114	0.957	830±110	0.814
	4.34±0.33	0.961		
P1	3.592±0.541	0.759	650±120	0.688

In the Baltic Sea regions, sediment accumulation rates are variable. Using a CF:CS model, sediment accumulation rates (SAR) were calculated assuming an exponential decrease in $^{210}Pb_{ex}$ with sediment depth (Robbins and Edgington, 1975). The best-fit least-squares method was used. The determined rates represent the maximum rates. The sediment accumulation rate was 1.153±0.102 mm·year^{-1} (R^2= 0.908) for the Gotland Basin, 3.592±0.541 mm·year^{-1} (R^2= 0.759) for the Gdańsk Basin (Fig. 29, 30). Two different sedimentation rates were found by the CF:CS model in each sediments profile sampled at the Bornholm Basin (78M) (Fig. 31), whose mean values are 1.071±0.114 mm·year^{-1} (R^2= 0.957) and 4.34±0.33 mm·year^{-1} (R^2= 0.961). These differences indicate that the sedimentation processes are distinct in each location, and various factors might influence sediment accumulation rates. The quantity of suspended matter in the water column and the extent of riverine water reaching the sea are key factors that directly impact the sedimentation process's intensity. Riverine water introduces significant amounts of organic and mineral materials into the sea. Simultaneously, the carried nutrients enhance primary production, leading to substantial phytoplankton blooms when weather conditions are favorable. When considering the influence of river discharge on suspended materials in seawater, we anticipate a more pronounced effect from the Vistula River in the Gdańsk Basin region compared to the

influence of the Oder River in the Bornholm Basin area. This contrast arises due to the moderating effects of the Szczecin Lagoon, which filters terrestrial materials and pollutants.

Consequently, the higher sedimentation rate observed in the Bornholm Basin can be attributed to distinct properties of the settling organic matter or specific hydrological conditions. Higher rates in the Gdańsk and Bornholm Basin might mean increased sediment supply from nearby land areas, potentially affected by factors like increased erosion or changes in land use. Conversely, the lower rates in the Gotland Basin could be linked to factors like lower sediment input or higher rates of sediment resuspension and transport by currents.

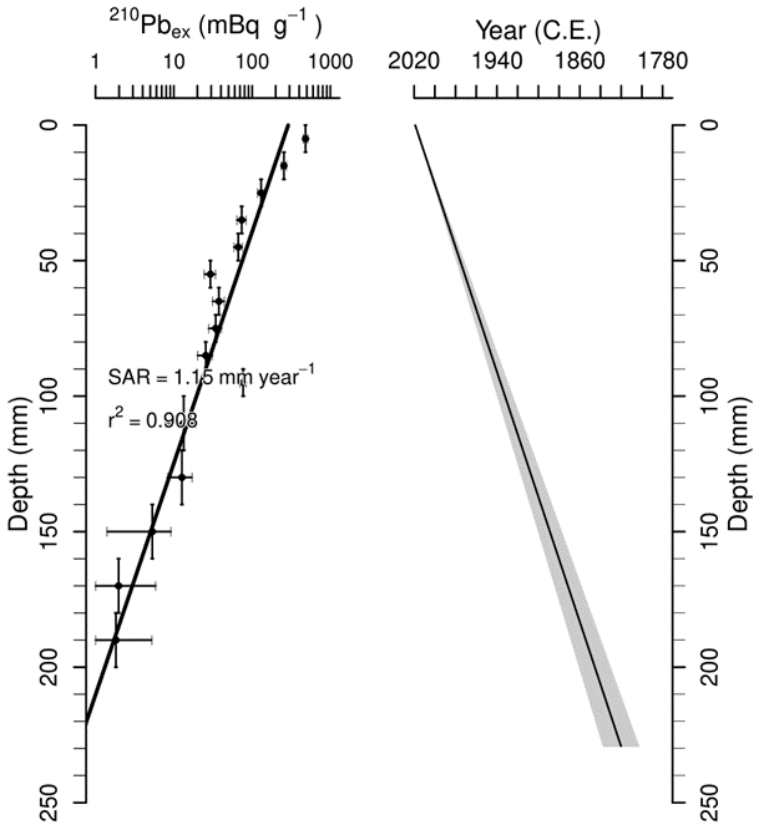

Figure 29. Age-depth model for Gotland Basin sediment core. From left to right: $^{210}Pb_{ex}$ and the CF:CS age model

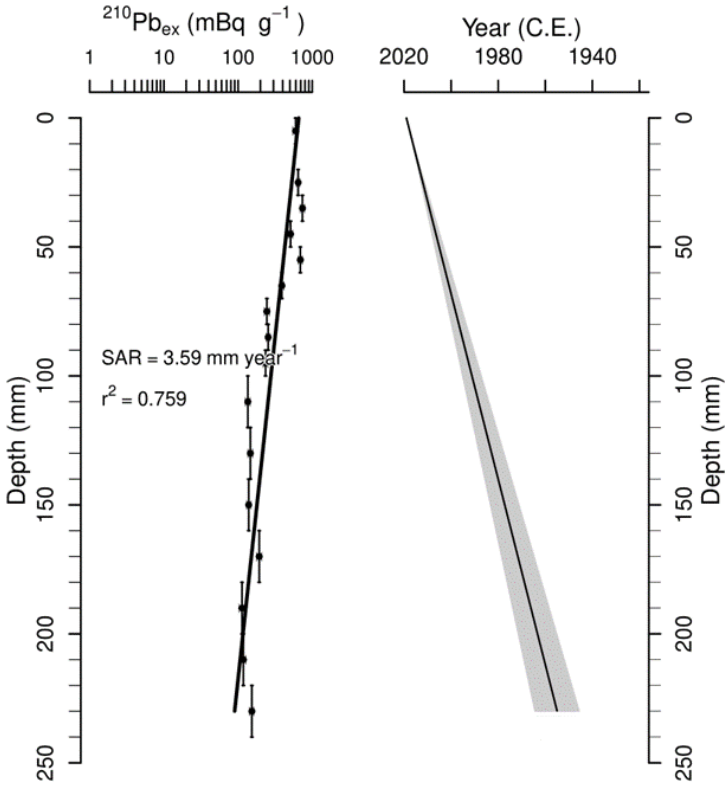

Figure 30. Age-depth model for Gdańsk Basin sediment core. From left to right: $^{210}Pb_{ex}$ and the CF:CS age model

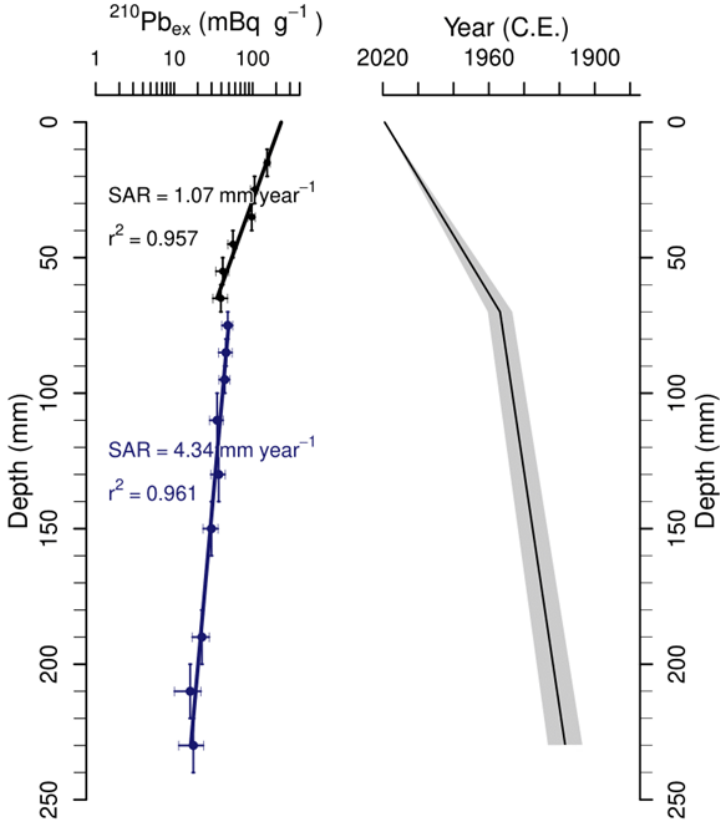

Figure 31. Age-depth model for Bornholm Basin sediment core. From left to right: $^{210}Pb_{ex}$ and the CF:CS age model

In two sediment cores (stations P1 and 78M), the disturbance of surface sediments, suggesting a variable sediment accumulation rate, was noticed; thus, a CRS model was applied to determine sediment layer age. The SAR and MAR values from the CRS model and calculated sediment age are shown in Table 16. The comparison of CF:CS and CRS age models is shown in Fig 32.

Comparing results from different sediment dating models can provide valuable validation and insight into sedimentation processes and dating accuracy. The consistency between the two models suggests that sedimentation processes may have been relatively stable over the period studied. However, discrepancies between the ages derived from the CRS and CSCF may indicate periods of sedimentary disturbance, changes in depositional environments, or changes in sediment supply.

Table 24. The age model (CFCS, CRS), sediment accumulation rates, and mass accumulation rates (CRS model) calculated from radiolead-dated cores from the Baltic Sea (extended uncertainty at k=2)

Layer [cm]	**CF:CS**	**CRS**		
	Year	**SAR [cm·year^{-1}]**	**MAR [g·cm^{-2}·year^{-1}]**	**Year**
78M – Bornholm Basin				
0	2019±0	0.18±0.02	0.01±0.01	2019±0
1	2010±1	0.28±0.04	0.05±0.03	2017±1
2	2000±2	0.25±0.04	0.05±0.03	2013±1
3	1991±3	0.48±0.09	0.10±0.04	2009±1
4	1982±4	0.45±0.10	0.06±0.03	2005±1
5	1972±5	0.41±0.10	0.10±0.06	2003±1
6	1963±6	0.35±0.09	0.08±0.05	2000±1
7	1954±7	0.83±0.20	0.18±0.05	1998±2
8	1951±7	0.62±0.14	0.04±0.02	1995±2
9	1949±7	0.41±0.09	0.06±0.03	1994±2
10	1947±7	0.30±0.07	0.07±0.05	1991±2
12	1942±8	0.18±0.05	0.06±0.09	1986±3
14	1938±8	0.19±0.05	0.06±0.09	1973±3
16	1933±9	0.15±0.05	0.03±0.07	1959±4
18	1928±9	0.22±0.10	0.06±0.12	1947±6
20	1924±9	0.14±0.07	0.01±0.04	1924±9
22	1919±10	0.44±0.07	0.11±0.04	1915±11
24	1914±10	0.44±0.07	0.10±0.04	1914±10

Table 25. continued

BY15 – Gotland Basin				
0–1	2019±0	0.00±0.00	0.00±0.00	2019±0
1–2	2010±1	0.18±0.03	0.012±0.002	2010±1
2–3	2002±2	0.19±0.03	0.021±0.003	2004±1
3–4	1993±2	0.22±0.04	0.031±0.006	1998±2
4–5	1984±3	0.21±0.04	0.028±0.005	1993±2
5–6	1976±4	0.40±0.09	0.057±0.012	1988±2
6–7	1967±5	0.31±0.07	0.041±0.009	1985±3
7–8	1958±5	0.19±0.05	0.039±0.010	1982±3
8–9	1950±6	0.28±0.08	0.044±0.012	1976±4
9–10	1941±7	0.06±0.01	0.013±0.003	1972±4
10–12	1932±8	0.18±0.09	0.038±0.020	1950±8
12–14	1915±9	0.13±0.07	0.027±0.014	1937±11
14–16	1898±11	0.16±0.16	0.032±0.032	1915±20
16–18	1880±12	0.22±0.48	0.052±0.115	1899±30
18–20	1863±14	0.19±0.40	0.041±0.088	1889±34
20–22	1845±15	0.12±0.28	0.029±0.067	1876±42
22–24	1828±17	0.06±0.16	0.010±0.028	1853±60
P1 – Gdańsk Basin				
0–1	2019±0	0.00±0.00	0.00±0.00	2019±0
1–2	2016±1	0.65±0.08	0.04±0.004	2018±0
2–3	2013±1	1.19±0.14	0.03±0.001	2017±0
3–4	2009±1	0.38±0.05	0.03±0.006	2016±0
4–5	2006±2	0.45±0.05	0.04±0.008	2013±0
5–6	2003±2	0.31±0.04	0.03±0.008	2011±1
6–7	2000±3	0.29±0.04	0.04±0.022	2007±1
7–8	1997±3	0.35±0.05	0.06±0.032	2004±1
8–9	1993±3	1.10±0.14	0.06±0.003	2001±1
9–10	1990±4	0.65±0.08	0.06±0.008	2000±1
10–12	1987±4	0.31±0.04	0.09±0.094	1998±1
12–14	1981±5	0.51±0.07	0.07±0.021	1991±1
14–16	1974±6	0.25±0.03	0.06±0.066	1987±1
16–18	1968±7	0.15±0.02	0.04±0.057	1978±2
18–20	1961±8	0.21±0.03	0.03±0.028	1960±2
20–22	1955±8	0.29±0.04	0.02±0.006	1949±2
22–24	1949±9	0.06±0.01	0.01±0.052	1941±3

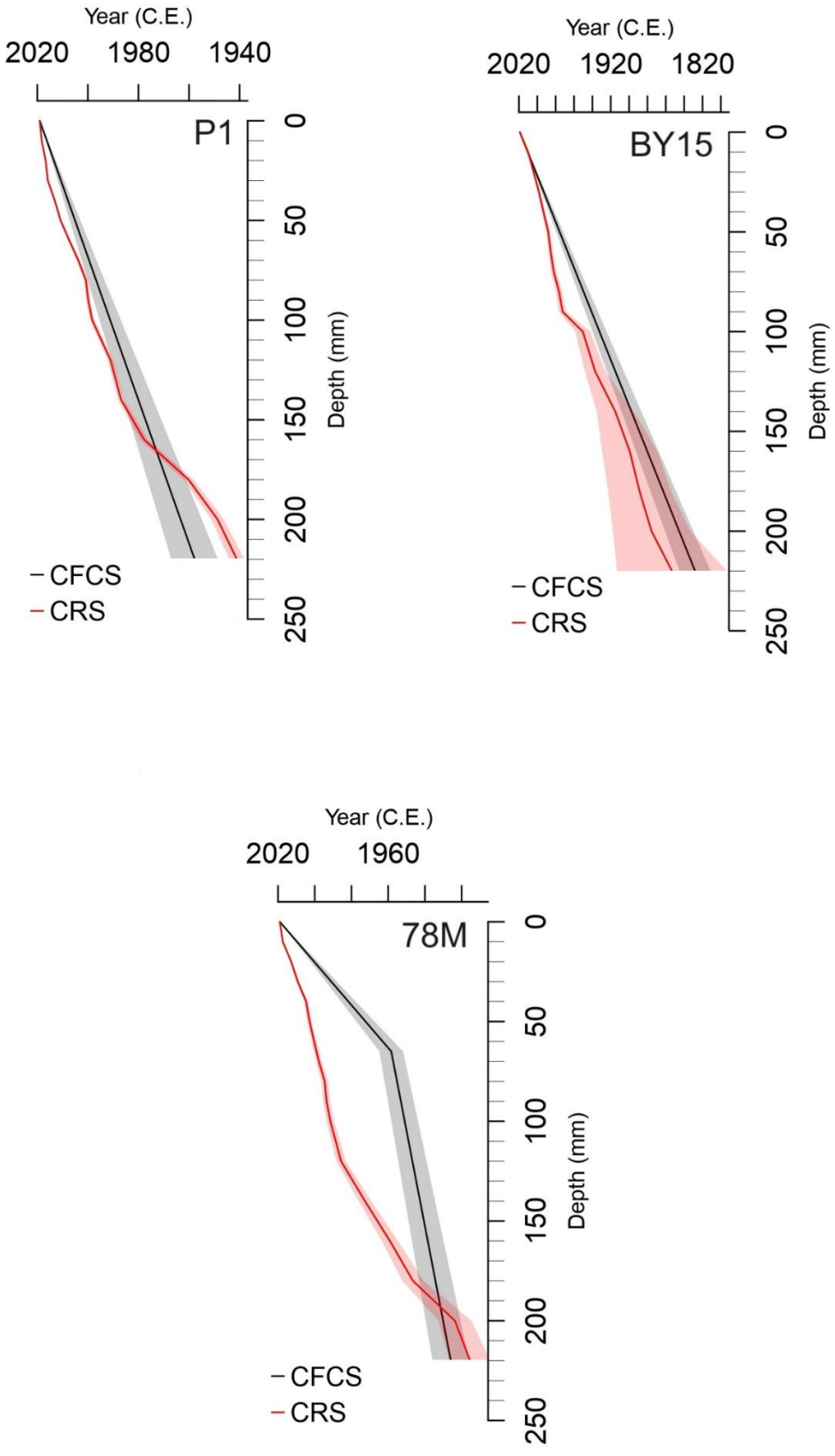

Figure 32. Comparison of CF:CS and CRS age models in analyzed sediments

The main distinction between the two models is that CF:CS assumes a constant atmospheric flux of ^{210}Pb to the sediment surface and constant sediment accumulation rate, whereas CRS assumes a constant atmospheric flux of ^{210}Pb and variable accumulation rate of sediments. The choice between CRS and CSCF models depends on the specific characteristics of the sediment environment.

6.1.2 Distribution of ^{137}Cs

To validate the accuracy of age determination using the ^{210}Pb method, an additional tracer is required, one with traceable concentration shifts linked to specific marine events. In the context of the Baltic Sea, the most suitable candidate is the entirely anthropogenic isotope ^{137}Cs. The HELCOM network has monitored radionuclides in the Baltic Sea seawater and sediments for over 25 years. The Institute of Meteorology and Water Management has monitored ^{137}Cs distribution in the Baltic seawater off the Polish coast since 1985 (Zalewska and Lipska, 2006; Zalewska and Saniewski, 2011). Over time, there has been a decrease in ^{137}Cs activity concentration from approximately 100 Bq m^3 during 1993-1998 to about 50 Bq m^3 in 2014. Recent studies have suggested that the activity concentration of radiocaesium in seawater is influenced by wind-induced transport from the heavily contaminated northern Baltic Sea (Zalewska and Lipska, 2006). Utilizing ^{137}Cs to verify age determination involves assuming that discernible historical incidents (such as nuclear weapons testing post-1945, with peak deposition in 1963, and the Chernobyl power plant disaster in 1986) should be distinctly recognizable as peaks within the isotope's variation curve across the sediment core.

Nevertheless, interpreting the results necessitates a cautious approach, given the intricate interplay of numerous processes that influence the ultimate representation of ^{137}Cs distribution within the sediment's vertical profile. This isotope can be a valuable tool for cross-referencing sediment chronology, particularly when post-depositional factors do not significantly impact this particular radionuclide (Díaz-Asencio et al., 2009). The results for ^{137}Cs in southern Baltic Sea bottom sediments are illustrated in Table 17.

Table 26. Activity concentration of ^{137}Cs in southern Baltic Sea bottom sediments (extended uncertainty at k=2)

Layer [cm]	^{137}Cs activity concentration [Bq·kg^{-1}]
78M – Bornholm Basin	
0–1	41.8±3.3
1–2	49.5±2.9
2–3	42.1±2.7
3–4	43.0±2.5
4–5	25.4±1.5
5–6	21.8±1.3
6–7	21.2±1.4
7–8	19.7±1.2
8–9	17.4±1.2
9–10	14.2±0.8
10–12	10.9±0.7
12–14	7.93±0.64
14–16	4.54±0.39
16–18	1.83±0.31
18–20	0.00±0.00
20–22	0.00±0.00
22–24	0.00±0.00
24–26	0.00±0.00
26–28	0.00±0.00
28–30	0.00±0.00
BY15 – Gotland Basin	
0–1	126±7
1–2	61.7±3.6
2–3	31.2±1.9
3–4	20.0±1.3
4–5	14.1±0.9
5–6	9.25±0.7
6–7	6.89±0.6
7–8	5.27±0.5
8–9	1.33±0.3
9–10	2.23±0.5
10–12	0.02±0.5
12–14	0.00±0.00
14–16	0.00±0.00
16–18	0.00±0.00
18–20	0.00±0.00

Table 27. continued

20–22	0.00±0.00
22–24	0.00±0.00
24–26	0.00±0.00
26–28	0.00±0.00
28–30	0.00±0.00
P1 – Gdańsk Basin	
0–1	103±8
1–2	149±8
2–3	129±7
3–4	167±11
4–5	149±8
5–6	176±10
6–7	169±9
7–8	149±8
8–9	138±7
9–10	118±7
10–12	61.8±3.3
12–14	51.8±3.1
14–16	45.5±2.4
16–18	42.9±2.6
18–20	35.2±2.0
20–22	35.6±2.0
22–24	37.8±2.1
24–26	23.0±1.4
26–28	15.1±0.9
28–30	10.0±0.7

The highest values of ^{137}Cs were observed in the Gdańsk Basin, where activity concentration exceeded 176±10.2 Bq·kg^{-1} in the 5–6 layer. The distinctly lower activities of ^{137}Cs measured in surface sediments from the Bornholm Basin (49.5±2.90 Bq·kg^{-1} in 1–2 cm layer) may indicate the influence of frequent flushes of the North Sea (Zalewska and Lipska, 2006) saline inflows in the near bottom layer, the water in the North Sea having a much lower content of ^{137}Cs. The ^{137}Cs concentration in the Gotland Basin surface sediments reached 126±6.82 Bq·kg^{-1}.

When plotting the ^{137}Cs activity concentration profile against the year of sediment deposition, the ^{137}Cs concentration peak appears after the 1980s and is

observed at stations BY15 (Gotland Basin) and 78M (Bornholm Basin). A clear peak in ^{137}Cs concentration at station P1 (Gdansk Deep), observed around 2010, occurred later than expected. Similarly, the maximum concentration of ^{137}Cs measured in surface sediments at stations BY15 and 78M can be attributed to post-deposition processes or very low sediment accumulation rates. These post-deposition sedimentation processes include physical and biological sediment mixing, sediment erosion, and redeposition. In addition, the continuous flushing of the heavily polluted Baltic Sea catchment by rivers and groundwater discharges may contribute to this phenomenon.

Moreover, ^{137}Cs can migrate in sediments through pore waters, leading to activity concentration peaks that do not necessarily correspond to dates of peak radionuclide deposition. Previous studies have found the highest concentrations of ^{137}Cs in recently deposited Baltic Sea surface sediments. The ^{137}Cs activity concentration increase to 220 Bq·kg^{-1} in Gdańsk Basin and 70 Bq·kg^{-1} in Bornholm Basin is observed in recent sediments (Zalewska et al., 2015). The graphs depicting variations in ^{137}Cs activity across different sediment layers and their corresponding years do not exhibit clear and distinct peaks (Figure 33). This lack of clarity can be attributed to the repositioning of radiocesium within the sediment column. This redistribution could stem from physical and biological blending near or at the sediment-water boundary and chemical diffusion or movement within the porewater. Potential inaccuracies in identifying the first ^{137}Cs atmospheric fallout become apparent when considering non-ideal deposition scenarios involving either diffusion (Delaval et al., 2020) or mixing (Sabatier et al., 2010). Additionally, challenges arise in pinpointing ^{137}Cs peaks when translocation or incomplete mixing processes come into play (Abril, 2004; Sabatier et al., 2010)

Furthermore, Wang et al. (2022) suggested that the migration of ^{137}Cs following its deposition in the marine environment, except for coastal regions influenced by river systems, renders it an inappropriate choice for validating ^{210}Pbex-based chronologies. Cesium is highly soluble in marine environments, making it challenging to use ^{137}Cs for effectively dating marine sediments (Koarashi et al., 2012). ^{137}Cs dating (using the time marker 1952) is problematic in most marine environments due to its post-depositional diffusion and high solubility. The shape of the ^{137}Cs activity curve can also be affected by changes in the capacity of the sorption complex and, thus, the ability to capture the

element – the ability of the sorption complex to capture ^{137}Cs from the environment and retain it in the sediment. For the radionuclides under analysis, the most important are fine particles of clay minerals and humic material (Milan et al. 1995).

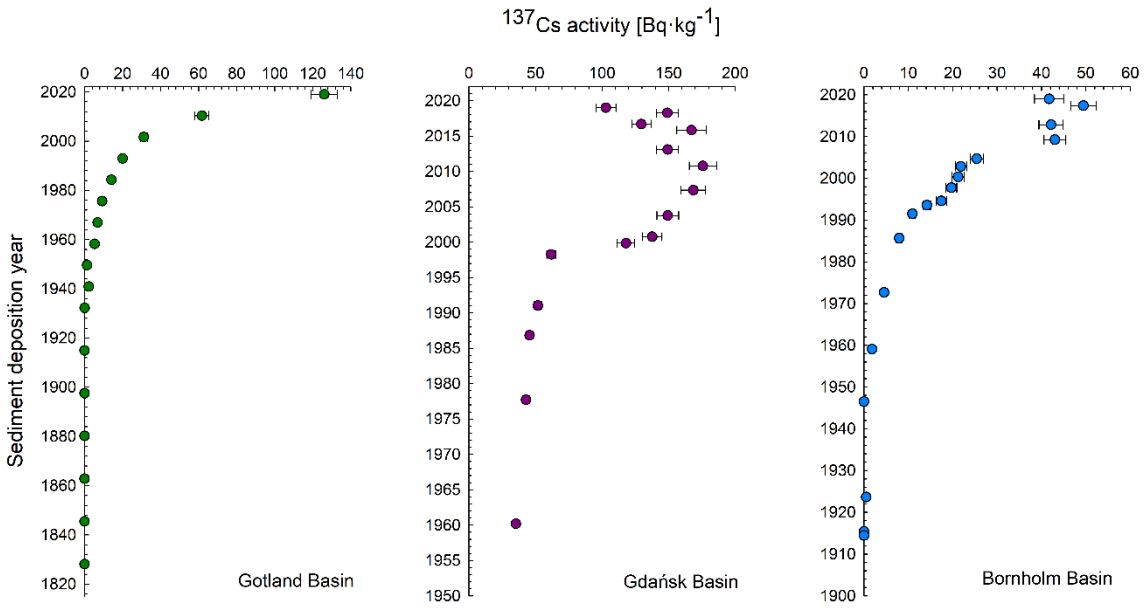

Figure 33. Deposition histories of ^{137}Cs in sediments from the southern Baltic Sea

The concentrations of ^{137}Cs in sediments differ depending on the sampling site and sampling depth. In most sediment cores investigated, a subsurface maximum of ^{137}Cs is evident. The expected peak value of ^{137}Cs in the Chernobyl accident fallout sediments has been smeared out, indicating a continuous influx of ^{137}Cs with Baltic seawater. Numerous studies on marine and lake sediment within the Baltic Sea and its surrounding areas have corroborated the association of this ^{137}Cs maximum (or a sharp surge in ^{137}Cs levels) with Chernobyl fallout (Jokinen et al., 2015; Moros et al., 2016; Reinikainen et al., 1997). The marked change in the curve slope of the Gdańsk Basin occurred after 1990 and is probably a direct influence of ^{137}Cs input from the accidental release in the Chernobyl power plant 1986. Though less spectacular, a change in the curve development was also detected in the Bornholm and Gotland Basin. After 2010, ^{137}Cs activity in sediments in the Bornholm Basin became stable, as indicated by an insignificant increase from 25.4±1.50 to 49.5±2.90 Bq·kg^{-1} observed in 6 years. Concentrations of ^{137}Cs in bottom sediments from all sampling areas decrease exponentially with depth. In the Gdańsk Basin, the influence of global fallout contamination was still observed in the deeper layers of the core. The area of the

Gdańsk Basin remains under the most severe anthropogenic pressure among the studied sedimentation areas. The presented trends in ^{137}Cs concentrations in sediment cores are not acceptable to verify fidelity of the ^{210}Pb dating. Differences in the deposition of ^{137}Cs between successive years, as observed at specific sampling locations, highlight the potential for significant variations in radionuclide concentrations, even within relatively small areas. Sedimentary material discharged by the Vistula is transported to deeper areas, indicating that the Gdansk Basin is a sink for fluvial matter. Understanding the role of the Gdansk Basin as a sink for fluvial sediment is crucial for assessing sedimentary processes, sediment budgets, and ecosystem dynamics in the Baltic Sea region.

6.2 ^{241}Am Activity Concentrations in Sediments

6.2.1 Sediments Cores Collected in 2010

The activity concentrations were determined based on the analysis of alpha-ray spectra. The bottom sediments collected in April 2010 from the Gotland and the Gdańsk Basins were analyzed for ^{241}Am, and the results are shown in Fig. 25 and 26 and detailed in Table 18. All results are given in Bq·kg^{-1} dry wt.

The highest ^{241}Am concentration levels were obtained in both deeps at the same sediment depths (0–1 cm). The ^{241}Am concentrations at the Gotland Basin ranged from 0.024±0.004 to 2.57±0.19 Bq·kg^{-1}. A significant spike in the presence of ^{241}Am at a depth of 7–8 cm was observed, measuring at 0.765±0.057 Bq·kg^{-1}.

The activity concentration of ^{241}Am in the samples from the Gdańsk Basin varied across the samples, ranging from 0.009±0.003 to 0.94±0.07 Bq·kg^{-1}. A significantly high activity concentration of ^{241}Am was found in a 2–3 cm layer. Due to the absence of layers 3–9, a notable rise in ^{241}Am activity within the 8–9 cm layer was anticipated, attributed to the influence of the Chernobyl accident. Furthermore, the higher layers exhibited a delayed inflow effect of ^{241}Am in the Gdańsk Basin region. However, the 10–11 and 12–13 layers showed comparatively lower contamination levels from ^{241}Am (Fig. 35).

Table 28. Activity concentrations of ^{241}Am in sediments from 2010 (extended uncertainty at k=2)

Sample ID	Layer [cm]	^{241}Am activity [Bq·kg^{-1}]
Got – Gotland Basin		
Got-1	0─1	2.568±0.189
Got-2	1─2	0.424±0.033
Got-3	2─3	0.092±0.022
Got-4	3─4	0.050±0.005
Got-5	4─5	0.028±0.004
Got-6	5─6	0.036±0.004
Got-7	6─7	0.074±0.006
Got-8	7─8	0.765±0.057
Got-9	8─9	0.024±0.004
Got-10	9─10	0.045±0.006
Got-12	10─12	0.077±0.007
Got-14	12─14	0.037±0.005
Got-16	14─16	0.061±0.005
Got-18	16─18	0.055±0.006
Got-20	18─20	0.057±0.005
Got-22	20─22	0.033±0.008
Got-24	22─24	0.043±0.005
Got-29	24─29	0.065±0.008
GG – Gdańsk Basin		
GG-1	0–1	0.938±0.070
GG-2	1–2	0.557±0.042
GG-3	2–3	0.790±0.062
GG-11	10–11	0.009±0.003
GG-13	12–13	0.029±0.004
GG-19	17–19	0.041±0.004
GG-20	19–20	0.089±0.007
GG-29	27–29	0.013±0.003
GG-31	29–31	0.020±0.003

The activity concentration of ^{241}Am in the samples from the Gdańsk Basin varied across the samples, ranging from 0.009±0.003 to 0.94±0.07 Bq·kg^{-1}. A significantly

high activity concentration of ^{241}Am was found in a 2–3 cm layer. Due to the absence of layers spanning from 1980 to 2000, a notable rise in ^{241}Am activity within the 8–9 cm layer was anticipated, attributed to the influence of the Chernobyl accident. Furthermore, the higher layers exhibited a delayed inflow effect of ^{241}Am in the Gdańsk Basin region. However, the 10–11 and 12–13 layers showed comparatively lower contamination levels from ^{241}Am (Fig. 35). The results obtained agree with the plutonium results measured in sediments collected in 1999. Corresponding 10–11 and 12–13 cm layers described in this study contained low ^{241}Pu activity concentration (1.5–4.7 Bq·kg^{-1} dm) and the values of ^{238}Pu/$^{239+240}$Pu activity ratio between 0.05 and 0.3, which is substantially below 0.56 (the value typical for the Chernobyl accident) (Strumińska-Parulska et al., 2012; Strumińska-Parulska, 2014). The results agreed with the plutonium results measured in sediments collected in 1999. Corresponding 10–11 and 12–13 cm layers described in this study contained low ^{241}Pu activity concentration (1.5–4.7 Bq·kg^{-1} dm) and the values of ^{238}Pu/$^{239+240}$Pu activity ratio between 0.05 and 0.3, which is substantially below 0.56 (the value typical for the Chernobyl accident) (Strumińska-Parulska et al., 2012; Strumińska-Parulska, 2014).

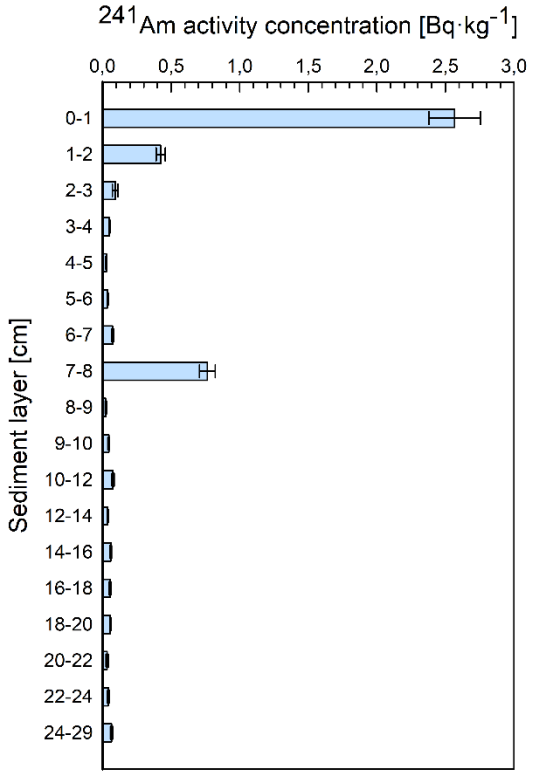

Figure 34. The activity concentrations of ^{241}Am in sediment collected in 2010 from the Gotland Basin

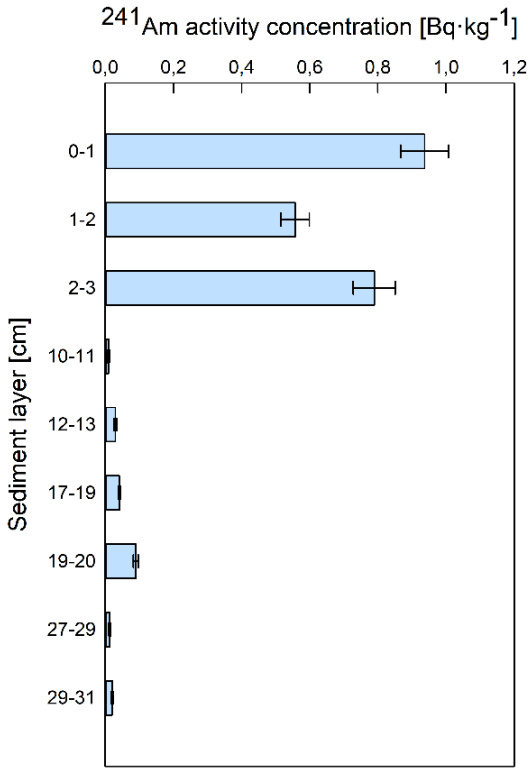

Figure 35. The activity concentrations of ^{241}Am in sediment collected in 2010 from the Gdańsk Basin

A more detailed description of the changes in ^{241}Am activity concentration in the Gotland Basin core over time can be found in the Historical View on ^{241}Am Activity Concentration Changes section.

6.2.2 Sediment Cores Collected in 2019

The bottom sediments collected in May 2019 from the Bornholm, the Gotland, and the Gdańsk Basins were analyzed for ^{241}Am, and the results are detailed in Table 19. The uneven contamination by anthropogenic radioactive isotopes in the southern Baltic is evident in its bottom sediments. The geographic distribution of isotopes is primarily shaped by the initial uneven contamination of Baltic seawater immediately following the Chernobyl accident. In addition, changes along vertical sediment profiles reflect historical events and the effects of radioactive decay (Suplińska, 2002; Suplińska and Pietrzak-Flis, 2008). Values are slightly higher in the Gdańsk and the Gotland Basins coastal regions, while the least contaminated sediments are found in the western part of the southern Baltic, in the Bornholm Basin. Results for ^{241}Am concentrations in the southern Baltic Sea sediments are presented below.

Table 29. Activities of ^{241}Am and the estimated age concerning the depth of the sediment cores 78M, BY15, and P1 (extended uncertainty at k=2)

Layer [cm]	^{241}Am activity concentration [Bq·kg^{-1}]	Year
78M – Bornholm Basin		
0–1	0.848±0.064	2019±0
1–2	0.387±0.029	2017±1
2–3	0.563±0.042	2013±1
3–4	0.368±0.027	2009±1
4–5	0.178±0.013	2005±1
5–6	0.281±0.022	2003±1
6–7	0.474±0.039	2000±1
7–8	0.277±0.020	1998±2
8–9	0.226±0.018	1995±2
9–10	0.424±0.031	1994±2
10–12	0.430±0.032	1991±2
12–14	0.372±0.028	1986±3
14–16	0.174±0.016	1973±3
16–18	0.110±0.009	1959±4
18–20	0.135±0.016	1947±6
20–22	0.055±0.005	1924±9
22–24	0.043±0.005	1915±11
24–26	0.045±0.006	1914±10
26–28	0.030±0.012	*1913±10*
28–30	0.039±0.003	*1912±10*
BY15 – Gotland Basin		
0–1	2.059±0.152	2019±0
1–2	2.249±0.165	2010±1
2–3	0.630±0.046	2002±2
3–4	0.064±0.005	1993±2
4–5	0.207±0.017	1984±3
5–6	1.950±0.144	1976±4
6–7	0.043±0.004	1967±5
7–8	0.022±0.002	1958±5
8–9	0.109±0.009	1950±6
9–10	0.053±0.005	1941±7
10–12	0.031±0.003	1932±8
12–14	0.017±0.001	1915±9
14–16	0.025±0.002	*1898±11*
16–18	0.028±0.002	*1880±12*
18–20	0.018±0.001	*1863±14*

Table 30. continued

20–22	0.020±0.008	*1845±15*
22–24	0.022±0.014	*1828±17*
24–26	0.017±0.006	*1824±17*
26–28	0.095±0.039	*1819±18*
28–30	0.025±0.009	*1815±18*
P1 – Gdańsk Basin		
0–1	2.176±0.149	2019±0
1–2	2.096±0.143	2018±0
2–3	0.585±0.039	2017±0
3–4	1.364±0.100	2016±0
4–5	0.683±0.041	2013±0
5–6	0.744±0.054	2011±1
6–7	0.760±0.055	2007±1
7–8	0.646±0.047	2004±1
8–9	1.234±0.090	2001±1
9–10	0.943±0.069	2000±1
10–12	0.742±0.054	1998±1
12–14	2.899±0.211	1991±1
14–16	0.953±0.071	1987±1
16–18	1.742±0.127	1978±2
18–20	3.185±0.232	1960±2
20–22	0.698±0.051	1949±2
22–24	0.666±0.048	1941±3
24–26	0.574±0.042	*1939±4*
26–28	0.454±0.033	*1938±5*
28–30	0.221±0.016	*1934±5*

6.2.2.1 Bornholm Basin Sediments

The ^{241}Am concentrations in the Bornholm Basin are shown in Figure 36. The results show heterogeneity in the distribution of americium ^{241}Am. Layer 1–2 cm shows the highest concentration of ^{241}Am, with a recorded value of 0.85±0.064 Bq·kg^{-1}. In contrast, the lowest concentration of ^{241}Am is observed in layers 26–28, where the concentration is 0.03±0.01 Bq·kg^{-1}. In the Bornholm Basin, ^{241}Am concentrations are almost constant from 20 cm onward. The Baltic Sea can be characterized as a partially enclosed body of water, and the process of water renewal, driven by interactions with

the North Sea, holds significant importance in the distribution of radionuclides. The Bornholm Basin, situated at its western reaches, experiences the influence of substantial inflows totaling around 100 km^3 (Szefer, 2002).

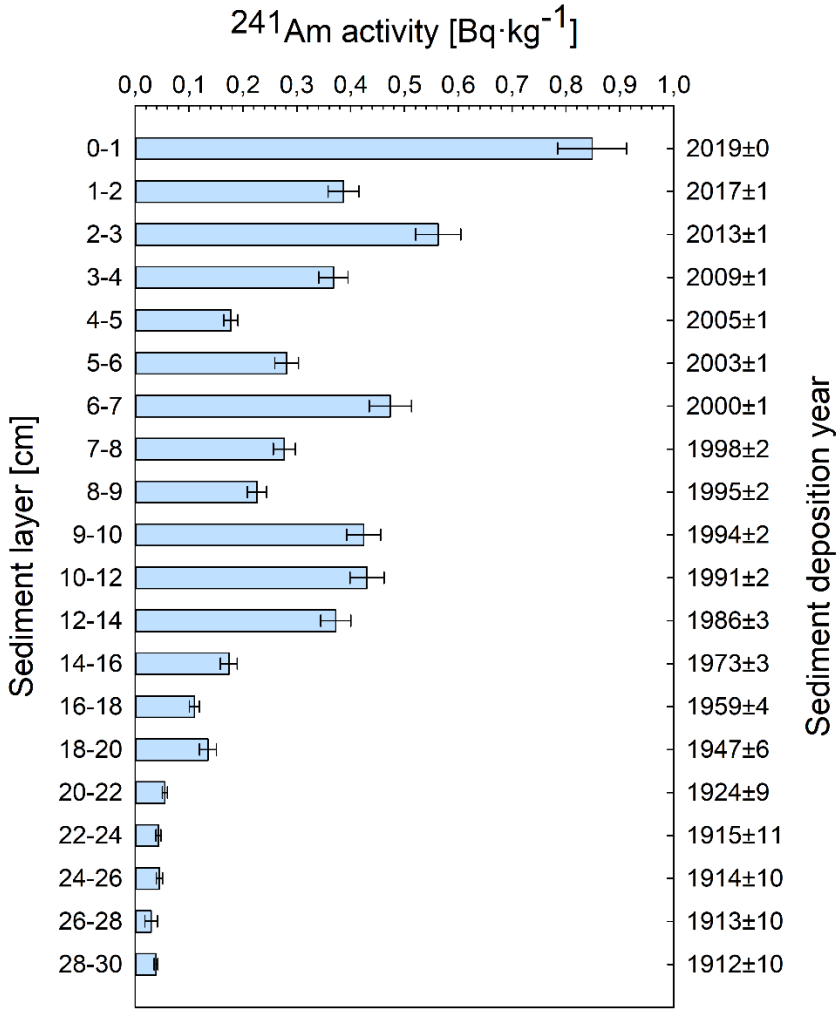

Figure 36. The activity concentrations of ^{241}Am in sediments collected in 2019 from Bornholm Basin

6.2.2.2 Gdańsk Basin Sediments

The ^{241}Am concentrations in the Gdańsk Basin are shown in Figure 37. The highest concentrations of ^{241}Am in Gdańsk Basin sediments were measured in layers 18─20 cm (3.16±0.23 $Bq \cdot kg^{-1}$), which is assumed to represent the global atmospheric fallout (1958─1970) when the United States and the Soviet Union conducted a large amount of nuclear weapons tests (Holm, 1995; Irlweck and Wicke, 1998). The 1990s

and 2000s show a mix of lower and moderate concentrations, suggesting potential changes in sources or environmental processes during this period. The highest activity concentrations were found in the Gdansk Deep (P1) area, where contaminated sediments flow in from other regions of the Baltic Sea, such as the Pomeranian Bay, as indicated by bottom currents from the direction of the Słupsk Bank (Piechura et al. 1997).

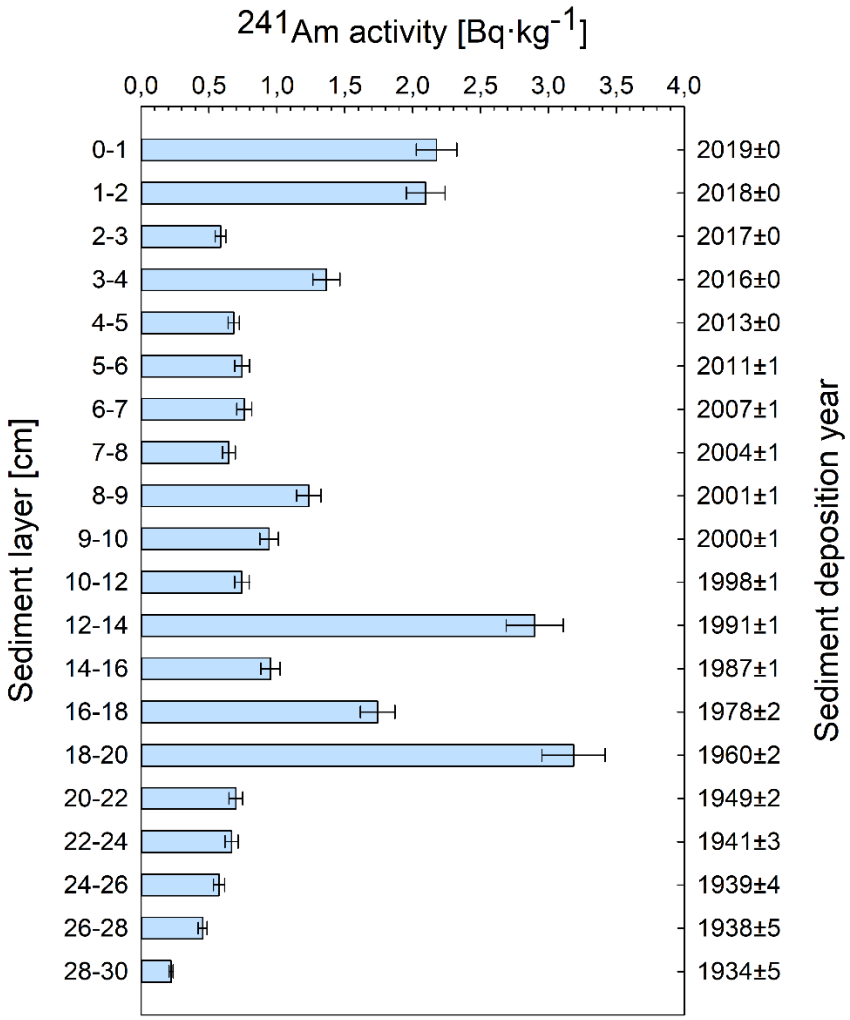

Figure 37. The activity concentrations of ^{241}Am in sediments collected in 2019 from the Gdańsk Basin

Rivers can serve as channels for transporting ^{241}Am from inland sources, such as industrial discharges or natural radioactive deposits in the catchment. The primary source of terrigenous material entering the Gulf of Gdańsk is the Vistula River, significantly influencing the region's sediment dynamics (Żbikowski et al., 2006). The Vistula River contributes a substantial flow rate of approximately 1027 $m^3 \cdot s^{-1}$ of water, making it a dominant hydrological feature in the area. In addition to water, the Vistula

transports considerable sediment in bedload and suspended load. Estimates suggest that the Vistula River transports between 0.4 to 1.4 tons per year of bedload, consisting of coarse sediment particles transported along the riverbed. This bedload contributes to the deposition of sediment in the Gulf of Gdańsk, particularly in areas where the river meets the sea (Szymczak and Galińska, 2013). Specific environmental conditions within each basin also play a role. For example, the presence of anaerobic zones in the Gdańsk hinterland can influence the mobility and speciation of ^{241}Am within the sediment column (Brocławik et al., 2020). Anaerobic conditions may promote the reduction of Am(III) to Am(II), which can enhance its solubility and mobility, potentially leading to higher concentrations in pore waters or release to overlying waters under certain conditions.

In contrast, strong currents or bioturbation in other basins may result in more efficient mixing and redistribution of ^{241}Am within the sediment matrix, influencing its vertical and lateral distribution patterns. The Basin of Gdansk is particularly exposed to heavy metal contamination, as well as radioactive nuclides, mainly from industrial activities in the Polish region and possibly from a Russian enclave (Kaliningrad Oblast) (Glasby et al., 2004; Zaborska et al., 2017). Peak levels of radionuclides, for example^{137}Cs, have been reported over the past 30 years, with concentrations observed in sediment samples ranging from 0.1 to 256.9 Bq·kg^{-1} (Zaborska et al., 2017). This contamination extends to the sediments of the Vistula River, where similar levels of radionuclides have been detected, exacerbating the contamination in the central Gulf of Gdansk (Glasby et al., 2004). The spread of contamination is not limited to the immediate vicinity of industrial areas. However, it extends more than 200 km from Poland eastward toward Germany, where the Oder River and its lagoons act as additional sources of contamination in the southern Baltic Sea (Meyer and Lampe, 1999). A study from 2003 highlighted the significant contribution of plutonium from the Vistula River to the pollution of the Baltic Sea. About 7% of the total plutonium entering the Baltic Sea came from the Vistula, underscoring its importance as a source of plutonium pollution in the region (Skwarzec et al., 2003). The finding raises an important question: could other radionuclides, such as ^{241}Am, also be transported via similar routes? Although the study focused on plutonium in particular, it raises the possibility that other radionuclides may follow comparable paths from the Vistula

catchment area to the Baltic Sea. However, definitive conclusions on the presence and transport of ^{241}Am require further research.

6.2.2.3 Gotland Basin Sediments

The ^{241}Am concentrations in the Gdańsk Basin are shown in Figure 38. The variation in ^{241}Am concentration values within the sediment from the Gotland Basin ranges from 0.017±0.001 to 2.25±0.17 Bq·kg^{-1}. The concentration tends to decrease with depth. Given that the Chernobyl nuclear disaster occurred in 1986, the peak in the sediment layer in years 5–6 may correspond to the fallout from Chernobyl.

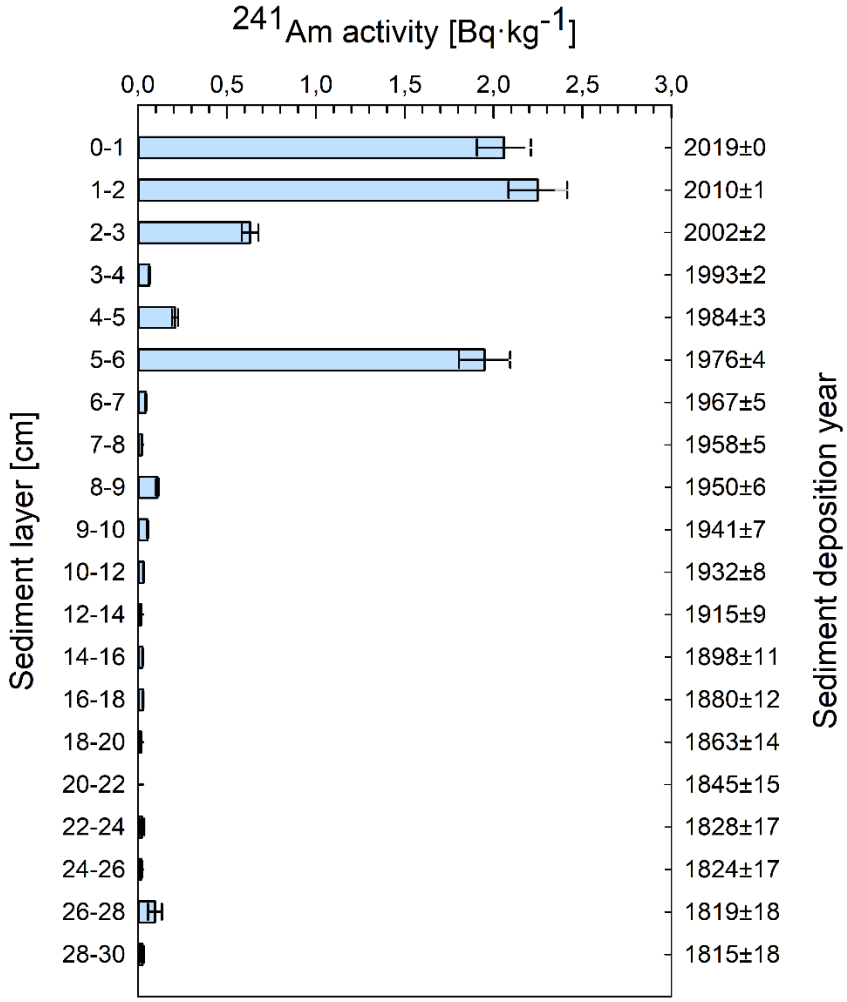

Figure 38. The activity concentrations of ^{241}Am in sediments collected in 2019 from Gotland Basin

The Gotland Deep is one of the main basins of Holocene sediment deposition in the Baltic Sea proper and a significant recipient of saline pulses from the North Sea. Since Gotland Deep is one of the few deep basins in the Baltic Sea with almost constant

anoxic bottom conditions, it is especially suitable for studying the effects of intrusion of oxygen-rich saline North Sea waters followed by oxygen depletion and anoxia (Alvi and Winterhalter 2001). In anoxic environments, the absence of dissolved oxygen alters biogeochemical processes and sedimentary conditions, affecting the mobility and fate of radionuclides. Specifically, in the context of ^{241}Am, anoxic conditions can impact its speciation, solubility, and sorption behavior within the sediment-water interface.

The differences in ^{241}Am concentrations observed among the bottom sediments of the Bornholm, Gotland, and Gdańsk Basins can be attributed to a combination of factors related to these regions' geographical, hydrological, and geological characteristics.

6.3 Comparison of the Obtained ^{241}Am Activities with Literature Values

Accurate determination of ^{241}Am activity is a crucial aspect in environmental studies, providing valuable insight into the distribution and behavior of this artificial radionuclide in different ecosystems. In this context, a comprehensive understanding of the ^{241}Am activity obtained requires comparison with existing literature values. Table 20 presents an overview of the distributions of ^{241}Am in sediments across specific geographical locations. Each coastal region has distinct characteristics, challenges, and importance regarding ecology, economy, and human activity.

Table 31. Distributions of ^{241}Am in sediments in some specific locations

Location	Concentration of ^{241}Am [Bq·kg^{-1}]	Reference
Black Sea coast	0.043–0.187	Mihai and Hurtgen, 1997
Irish Sea	2.61–1894	Kim et al., 1992
Ligurian Sea	0.09–0.14	Desideri et al., 2004
Northwest Pacific Ocean	0.44–10	Lee et al., 2005
Aegean Turkish coast	0.003–0.33	Uğur (Tanbay) and Yener, 2002
south-eastern Baltic Sea and Curonian Lagoon	0.01–0.38	Lujanienė et al., 2014

The concentrations of ^{241}Am in these specific locations serve as critical indicators, influencing our understanding of this artificial radionuclide environmental dynamics and potential sources. The magnitude of ^{241}Am concentrations at the study locations in the Gotland Basin (from 0.017±0.001 to 2.25±0.17 Bq·kg^{-1}), Bornholm Basin (0.03±0.01 to 0.85±0.06 Bq·kg^{-1}) and Gdańsk Basin (0.221±0.016 to 3.185±0.232 Bq·kg^{-1}) are within or comparable to concentration ranges reported in the literature for other marine and coastal areas. Concentrations in the Gotland Basin and Bornholm Basin coincide well with ranges observed on the Black Sea, Ligurian, and Turkish Aegean coasts. Compared to the Black Sea (0.043 to 0.187 Bq·kg^{-1}), ^{241}Am concentrations are slightly lower than in this study. Located in Eastern Europe, the Black Sea coast is characterized by its unique hydrology, including limited exchange with the Mediterranean Sea, which results in low oxygen levels in deeper waters. It also faces environmental issues like pollution and eutrophication. The Baltic and Black Seas have fine-grained sediments, favoring the adsorption and retention of ^{241}Am. In addition, both regions have experienced the impact of anthropogenic activities, including the global radioactive fallout after nuclear weapon tests in open environments peaked in the early 1960s and the atmospheric fallout caused by the accidental release from the Chernobyl Nuclear Power Plant on April 26, 1986, and followed by riverine discharge of significant quantities of radioactivity during early years after the accident (UNSCEAR, 2000; Gulin et al., 2002; Polikarpov et al., 2008). The literature indicates that the Irish Sea shows exceptionally high concentrations of ^{241}Am compared to other locations. Sediments in the Irish Sea are predominantly sandy or muddy, influenced by strong tidal currents and riverine inputs. The notable disparity in ^{241}Am concentrations between the sediments from the Irish Sea (2.61–1894 Bq·kg^{-1}) and investigated sediments from the Baltic Sea can be explained by a confluence of factors, mainly influenced by various anthropogenic activities, historical nuclear practices, and geographic features specific to each region. The Irish Sea shows much higher levels of ^{241}Am, primarily attributed to its proximity to the Sellafield nuclear facility on the northwest coast of England. Americium discharge from Sellafield was reported as being reduced and highly particle-reactive Am(III) (Pentreath et al., 1986; Mitchell et al., 1995).

In contrast, while subject to various anthropogenic influences, the Baltic Sea does not have a reprocessing facility of a scale comparable to Sellafield. Sediments in

the southeastern Baltic Sea and Curonian Lagoon with ^{241}Am concentrations between 0.01 to 0.38 Bq·kg^{-1} are characterized by fine-grained silts and clays, with organic-rich layers in some areas. Freshwater inputs, agricultural runoff, and historical pollution from industrial activities influence these sediments. Activity levels of ^{241}Am in the Baltic Sea are relatively low, as confirmed by our research. Published literature regarding ^{241}Am isotope in the Baltic Sea and the Curonian Lagoon is scarce. Furthermore, no available data have been published regarding the redistribution and transport behavior of these radionuclides in the studied region (Lujanienė et al., 2014).

This work explores the distribution of ^{241}Am in the Gdansk Deep of the Baltic Sea for the first time. The Gdańsk Basin is distinguished by a broader range of concentrations compared to literature data. This local variability suggests unique factors influencing the distribution of ^{241}Am in this particular Baltic Sea region. In the case of the Gdansk Deep, with its anaerobic zones and lack of currents, this can lead to specific chemical and physical conditions that affect the behavior and distribution of ^{241}Am in marine sediments. Chemical processes under anaerobic conditions can affect the binding and release of ^{241}Am from sediments, leading to local variations in its concentrations.

6.4 Statistical Analysis of ^{241}Am Activity Concentrations

The concentration values of ^{241}Am in sediments collected in 2019 differ notably depending on the sampling site and sampling depth. This study shows differences in ^{241}Am activity concentrations in the southern Baltic sediments from different areas (the Kruskal-Wallis test statistic confirmed there is a statistically significant difference at p = <0,001) and provides a summary of the distribution of the activities of ^{241}Am in other regions, allowing identifying the range and central tendency of the activity in the whole core of sediment, as well as any unusual or extreme values (Fig. 39).

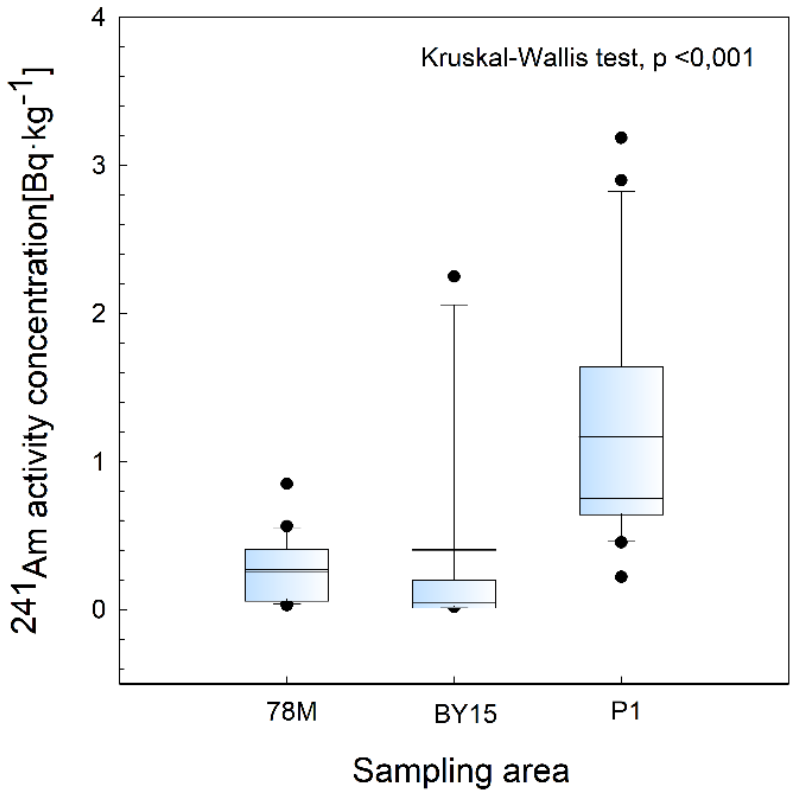

Figure 39. Boxplot of ^{241}Am concentration in all studied samples from different areas. 78M: Bornholm Basin, BY15: Gotland Basin, P1: Gdańsk Basin

For the statistical analysis of a dataset, the R programming language was employed, and various statistical measures, including range, mean, median, standard deviation (SD), minimum (Min), maximum (Max), skewness, kurtosis, and conducted a Shapiro-Wilk test for normality were computed (Table 21). The distribution of all values of ^{241}Am activity concentration in every sediment was asymmetric (skewness > 0), with larger tails than for a normal distribution (kurtosis > 0). A normality test was performed using Shapiro-Wilks tests and gave *p*-values <0 for ^{241}Am activity concentrations, suggesting that the data in Gdańsk Basin and Gotland Basin may deviate from a normal distribution. In the case of the Bornholm Basin, the data indicates a moderate concentration level with a relatively low standard deviation, suggesting a somewhat consistent level of ^{241}Am. The skewness and kurtosis values suggest a distribution that may be slightly skewed to the right and have heavier tails than a normal distribution. However, the Shapiro-Wilk test *p*-value is above 0.05, indicating that the departure from normality is not statistically significant at the conventional significance level.

Table 32. Descriptive statistics of radionuclide ^{241}Am concentration in bottom sediments of the southern Baltic Sea

	^{241}Am		
Statistical parameters	**Bornholm Basin**	**Gdańsk Basin**	**Gotland Basin**
N	20	20	20
Missing	0	0	1
Mean	0.273	1.168	0.403
SD	0.214	0.828	0.763
SD error	0.0478	0.185	0.175
Range	0.819	2.964	2.232
Max	0.848	3.185	2.249
Min	0.0295	0.221	0.0173
Median	0.252	0.752	0.0433
Skewness	0.977	1.346	1.935
Kurtosis	1.143	0.929	2.170
SWilk W	0.910	0.824	0.551
SWilk Prob	0.064	0.002	<0,001

Activity concentration for radionuclides in sediments is given in $Bq \cdot kg^{-1}$

* N = Number; SD = Standard deviation; Max = Maximum; Min = Minimum; SWilk W=W statistic; SWilk Prob=p-value

Table 22. provides results from a statistical analysis that includes a Kruskal-Wallis test and subsequent pairwise comparisons using Dunn's Method. The Kruskal-Wallis test, applied to assess differences among multiple groups, yielded a highly significant result with a test statistic (*H*) of 26.480 and a *p-value* of less than 0.001, indicating a significant overall difference among the groups. Following the Kruskal-Wallis test, Dunn's Method was employed for pairwise comparisons. The first comparison, P1 vs. BY15, revealed a (*Q*) statistic of 4.901 and a significant difference, supported by a difference of ranks of 26.966 and a *p-value* less than 0.05.

Similarly, the comparison between P1 and 78M exhibited a (*Q*) statistic of 3.784, a difference of ranks of 20.55, and a significant *p-value*. On the other hand, the comparison between 78M and BY15 showed a (*Q*) statistic of 1.166, a difference of ranks of 6.416, and a *p-value* greater than 0.05, suggesting no significant difference between these two groups. The results indicate a significant overall difference among the groups, with specific pairwise comparisons revealing substantial differences

between P1 and BY15 and 78M. However, no significant difference was detected between 78M and BY15.

Table 33. Summary of Kruskal-Wallis Test and Dunn's Method Pairwise Comparisons for radionuclide ^{241}Am concentration in bottom sediments of the southern Baltic Sea

	Test Statistic	**P-value**	**Q Statistic**	**Significant**
Kruskal-Wallis Test	H = 26.480	<0.001	-	Yes
Dunn's Method	P1 vs. BY15	Q = 4.901	26.966	Yes
Dunn's Method	P1 vs. 78M	Q = 3.784	20.55	Yes
Dunn's Method	78M vs. BY15	Q = 1.166	6.416	No

6.5 Historical View on ^{241}Am Activity Concentration Changes

Based on the results of ^{241}Am activity concentrations in bottom sediments from the Bornholm Basin, Gotland Basin, and Gdańsk Basin of the Baltic Sea, an attempt was made to look historically at the changes in ^{241}Am activity concentrations. The research involved a comparative analysis of samples collected in 2010 and 2019. The ^{241}Am concentrations in the first layers of the studied sediments increased significantly over the years, which indicated a substantial increase in ^{241}Am accumulation or input in the surface sediments of examined areas. However, understanding the distribution of ^{241}Am in the sediment cores is not as straightforward as expected based on geochronology. Several factors could explain the observed increase in ^{241}Am accumulation. First, there may have been an increase in the influx of particles containing americium from external sources, such as atmospheric deposition or fluvial inputs. This could be contributing to higher ^{241}Am concentrations in the surface sediments. Changes in environmental conditions or human activities might have influenced sedimentation patterns, increasing the input of americium-containing particles. Second, the mobility of americium within sediments is influenced by various factors, including pH levels, redox conditions, and specific minerals or organic matter. Third, physical disturbances, like sediment resuspension caused by currents, waves, or bioturbation (the mixing of sediments by bottom-dwelling organisms), can remobilize ^{241}Am. These remobilized isotopes can settle again onto the sediment bed, resulting in higher concentrations in the surface sediments. Various physical processes, including sediment mixing, can affect the distribution of ^{241}Am within the sediment layers.

Furthermore, the increase in ^{241}Am over time is influenced by the half-life of its parent nuclide, ^{241}Pu. If there were a hypothetical scenario involving increased deposition of ^{241}Pu-containing particles onto the sediments, it would lead to higher ^{241}Am concentrations due to the ingrowth of ^{241}Am. This could result in unexpected patterns in dated sediments.

To confirm the results, additional measurements of ^{241}Am were carried out on sediment samples dating back to 2010. These additional measurements confirm the observed trends in ^{241}Am activity over time. Gotland Basin sediment analysis conducted in 2010 showed results comparable to the 2019 measurements, further confirming the recorded ^{241}Am activity over this period. The highest ^{241}Am concentration levels were obtained in both deeps (from 2010 and 2019) at the same sediment depths (0–1 cm). A significant spike in the presence of ^{241}Am at a depth of 7–8 cm was observed, measuring at 0.765±0.057 Bq·kg^{-1}. This peak coincided with 1988±2, which may have come from the Chernobyl catastrophe. The 1986 Chernobyl disaster and potential fallout may have influenced the observed changes, especially given the elevated concentrations in the years following the event. The most significant differences were observed in sediment dated 1988 and 1976. The observed differences in ^{241}Am concentration levels between sediment samples collected from the Gotland Basin in 2010 and 2019 can be attributed to several factors. These include natural processes such as sediment mixing, bioturbation, chemical mobility, and anthropogenic activities such as resuspension. Sediment mixing, driven by currents and other hydrodynamic forces, can redistribute ^{241}Am in the sediment column, leading to changes in concentration levels over time. The chemical mobility of ^{241}Am, influenced by factors such as pH and redox conditions, can affect its retention or release from sediment particles. Fluctuations in these environmental parameters can cause changes in the concentration of ^{241}Am in the sludge. In addition, the possibility of errors during laboratory analyses, including instrument calibration problems and procedural errors, cannot be excluded. Such errors may contribute to discrepancies between measured ^{241}Am concentrations in sediment samples from different periods.

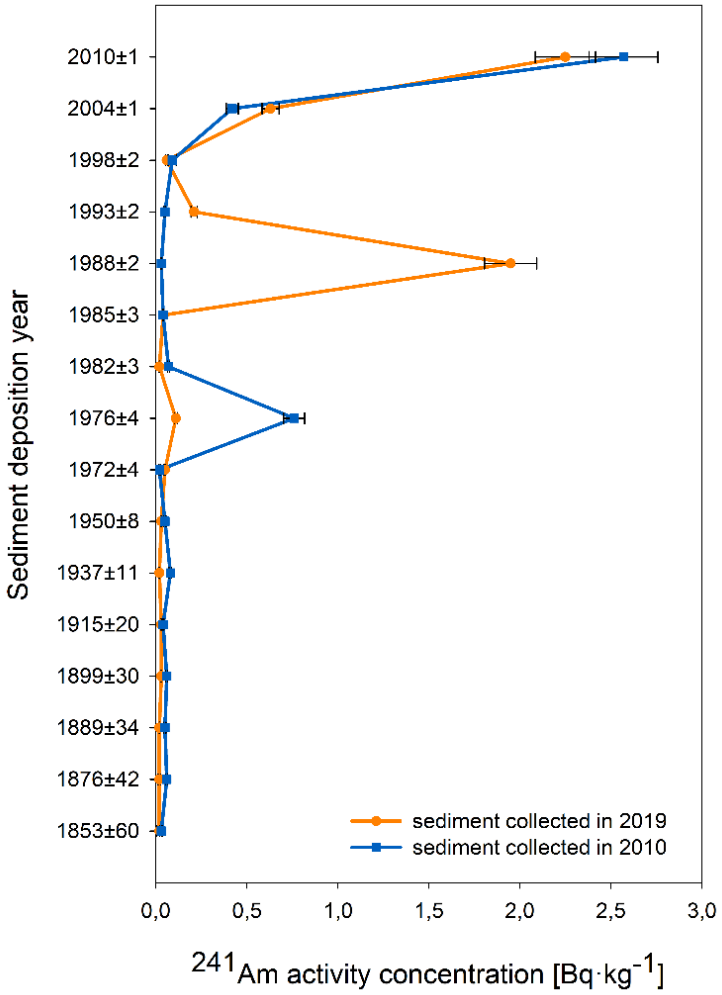

Figure 40. The activity concentrations of ^{241}Am in sediments from Gotland Basin collected in 2010 and 2019

The Chernobyl NPP accident impact is still visible as a potential transport of Chernobyl-originated americium and plutonium from the terrestrial environment to the studied areas of the Baltic Sea, especially in the surface layers of sediments studied (Fig. 41, 42, and 43).

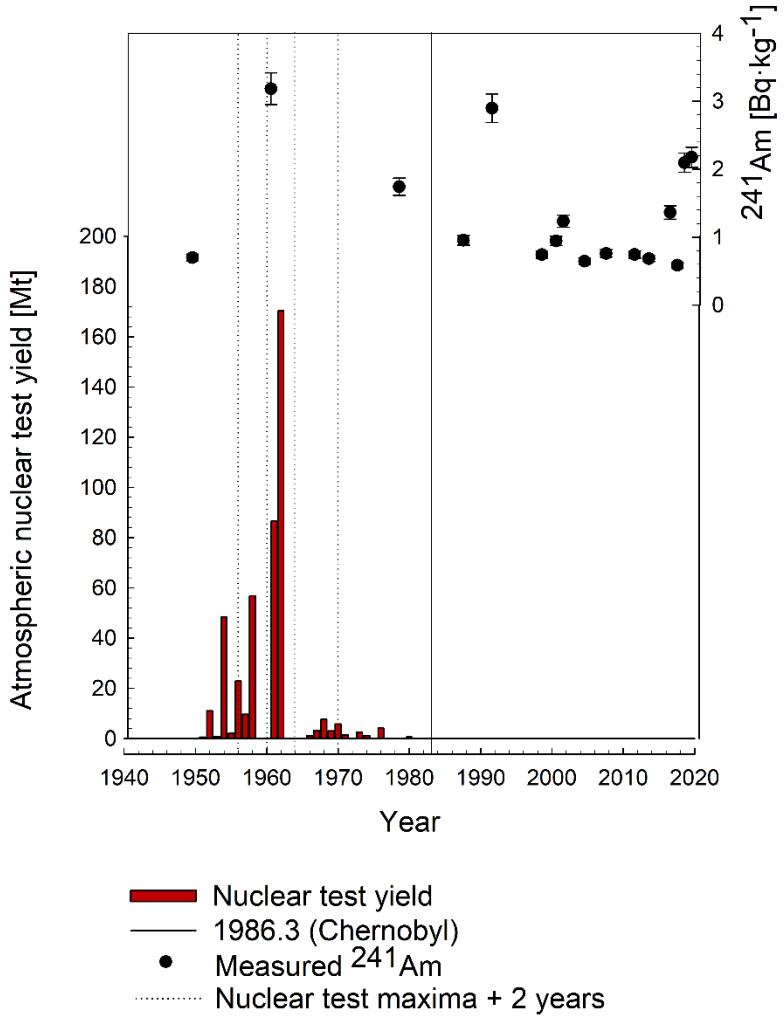

Figure 41. The activity concentrations of ^{241}Am in sediments from Gdańsk Basin in reference to the history of atmospheric nuclear weapon tests

In the early 20th century (1930s–1950s), activity concentrations of ^{241}Am in the Gdańsk Basin were relatively low, ranging from 0.221 to 0.698 Bq·kg^{-1}. This period corresponds to minimal anthropogenic influence on environmental radioactivity. During the mid-20th century (1960s–1970s), there was a significant increase in ^{241}Am activity concentrations, with values ranging from 1.742 to 3.185 Bq·kg^{-1}. This surge likely reflects the impact of nuclear weapons testing and the establishment of nuclear facilities during this period. In the late 20th century (1980s–1990s), activity concentrations of ^{241}Am remained relatively high, indicating ongoing inputs from nuclear activities. Concentrations ranged from 0.742 to 2.899 Bq·kg^{-1} during this time frame. In the 21st century (2000s–2019), activity concentrations fluctuated, reflecting changes in nuclear

policies and advancements in nuclear technology. Concentrations varied from 0.585 to 2.176 $Bq \cdot kg^{-1}$, with potentially lower values in recent years.

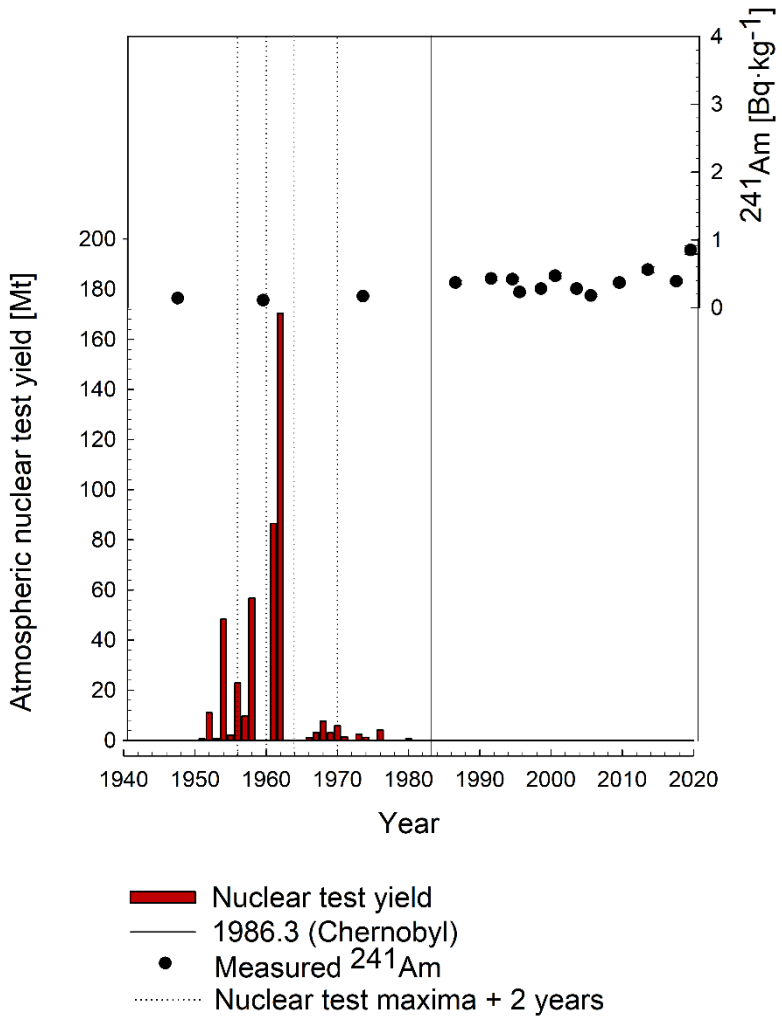

Figure 42. The activity concentrations of ^{241}Am in sediments from Bornholm Basin in reference to the history of atmospheric nuclear weapon tests

In sediments from the Bornholm Basin in the early 20th century (1912–1940), the influence of artificial sources on ^{241}Am levels was limited. Sediment layers showed low activity concentrations, indicating minimal anthropogenic influence on environmental radioactivity. In the mid-20th century (1950–1970), there was a slight increase in ^{241}Am concentrations, especially after 1950. This increase coincided with the era of nuclear weapons testing and the establishment of nuclear facilities for energy production and research. The increased flow of ^{241}Am into the environment from nuclear activities contributed to higher concentrations in sedimentary layers during this

period. In the late 20th century (1980s–1990s), the influx of ^{241}Am from nuclear activities continued, including from events such as nuclear weapons tests and accidents such as Chernobyl (in 1986). Fluctuations in activity concentrations have been influenced by changes in nuclear policy, advances in nuclear technology, and environmental regulations. In the 21st century (2000–2019), ^{241}Am continued to persist in sediment layers, reflecting its long half-life and continued presence in the environment. Fluctuations in activity concentrations resulted from a combination of anthropogenic and natural processes, including changes in nuclear activity and sedimentation rates.

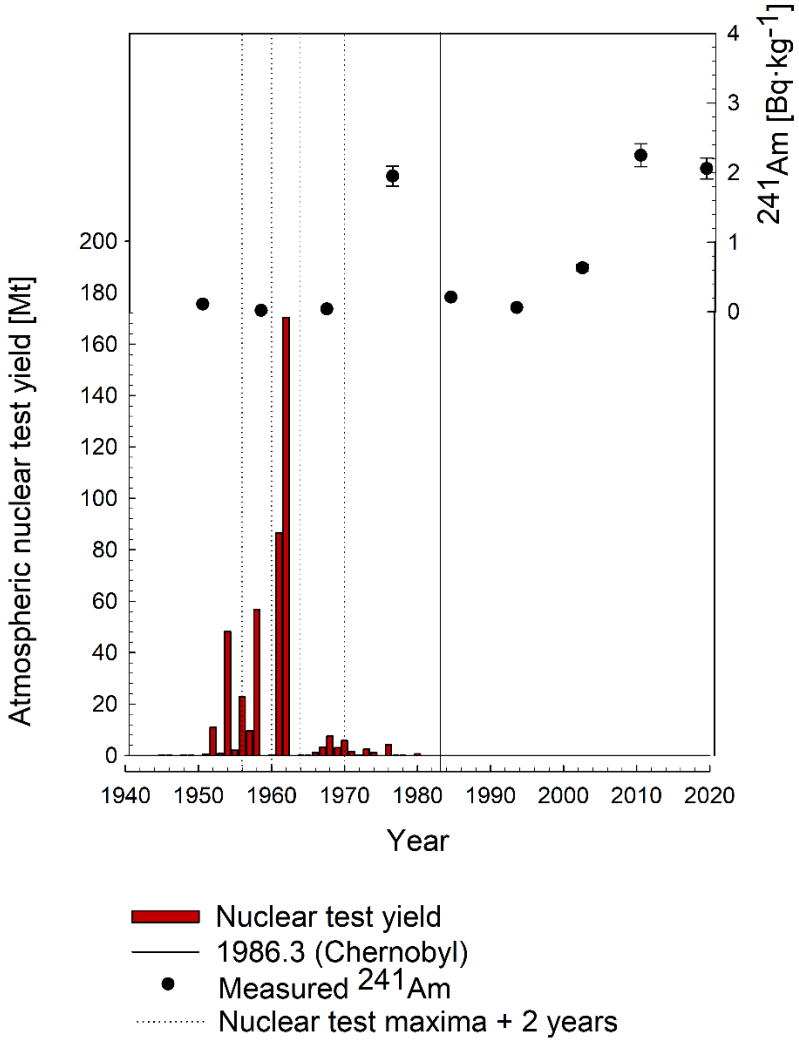

Figure 43. The activity concentrations of ^{241}Am in sediments from Gotland Basin in reference to the history of atmospheric nuclear weapon tests

At the end of the 19th century (1800–1900s), concentrations of ^{241}Am activity were relatively low in the Gotland Basin, consistent with minimal anthropogenic impact on environmental radioactivity. Sediment layers from this period showed concentrations of 0.017 to 0.028 Bq·kg^{-1}. In the early and mid-20th century (1900–1950s), there was a gradual increase in ^{241}Am concentrations. This increase can be attributed to increasing industrialization and the emergence of nuclear activities during this period. Concentrations ranged from 0.017 to 2.249 Bq·kg^{-1}. During the second half of the 20th century (1960–1990), variable concentrations of ^{241}Am activity were observed, reflecting changes in nuclear policy, advances in nuclear technology, and environmental regulations. Concentrations ranged from 0.022 to 1.950 Bq·kg^{-1} during this period. In the 21st century (2000–2019), activity concentrations have remained relatively stable compared to previous decades. However, there have been significant spikes in concentrations in the uppermost layers of sediments, reflecting ^{241}Am long half-life and continued presence in the environment.

6.6 ^{241}Am and ^{137}Cs as Markers in Sediment Chronology

For validation of ^{210}Pb geochronology, it is necessary to use at least one independent marker to ensure an unambiguous time-stratigraphic horizon. Validation is critical to eliminate limitations and potential misapplications of ^{210}Pb dating. The purpose of using an independent tracer is to have an external reference point that can confirm or verify age estimates obtained from ^{210}Pb dating. The term "time-stratigraphic horizon" refers to a specific layer or depth in the sediment that represents a distinct point in time. An unambiguous time-stratigraphic horizon means that the selected independent marker clearly and accurately points to a specific historical event or time period. Sedimentation models often assume certain patterns of deposition and mixing, and the independent tracer is used to verify that these assumptions are correct (Smith, 2001). It is common to encounter applications of the ^{210}Pb method that ignore the complexities of sedimentary processes, including compaction, local mixing (both physical mixing and bioturbation), erosion or episodic sedimentation. These processes have the potential to significantly disrupt the vertical profile of ^{210}Pb and threaten the basic principles of the ^{210}Pb dating models used. Various mechanisms affect the vertical distribution of excess ^{210}Pb (Barsanti et al., 2020).

In this research, the method's reliability was verified using radioactivity, ^{137}Cs, and ^{241}Am by assigning specific changes in their activity concentrations to relevant and known historical events. Using ^{241}Am and ^{137}Cs as markers in sediment chronology has various advantages and disadvantages. ^{241}Am exhibits high particle reactivity, leading to rapid sedimentary burial. Furthermore, its immobile behavior after deposition minimizes redistribution, resulting in sharp peaks in undisturbed sediments. Moreover, the frequency of atmospheric nuclear bomb testing can be precisely identified through high-resolution sampling of geological archives, ensuring more trustworthy age determinations (Schnetger et al., 2013). However, ^{241}Am is typically present in sediments at lower concentrations than ^{137}Cs, presenting challenges in accurate detection and quantification. Its complex decay chain, involving several intermediates, further complicates age estimation. ^{137}Cs, on the other hand, is an abundant source, produced on a large scale during nuclear weapons testing and accidents, resulting in higher concentrations in sediments. Its sharp signal peak facilitates precise identification and dating of sediment layers corresponding to specific events. However, using ^{137}Cs as a time marker may also be associated with uncertainties associated with using this isotope, as it may migrate in the sediment column (Ligero et al., 2005). Due to the much longer half-life of ^{241}Am compared to ^{137}Cs, this tracer can be used when ^{137}Cs cannot be detected in the environment anymore. For instance, ^{137}Cs in 1962 sediment layers will be decayed after approximately eight half-lives in 2075. In addition, sediment data from the euxinic Landsort and Gotland Deeps indicate a significant influence on ^{137}Cs and ^{210}Pb burial over time due to the Mn-pump within the redoxcline (Schnetger et al., 2013).

^{137}Cs was introduced to the northern hemisphere in 1945, with the highest atmospheric concentration noted in 1963 during intense nuclear weapon tests. However, in the Baltic Sea region, the most significant event contributing to environmental contamination by ^{137}Cs was the Chernobyl accident in 1986. The fallout from this disaster typically supersedes any previous contamination by this radionuclide (Knapińska-Skiba et al., 2001; Zaborska et al., 2014). The total amount of ^{137}Cs introduced into the Baltic Sea after the Chernobyl accident is estimated at 4700 TBq, constituting a substantial 82% of the overall quantity present in the Baltic Sea (HELCOM, 1995; Nielsen et al., 1999; HELCOM, 2003). It is estimated that the overall amount of ^{137}Cs accumulated in sediments by 1998 was 2210 TBq (HELCOM, 2007).

This is approximately 8 times more than in the entire 1980s (277 TBq). In the area encompassing the Polish economic zone of the Baltic Sea, the accumulated 137Cs increased from 11 TBq to 46 TBq due to the Chernobyl accident. Therefore, ^{137}Cs can be utilized for verifying dating based on the activity concentrations ^{210}Pb (Zalewska et al., 2020).

Various factors come into play when considering the effectiveness of different time markers, such as ^{241}Am and ^{137}Cs, in dating sediments. ^{241}Am, with a half-life of 432.2 years, can date sediments with a longer historical record, potentially spanning several centuries. However, its analysis is more complicated, tedious, and time-consuming. In contrast, ^{137}Cs, with a shorter half-life of 30.17 years, is suitable for dating sediments deposited within the last few decades. It is particularly effective in identifying sediment layers corresponding to specific nuclear events, such as nuclear weapons tests and accidents such as Chernobyl. ^{137}Cs analysis is generally cheaper and faster than ^{241}Am, making it the preferred choice for time-limited studies.

6.7 Limitations and Future Directions

Studying the nature of radionuclides in the environment is a complicated matter. This chapter discusses the limitations encountered in the current study and shows future research directions.

This study may have been limited by sediment composition, which can vary widely over short distances, and the number and locations of samples taken may not fully capture this variability. Future studies could explore more extensive and targeted sampling strategies to account for such variability. While our current methodologies have yielded valuable insights, one should further refine our assessments. One significant limitation is the exclusive reliance on sediment samples to assess radionuclide impacts. Recognizing the dynamic nature of marine ecosystems, including data from water samples, becomes essential to capture a more complete picture.

Beneficial future directions could be long-term monitoring. Implementing extended monitoring programs can help elucidate trends and patterns in ^{241}Am accumulation over time. This would provide a more robust foundation for

understanding the dynamics of radionuclide deposition and sediment interactions in the Southern Baltic Sea.

Future studies could investigate the presence of ^{241}Am from the Vistula catchment area to the Baltic Sea. Such studies would help elucidate the dynamics of radionuclide transport, including ^{241}Am, from river catchment areas to the marine environment and provide valuable information on the broader pollution of the Baltic Sea ecosystem.

The next promising direction with significant potential for further research is using the ERICA (Environmental Risk from Ionizing Contaminants: Assessment and Management) tool to include sediment and water samples. Future studies could incorporate bioaccumulation analyses and ecological assessments. Investigating the uptake and accumulation of ^{241}Am by aquatic organisms can provide a more holistic understanding of the environmental impact.

7. CONCLUSIONS

This dissertation presents the results of the occurrence of ^{241}Am isotope in the southern Baltic Sea sediments. For the study, marine sediment samples were taken from 3 cores from stations in the Baltic Sea in 2019. In addition, two cores collected in 2010 from stations overlapping with the current study were also analyzed. The results of a study on the ^{241}Am isotope in the bottom sediments of the southern Baltic Sea indicated.

- Americium ^{241}Am is present in the seabed of the southern Baltic Sea.
- The research evaluates the current state of ^{241}Am contamination levels in the bottom sediments of the southern Baltic Sea; measured activity concentrations of ^{241}Am exhibited significant variations among sampling stations and varied with the depth of the sediment core; the highest levels were in the Gotland Basin, and the lowest were in the Bornholm Basin.
- Generally, there is a decreasing trend in ^{241}Am activity concentration with increasing depth of the sediment core; the highest ^{241}Am concentrations were found in surface sediments.
- The research anticipates a rise in ^{241}Am quantity in the Baltic Sea due to the decay of ^{241}Pu, emphasizing the imperative for sustained monitoring over the coming decades.
- Ongoing monitoring is important, especially with the upcoming operation of a new nuclear power plant in northern Poland and other European activities connected to the nuclear industry, civil or military.
- In order to determine the sedimentation rate - SAR and mass accumulation rate - MAR, and to assign ages to individual bottom sediment layers in the South Baltic region, a dating method based on analysis of changes in the ^{210}Pb lead isotope in sediment cores using the Constant Rate of Supply - CRS and Constant Flux - Constant Sedimentation – CF:CS models used. Sedimentation rates, as determined by depth-age profiles, varied across the Baltic basins, reflecting the complex dynamics of radionuclide distribution.
- The study successfully demonstrated the potential utility of ^{241}Am in future sediment dating studies (Gdańsk and Gotland cores). The time distributions obtained from the depth-age profiles point to ^{241}Am as a meaningful additional tool for assessing sedimentary processes and environmental changes.

- The concentration of ^{241}Pu activity for many of the reference materials used for ^{241}Am analysis is unknown, and their use could potentially introduce errors in the quality control and method validation process. A review of reference materials suitable for ^{241}Am validation was done.

REFERENCES

Aarkrog, A. (1991). Source of terms and inventories of anthropogenic radionuclides, Environmental Science and Technology Dept./Ecology Section, Riso National Laboratory, Roskilde, Denmark

Aarkrog, A. (2005). Worldwide marine radioactivity studies (WOMARS). Radionuclide levels in oceans and seas. In Worldwide marine radioactivity studies (WOMARS). Radionuclide levels in oceans and seas (Vol. IAEA-TECDOC-1429) /www-pub.iaea.org/MTCD/publications/PDF/TE_1429_web.pdf Retrieved January 2024

Abril, J. M. (2019). Radiometric dating of recent sediments: On the performance of ^{210}Pb-based CRS chronologies under varying rates of supply. Quaternary Geochronology, 51, 1–14. doi.org/10.1016/j.quageo.2018.12.003

Agency for Toxic Substances and Disease Registry (ATSDR) (2004). Toxicological profile for americium. U.S. Dept. of Health and Human Services, Public Health Service, Agency for Toxic Substances and Disease Registry. www.atsdr.cdc.gov/ToxProfiles/tp156.pdf

Aggarwal, S. K. (2018). A review on the mass spectrometric studies of americium: Present status and future perspective. *Mass Spectrometry Reviews*, *37*(1), 43–56. doi.org/10.1002/mas.21506

Alvi, K. and Winterhalter, B. (2001). Authigenic mineralization in the temporally anoxic Gotland Deep, the Baltic Sea.Baltica, Vol 14.

Amoudry F. (1990). L'analyse par spectrometrie alpha. INSTN ref. from Leblanc, 2006

Apler, A., and Josefsson, S. (2016). Swedish status and trend monitoring program chemical contamination in offshore sediments 2003–2014

Appleby, P. G., and Oldfield, F. (1978). The calculation of lead-210 dates assuming a constant rate of supply of unsupported ^{210}Pb to the sediment. CATENA, 5(1), 1–8. doi.org/10.1016/s0341-8162(78)80002-2

Appleby, P. G., and Oldfield, F. (1983). The assessment of ^{210}Pb data from sites with varying sediment accumulation rates. Hydrobiologia, 103(1), 29–35. doi.org/10.1007/bf00028424

Appleby, P. G., Richardson, N., and Nolan, P. J. (1991). ^{241}Am dating of lake sediments. Hydrobiologia, 214(1), 35–42. doi.org/10.1007/bf00050929

Arnaud, F., Magand, O., Chapron, E., Bertrand, S., Boes, X., Charlet, F., and Melieres, M. A. (2006). Radionuclide dating (^{210}Pb, ^{137}Cs, ^{241}Am) of recent lake sediments in a highly active geodynamic setting (Lakes Puyehue and Icalma—Chilean Lake District). Science of The Total Environment, 366, 837–850. doi.org/10.1016/j.scitotenv.2005.08.013

Asprey, L. B., and Penneman, R. A. (1962). Preparation and Properties of Aqueous Tetravalent Americium. Inorganic Chemistry, 1(1), 134–136. doi.org/10.1021/ic50001a025

Asprey, L. B., Stephanou, S. E., and Penneman, R. A. (1951). Hexavalent Americium. Journal of the American Chemical Society, 73(12), 5715–5717. doi.org/10.1021/ja01156a065

Balaram, V., and Subramanyam, K. S. V. (2022). Sample preparation for geochemical analysis: Strategies and significance. Advances in Sample Preparation, 1, 100010. doi.org/10.1016/j.sampre.2022.100010

Barsanti, M., Garcia-Tenorio, R., Schirone, A., Rozmaric, M., Ruiz-Fernández, A. C., Sanchez-Cabeza, J. A., Delbono, I., Conte, F., De Oliveira Godoy, J. M., Heijnis, H., Eriksson, M., Hatje, V., Laissaoui, A., Nguyen, H. Q., Okuku, E., Al-Rousan, S. A., Uddin, S., Yii, M. W., and Osvath, I. (2020). Challenges and limitations of the ^{210}Pb sediment dating method: Results from an IAEA modelling interlaboratory comparison exercise. Quaternary Geochronology, 59, 101093. doi.org/10.1016/j.quageo.2020.101093

Baskaran, M., Asbill, S., Santschi, P., Brooks, J., Champ, M., Adkinson, D., Colmer, M. R., and Makeyev, V. (1996). Pu, ^{137}Cs, and excess ^{210}Pb in Russian Arctic sediments. Earth and Planetary Science Letters, 140(1-4), 243–257. doi.org/10.1016/0012-821x(96)00040-4

Bateman, H. (1910). Solution of a system of differential equations occurring in the theory of radioactive transformations. Proc. Cambridge Philos. Soc. 15, 423–427

Batlle, J. V. I., Aoyama, M., Bradshaw, C., Brown, J., Buesseler, K. O., Casacuberta, N., Christl, M., Duffa, C., Impens, N., Iøsjpe, M., Masqué, P., and Nishikawa, J. (2018). Marine radioecology after the Fukushima Dai-ichi nuclear accident: Are we better positioned to understand the impact of radionuclides in marine ecosystems? Science of the Total Environment, 618, 80–92. doi.org/10.1016/j.scitotenv.2017.11.005

Bełdowski, J., Klusek, Z., Szubska, M., Turja, R., Bulczak, A. I., Rak, D., Brenner, M., Lang, T., Kotwicki, L., Grzelak, K., Jakacki, J., Fricke, N., Östin, A., Olsson, U., Fabisiak, J., Garnaga, G., Nyholm, J. R., Majewski, P., Broeg, K., ... Schmidt, B. (2016). Chemical Munitions Search and Assessment—An evaluation of the dumped munitions problem in the Baltic Sea. Deep Sea Research Part II: Topical Studies in Oceanography, 128, 85–95. doi.org/10.1016/j.dsr2.2015.01.017

Bellucci, L. G., Frignani, M., Cochran, J. K., Albertazzi, S., Zaggia, L., Cecconi, G., and Hopkins, H. (2007). ^{210}Pb and ^{137}Cs as chronometers for salt marsh accretion in the Venice Lagoon – links to flooding frequency and climate change. Journal of Environmental Radioactivity, 97(2-3), 85–102. doi.org/10.1016/j.jenvrad.2007.03.005

Bennett, B. G. (1978). Environmental aspects of americium (No. EML-348). Department of Energy, New York. doi.org/10.2172/6592513

Bergkvist, N. O. and Ferm R. (2000). Nuclear Explosions 1945-1998. Report FOA-R--00-01572-180–SE, Defense Research Establishment, Division of Systems and Underwater Technology, Stockholm, Sweden

Bergstrom S., Carlsson B. (1994), River runoff to the Baltic Sea: 1950–1990, Ambio, 23 (4–5), 280–287

Bindler, R., Renberg, I., Rydberg, J., and Andrén, T. (2009). Widespread waterborne pollution in central Swedish lakes and the Baltic Sea from pre-industrial mining and metallurgy. Environmental Pollution, 157(7), 2132–2141. doi.org/10.1016/j.envpol.2009.02.003

BiPM, I. E. C., IFCC, I., IUPAC, I., ISO, O. (2012). The international vocabulary of metrology—basic and general concepts and associated terms (VIM)

Bouisset, P., Nohl, M., Cossonnet, C., Boulet, B., Thomas, S., Cariou, N., and Salaun, G. (2021). Contribution of close-in fallout from the French atmospheric tests in inventories of ^{137}Cs, ^{241}Am, and plutonium (238, 239, 240) in Gambier Islands (French Polynesia)—signatures of stratospheric fallout in the Southern Hemisphere. Journal of Environmental Radioactivity, 235–236, 106624. doi.org/10.1016/j.jenvrad.2021.106624

Boulyga, S. F., Desideri, D., and Meli, M. A. (2003). Plutonium and americium determination in mosses by laser ablation ICP-MS combined with isotope dilution technique. International Journal of Mass Spectrometry, 226, 329-339. doi:10.1016/S1387-3806(03)00024-1

Bourges, J. Y., Guillaume, B., Koehly, G., Hobart, D. E., and Peterson, J. R. (1983). Coexistence of americium in four oxidation states in sodium carbonate-sodium bicarbonate medium. Inorganic Chemistry, 22(8), 1179–1184. doi.org/10.1021/ic00150a007

Bricker-Urso, S., Nixon, S. W., Cochran, J. K., Hirschberg, D. J., and Hunt, C. (1989). Accretion Rates and Sediment Accumulation in Rhode Island Salt Marshes. Estuaries, 12(4), 300. doi.org/10.2307/1351908

Brocławik, O., Łukawska-Matuszewska, K., Brodecka-Goluch, A., and Bolałek, J. (2020). Impact of methane occurrence on iron speciation in the sediments of the Gdansk Basin (Southern Baltic Sea). Science of The Total Environment, 721, 137718. doi.org/10.1016/j.scitotenv.2020.137718

Brown, J., Campbell, C., Carrigan, C., Carrott, M., Greenough, K., Maher, C., McLuckie, B., Mason, C., Gregson, C., Griffiths, T., Holt, J., Sarsfield, M., Stephenson, K., Taylor, R., and Tinsley, T. (2018). Americium and Plutonium Purification by Extraction (the AMPPEX process): Development of a new method to separate ^{241}Am from aged plutonium dioxide for use in space power systems. Progress in Nuclear Energy, 106, 396–416. doi.org/10.1016/j.pnucene.2018.02.008

Browne, E., and Firestone, R. B., 1986. Table of Radioactive Isotopes. John Wiley and Sons

Bruel, R., Sabatier, P., (2020). Serac: an R package for ShortlivEd RAdionuclide chronology of recent sediment cores. Journal of Environmental Radioactivity 225, 106449. doi.org/10.1016/j.jenvrad.2020.106449

Brunnengräber, A., and Di Nucci, M. R. (Red.). (2019). Conflicts, Participation and Acceptability in Nuclear Waste Governance. Springer Fachmedien Wiesbaden. doi.org/10.1007/978-3-658-27107-7

Budd, J. R., Weykamp, C., Rej, R., MacKenzie, F., Ceriotti, F., Greenberg, N., Camara, J. E., Schimmel, H., Vesper, H. W., Keller, T., Delatour, V., Panteghini, M., Burns, C., Miller, W. G. (2018). IFCC Working Group Recommendations for Assessing Commutability Part 3: Using the Calibration Effectiveness of a Reference Material. Clinical Chemistry, 64(3), 465–474. doi.org/10.1373/clinchem.2017.277558

Buesseler, K., Dai, M., Aoyama, M., Benitez-Nelson, C., Charmasson, S., Higley, K., Maderich, V., Masqué, P., Oughton, D., and Smith, J.N. (2017). Fukushima Daiichi–derived radionuclides in the ocean: Transport, fate, and impacts. Annual Review of Marine Science, 9, 173–203. doi:10.1146/annurev-marine-010816-060733

Bulczak, A.I., Rak, D., Schmidt, B., Bełdowski, J. (2016). Observations of near-bottom currents in Bornholm Basin, Słupsk Furrow, and Gdansk Deep. Deep-Sea Res. II, 128, 96-113. doi:10.1016/j.dsr2.2015.02.021

Bunke, D. (2017). Sediment mixing processes and accumulation patterns in the south-western Baltic Sea (Doctoral dissertation).

Bunzl, K., Kracke, W. (1988). Cumulative deposition of ^{137}Cs, ^{238}Pu, $^{239+240}$Pu, and ^{241}Am from global fallout in soils from forest, grassland, and arable land in Bavaria (FRG). J. Environ. Radioact., 8(1), 1-14. doi:10.1016/0265-931X(88)90010-0

Cambray, R.S., Cawse, P.A., Garland, J.A., Gibson, J.A.B., Johnson, P., Lewis, G.N.J., Newton, D., Salmon, L., and Wade, B.O. (1987). Observations on radioactivity from the Chernobyl accident. Nucl. Energy 26: 77- 101

Carpenter, R., Beasley, T. M., Zahnle, D., and Somayajulu, B. L. K. (1987). Cycling of fallout (Pu, ^{241}Am, ^{137}Cs) and natural (U, Th, ^{210}Pb) radionuclides in Washington

continental slope sediments. Geochimica et Cosmochimica Acta, 51(7), 1897–1921. doi.org/10.1016/0016-7037(87)90181-5

Carstensen, J., Andersen, J. H., Gustafsson, B. G., and Conley, D. J. (2014). Deoxygenation of the Baltic Sea during the last century. Proceedings of the National Academy of Sciences, 111(15), 5628–5633. doi.org/10.1073/pnas.1323156111

Castrillejo, M., Casacuberta, N., Breier, C. F., Pike, S. M., Masqué, P., and Buesseler, K. O. (2015). Reassessment of ^{90}Sr, ^{137}Cs, and ^{134}Cs in the Coast of Japan Derived from the Fukushima Dai-ichi Nuclear Accident. Environmental Science and Technology, 50(1), 173–180. doi.org/10.1021/acs.est.5b03903

Cetnar, J. (2006). General solution of Bateman equations for nuclear transmutations. Annals of Nuclear Energy, 33(7), 640–645. doi.org/10.1016/j.anucene.2006.02.004

Chassard-Bouchaud C. (1996). Analytical microscopy and environment. Current developments using bioindicators of pollution by stable and radioactive elements. Cell Mol Biol 42(3):361-383

Choppin, G. R., liljenzin J. O., and Rydberg, J. (1995). Radiochemistry and Nuclear Chemistry (2nd ed.). Oxford: Butterworth-Heinnemann

Choppin, G. R., Liljenzin, J.-O., and Rydberg, J. (2002). Unstable Nuclei and Radioactive Decay. W Radiochemistry and Nuclear Chemistry (s. 58–93). Elsevier. doi.org/10.1016/b978-075067463-8/50004-2

Choppin, G.R., Liljenzin, J.O. and Rydberg, J. (2002) Radiochemistry and Nuclear Chemistry. 3rd Edition, Butterworth-Heinemann, Woburn

Christoffersen, P. L., Christiansen, C., Jensen, J. B., Leipe, T., and Hille, S. (2007). Depositional conditions and organic matter distribution in the Bornholm Basin, Baltic Sea. Geo-Marine Letters, 27(5), 325–338. doi.org/10.1007/s00367-007-0054-6

Cieślikiewicz, W., Dudkowska, A., Gic-Grusza, G., and Jędrasik, J. (2017). Extreme bottom velocities induced by wind wave and currents in the Gulf of Gdańsk. Ocean Dynamics, 67(11), 1461–1480. doi.org/10.1007/s10236-017-1098-4

Clark, D.L., Hecker, S.S., Jarvinen, G.D., Neu, M.P. (2010). Plutonium. In L. R. Morss, N. M. Edelstein, and J. Fuger (Eds.), The Chemistry of the Actinide and Transactinide Elements. Springer

Cochran, J.K., 1982. The oceanic chemistry of the U- and Th-series nuclides. In: Ivanovich, M., Harmon, S. (Eds.), Uranium Series Disequilibrium: Applications to Environmental Problems. Clarendon Press, Oxford

Conley, D.J., Carstensen, J., Vaquer-Sunyer, R., Duarte, C.M. (2009). Ecosystem thresholds with hypoxia. In: Andersen, J.H., Conley, D.J. (eds) Eutrophication in Coastal Ecosystems. Developments in Hydrobiology, vol 207. Springer, Dordrecht. doi.org/10.1007/978-90-481-3385-7_3

Corcho-Alvarado, J. A., Diaz-Asencio, M., Froidevaux, P., Bochud, F., Alonso-Hernández, C. M., and Sanchez-Cabeza, J. A. (2014). Dating young Holocene coastal sediments in tropical regions: Use of fallout ^{239,240}Pu as alternative chronostratigraphic marker. Quaternary Geochronology, 22, 1–10. doi.org/10.1016/j.quageo.2014.02.001

Cundy, A. B., and Croudace, I. W. (1996). Sediment Accretion and Recent Sea-level Rise in the Solent, Southern England: Inferences from Radiometric and Geochemical Studies. Estuarine, Coastal and Shelf Science, 43(4), 449–467. doi.org/10.1006/ecss.1996.0081

Cundy, A. B., Croudace, I. W., Warwick, P. E., Oh, J., and Haslett, S. K. (2002). Accumulation of COGEMA-La Hague-derived reprocessing wastes in French salt marsh sediments. Environmental Science and Technology, 36(20), 4990–4997. doi.org/10.1021/es020098c

Cuney, M. (2021). Nuclear Geology. W Encyclopedia of Geology (s. 723–744). Elsevier. doi.org/10.1016/b978-0-08-102908-4.00024-2

Currie, L. A. (1968). Limits for qualitative detection and quantitative determination. Application to radiochemistry. Analytical Chemistry, 40(3), 586–593. doi.org/10.1021/ac60259a007

Czub, M., Kotwicki, L., Lang, T., Sanderson, H., Klusek, Z., Grabowski, M., Szubska, M., Jakacki, J., Andrzejewski, J., Rak, D., and Bełdowski, J. (2018). Deep

sea habitats in the chemical warfare dumping areas of the Baltic Sea. Science of The Total Environment, 616-617, 1485–1497. doi.org/10.1016/j.scitotenv.2017.10.165

Dadey, K. A., Janecek, T., Klaus, A. (1992). Dry-Bulk Density: Its Use and Determination. W Proceedings of the Ocean Drilling Program, 126 Scientific Results. Ocean Drilling Program. doi.org/10.2973/odp.proc.sr.126.157.1992

Damrat, M., Zaborska, A., and Zajączkowski, M. (2013). Sedimentation from suspension and sediment accumulation rate in the River Vistula prodelta, Gulf of Gdańsk (Baltic Sea)**The project within which this paper was prepared was funded by the Institute of Oceanology, Polish Academy of Sciences, and the National Science Centre, grant No. 011/01/B/ST10/06529. Oceanologia, 55(4), 937–950. doi.org/10.5697/oc.55-4.937

Dares, C. J., Lapides, A. M., Mincher, B. J., and Meyer, T. J. (2015). Electrochemical oxidation of ^{243}Am(III) in nitric acid by a terpyridyl-derivatized electrode. Science, 350(6261), 652–655. doi.org/10.1126/science.aac9217

Darmawan and Wada, S. I. (2002). Effect of clay mineralogy on the feasibility of electrokinetic soil decontamination technology. Applied Clay Science, 20(6), 283–293. doi.org/10.1016/s0169-1317(01)00080-1

Das, D. K., Kumar, S., Pathak, P. N., Tomar, B. S., and Manchanda, V. K. (2011). Sorption of Am(III) on natural sediment: experiment and modeling. In Journal of Radioanalytical and Nuclear Chemistry (Vol. 289, Issue 1, pp. 137-143). Springer Science and Business Media LLC. doi.org/10.1007/s10967-011-1045-7

De Cort, M., Dubois, G., Fridman, Sh. D., Germenchuk, M. G., Izrael, Yu. A., Janssens, A., Jones, A. R., Kelly, G. N., Kvasnikova, E. V., Matveenko, I. I., Nazarov, I. M., Pokumeiko, Yu. M., Sitak, V. A., Stukin, E. D., Tabachny, L. Ya., Tsaturov, Yu. S., and Avdyushin, S. I. (1998). Atlas of caesium deposition on Europe after the Chernobyl accident. Office for Official Publications of the European Communities. ISBN 92-828-3140-X

Delaval, A., Duffa, C., Radakovitch, O. (2020). A review on cesium desorption at the freshwater-seawater interface. Journal of Environmental Radioactivity, 218, 106255. doi.org/10.1016/j.jenvrad.2020.106255

Deng, D., Zhang, L., Dong, M., Samuel, R. E., Ofori-Boadu, A., and Lamssali, M. (2020). Radioactive waste: A review. Water Environment Research, 92(10), 1818–1825. doi.org/10.1002/wer.1442

Desideri, D., Giuliani, S., Meli, M. A., Testa, C., Triulzi, C., and Vaghi, M. (2004). Presence of137Cs, Pu isotopes and ^{241}Am in ligurian and Tyrrhenian Seas sediments. Journal of Radioanalytical and Nuclear Chemistry, 260(1), 9–12. doi.org/10.1023/b:jrnc.0000027054.61685.b4

Dezileau, L., Lehu, R., Lallemand, S., Hsu, S.-K., Babonneau, N., Ratzov, G., Lin, A. T., and Dominguez, S. (2016). Historical Reconstruction of Submarine Earthquakes Using ^{210}Pb, ^{137}Cs, and ^{241}Am Turbidite Chronology and Radiocarbon Reservoir Age Estimation off East Taiwan. Radiocarbon, 58(1), 25–36. doi.org/10.1017/rdc.2015.3

Diaz, R. J., and Rosenberg, R. (2008). Spreading Dead Zones and Consequences for Marine Ecosystems. Science, 321(5891), 926–929. doi.org/10.1126/science.1156401

Díaz-Asencio, M., Alonso-Hernández, C. M., Bolanos-Álvarez, Y., Gómez-Batista, M., Pinto, V., Morabito, R., Hernández-Albernas, J. I., Eriksson, M., Sanchez-Cabeza, J. A. (2009). One century sedimentary record of Hg and Pb pollution in the Sagua estuary (Cuba) derived from ^{210}Pb and ^{137}Cs chronology. Marine Pollution Bulletin, 59(4-7), 108–115. doi.org/10.1016/j.marpolbul.2009.02.010

Díaz-Asencio, M., Sanchez-Cabeza, J.-A., Ruiz-Fernández, A. C., Corcho-Alvarado, J. A., and Pérez-Bernal, L. H. (2020). Calibration and use of well-type germanium detectors for low-level gamma-ray spectrometry of sediments using a semi-empirical method. Journal of Environmental Radioactivity, 225, 106385. doi.org/10.1016/j.jenvrad.2020.106385

DOE. (1996). Radiological bioconcentration factors for aquatic, terrestrial, and wetland ecosystems at the Savannah River Site (U). Savannah River Site. U.S. Department of Energy. WSRC-TR-96-0231. DE-AC09-89SR18035

Elmgren, R. (2001). Understanding Human Impact on the Baltic Ecosystem: Changing Views in Recent Decades. AMBIO: A Journal of the Human Environment, 30(4), 222–231. doi.org/10.1579/0044-7447-30.4.222

Emeis, KC., Endler, R., Struck, U., Kohly, A. (2002). The Post-Glacial Evolution of the Baltic Sea. In: Wefer, G., Berger, W.H., Behre, KE., Jansen, E. (eds) Climate Development and History of the North Atlantic Realm. Springer, Berlin, Heidelberg. doi.org/10.1007/978-3-662-04965-5_14

Emelyanov, E. M. (1995). Baltic Sea: geology, geochemistry, paleoceanography, pollution. PP Shirshov Institute of Oceanology RAS, Atlantic Branch/Baltic Ecological Institute of Hydrosphere/Academy of Natural Sciences, RF

Emelyanov, E. M. (2014). Biogenic components of the Baltic Sea sediments. Russian Geology and Geophysics, 55(12), 1404–1417. doi.org/10.1016/j.rgg.2014.11.005

Evans, L.J. (1989), "Chemistry of Metal Retention by Soils, Environ. Sci. Tech., 23: 1046-1056

Everett, S. E., Tims, S. G., Hancock, G. J., Bartley, R., and Fifield, L. K. (2008). Comparison of Pu and 137Cs as tracers of soil and sediment transport in a terrestrial environment. Journal of Environmental Radioactivity, 99(2), 383–393. doi.org/10.1016/j.jenvrad.2007.10.019

Fisher, N. S., Bjerregaard, P., and Fowler, S. W. (1983). Interactions of marine plankton with transuranic elements. Marine Biology, 75(2–3), 261–268. doi.org/10.1007/bf00406011

Fisher, N.S., Teyssie, J.L., Fowler, S.W., and Wang, W. (1996). Accumulation and retention of metals in mussels from food and water : A comparison under field and laboratory conditions. Environmental Science and Technology, 30, 3232-3242

Fitzgerald, R., Inn, K. G. W., Horgan, C. (2015). How old is it?—^{241}Pu/^{241}Am nuclear forensic chronology reference materials. Journal of Radioanalytical and Nuclear Chemistry, 307(3), 2521–2528. doi.org/10.1007/s10967-015-4565-8

Fonselius, S. H. (1970). On the stagnation and recent turnover of the water in the Baltic. Tellus, 22, 533-544

Fonselius, S., and Valderrama, J. (2003). One hundred years of hydrographic measurements in the Baltic Sea. Journal of Sea Research, 49(4), 229–241. doi.org/10.1016/s1385-1101(03)00035-2

Fowler, S.W., Ballestra, S., La Rosa, J., Fukai, R. (1983). Vertical transport of particulateassociated plutonium and americium in the upper water column of the Northeast Pacific. Deep-Sea Res. 30, 1221–1233. doi.org/10.1016/0198-0149(83)90081-X

Franck, H., Matthäus, W., and Sammler, R. (1987). Major inflows of saline water into the Baltic Sea during the present century.

Friedrichs, C. T., and Wright, L. D. (1995). Resonant internal waves and their role in transport and accumulation of fine sediment in Eckernförde Bay, Baltic Sea. Continental Shelf Research, 15(13), 1697–1721. doi.org/10.1016/0278-4343(95)00035-y

Gaebler, P., Ceranna, L., Nooshiri, N., Barth, A., Cesca, S., Frei, M., Grünberg, I., Hartmann, G., Koch, K., Pilger, C., Ross, J. O., and Dahm, T. (2019). A multi-technology analysis of the 2017 North Korean nuclear test. Solid Earth, 10(1), 59–78. doi.org/10.5194/se-10-59-2019

Ghiorso, A., R. A. James, L. O. Morgan and G. T. Seaborg, (1950). Preparation of Transplutonium Isotopes by Neutron Irradiation. Physical Review, 78(4), 472–472

Goff, G.S., Long, K.M., Reilly, S.D., Jarvinen, G.D., and Runde, W.H. (2012). Americium/Lanthanide Separations in Alkaline Solutions for Advanced Nuclear Fuel Cycles. In: 36th Actinide Separations Conference: May 5, 2012; Chattanooga, TN

Goldberg, E. D. (1963). Geochronology with ^{210}Pb. Symposium on Radiactive Dating. In International Atomic Energy (IEAE) Symposium Proceedings (pp. 121-131)

Grandin, K., Jagers, P., and Kullander, S. (2010). Nuclear Energy. AMBIO, 39(S1), 26–30. doi.org/10.1007/s13280-010-0061-0

Gudelis, V. K., and Litvin, V. M. (1976). The Bottom Geomorphology. In Geologiya Baltiiskogo morya (pp. 25-34). Vilnius: Mokslas

Gulin, S.B., Polikarpov, G.G., Egorov, V.N., Martin, J.-M., Korotkov, A.A., Stokozov, N.A. (2002). Radioactive contamination of the north-western Black Sea

sediments. Estuar. Coast Shelf Sci. 54 (3), 541–549. doi.org/10.1006/ecss.2000.0663

Haddad, P. R. (2005). ION EXCHANGE | Overview. W Encyclopedia of Analytical Science (s. 440–446). Elsevier. doi.org/10.1016/b0-12-369397-7/00283-1

Håkanson, L. (1991). Physical Geography of the Baltic. The Baltic Sea Environment : 1. Uppsala: The Baltic University Programme, Uppsala University

Hallberg, R. O. (1991). Environmental implications of metal distribution in Baltic Sea sediments. Ambio, 20, 309–316

Hancock, G. J., Leslie, C., Everett, S. E., Tims, S. G., Brunskill, G. J., and Haese, R. (2011). Plutonium as a chronomarker in Australian and New Zealand sediments: a comparison with ^{137}Cs. Journal of Environmental Radioactivity, 102(10), 919–929. doi.org/10.1016/j.jenvrad.2009.09.008

Harmon, H. D., Peterson, J. R., Bell, J. T., and McDowell, W. J. (1972). A spectrophotometric study of the formation of americium thiocyanate complexes. Journal of Inorganic and Nuclear Chemistry, 34(5), 1711–1719. doi.org/10.1016/0022-1902(72)80296-3

He, Q. and Walling, D. E. (1997). The distribution of fallout ^{137}Cs and ^{210}Pb in undisturbed and cultivated soils. Applied Radiation and Isotopes, 48(5), 677–690. doi.org/10.1016/s0969-8043(96)00302-8

HELCOM, (2004).The Fourth Baltic Sea Pollution Load Compilation (PLC-4). Baltic Sea Environ. Proc. No. 93

HELCOM, (2009): Radioactivity in the Baltic Sea, 1999–2006 HELCOM thematic assessment. – Baltic Sea environment proceedings No. 117, Helsinki

HELCOM. (1995). Radioactivity in the Baltic sea 1984-1991, In: Baltic Sea Environment Proceedings, 61, Helsinki Commission, Helsinki, Finland

HELCOM. (2003). Radioactivity in the Baltic Sea 1992-1998. Baltic Sea Environment Proceedings No 61, 5-15

HELCOM. (2006). Development of tools for assessment of eutrophication in the Baltic Sea. BSEP 104. Helsinki

HELCOM. (2007). Long-lived radionuclides in the seabed of the Baltic Sea. Report of the Sediment Baseline Study of HELCOM MORS-PRO in 2000–2005. Baltic Sea Environment Proceedings No. 110

HELCOM. (2018). State of the Baltic Sea - Second HELCOM holistic assessment 2011-2016

Hendożko, E., Szefer, P., and Warzocha, J. (2010). Heavy metals in Macoma balthica and extractable metals in sediments from the southern Baltic Sea. Ecotoxicology and Environmental Safety, 73(2), 152–163. doi.org/10.1016/j.ecoenv.2009.09.006

Hewitt, A. E. (1996). Estimating surface erosion using ^{137}Cs at a semi-arid site in Central Otago, New Zealand. Journal of the Royal Society of New Zealand, 26(1), 107–118. doi.org/10.1080/03014223.1996.9517506

Hindmann FD. (1983). Neodymium fluoride mounting for a spectrometric determination of uranium, plutonium, and americium. Anal Chem 55:2460-2461

Hinton, T. G., Garnier-Laplace, J., Vandenhove, H., Dowdall, M., Adam-Guillermin, C., Alonzo, F., Barnett, C., Beaugelin-Seiller, K., Beresford, N. A., Bradshaw, C., Brown, J., Eyrolle, F., Fevrier, L., Gariel, J. C., Gilbin, R., Hertel-Aas, T., Horemans, N., Howard, B. J., Ikäheimonen, T., ... Vives i Batlle, J. (2013). An invitation to contribute to a strategic research agenda in radioecology. Journal of Environmental Radioactivity, 115, 73–82. doi.org/10.1016/j.jenvrad.2012.07.011

Hoffman D. C. (2002) In Memory of Glenn Theodore Seaborg [19 April 1912-25 February 1999] Glenn T. Seaborg's Multi-Faceted Career, Journal of Nuclear Science and Technology, doi: 10.1080/00223131.2002.10875397

Högberg, L. (2013). Root Causes and Impacts of Severe Accidents at Large Nuclear Power Plants. AMBIO, 42(3), 267–284. doi.org/10.1007/s13280-013-0382-x

Holcomb, H. P. (1965). Analytical Oxidation of Americium with Sodium Perxenate. Analytical Chemistry, 37(3), 415. doi.org/10.1021/ac60222a002

Holm E. and Ballestra S. (1989). Methods for Radiochemical Analyses of Plutonium, Americium and Curium, within the "Measurements of Radionuclides in

Food and the Environment - A Guidebook", IAEA Technical Report Series No. 295, IAEA

Holm, E. (1995). Plutonium in the Baltic Sea. Applied Radiation and Isotopes, 46(11), 1225-1229. doi:10.1016/0969-8043(95)00164-9

Horikoshi, T., Nakajima, A., and Sakaguchi, T. (1981). Studies on the accumulation of heavy metal elements in biological systems. European Journal of Applied Microbiology and Biotechnology, 12(2), 90–96. doi.org/10.1007/bf01970040

Horwitz, E.P., Chiarizia, R., Dietz, M.L., Diamond, H., Nelson, D.M., (1993). Separation and preconcentration of actinides from acidic media by extraction chromatography. Anal. Chim. Acta 281, 361-372

Hu, Q.-H., Weng, J.-Q., and Wang, J.-S. (2010). Sources of anthropogenic radionuclides in the environment: a review. Journal of Environmental Radioactivity, 101(6), 426–437. doi.org/10.1016/j.jenvrad.2008.08.004

Hunt, J., Leonard, K., and Hughes, L. (2013). Artificial radionuclides in the Irish Sea from Sellafield: remobilization revisited. Journal of Radiological Protection, 33(2), 261–279. doi.org/10.1088/0952-4746/33/2/261

Hutchins, D. A., Stupakoff, I., and Fisher, N. S. (1996). Temperature effects on accumulation and retention of radionuclides in the sea star, Asterias forbesi: implications for contaminated northern waters. Marine Biology, 125(4), 701–706. doi.org/10.1007/bf00349252

IAEA. (1998). The radiological situation at the atolls of Mururoa and Fangataufa: Main report (STI/PUB/1028). /www-pub.iaea.org/MTCD/Publications/PDF/Pub1028_web.pdf. Retrieved January 2024

IAEA. (2004). Quantifying Uncertainty in Nuclear Analytical Measurements, IAEA-TECDOC-1401, IAEA, Vienna

IAEA. (2008). Worldwide proficiency test: determination of naturally occurring radionuclides in phosphogypsum and water. IAEA-CU-2008-03

IAEA. (2009). A procedure for the rapid determination of Pu isotopes and Am-241 in soil and sediment samples by alpha spectrometry. Analytical Quality in Nuclear Applications No. IAEA/AQ/11. Vienna: IAEA. ISSN 2074–765

IAEA. (2012). Fukushima Daiichi status report. /www.iaea.org/newscenter/focus/fukushima/statusreport280612.pdf. Retrieved January 2024

Ikäheimonen, T.K., Saxen, R. (2002). Transuranic elements in fishes compared to ^{137}Cs in certain lakes in Finland. Boreal Environ. Res. 7, 99–104. /www.borenv.net/ BER/archive/pdfs/ber7/ber7-099.pdf

Ikäheimonen, TK. (2003). Determination of transuranic elements, their behaviour and sources in the aquatic environment (thesis). Report STUK-A194, Helsinki, 82 pp + Annexes

Ilus E. (1998). Dating of sediments and sedimentation rate, STUK-A 145, Proceedings of a seminar held in Helsinki 2-3.04.1997

Ilus, E. (2007). The Chernobyl accident and the Baltic Sea. Boreal Environ. Res., 12, 1-10. helda.helsinki.fi/bitstream/handle/10138/235348/ber12-1-001.pdf

Ilus, E., Ilus, T., (2000). Sources of radioactivity. In: Nielsen, S.P. (Ed.), The Radiological Exposure of the Population of the European Community to Radioactivity in the Baltic Sea, Marina-Balt project, Radiation Protection 110:9–76, EUR 19200, European Commission, Luxembourg

Imanaka, T., Hayashi, G., Endo, S. (2015). Comparison of the accident process, radioactivity release and ground contamination between Chernobyl and Fukushima-1. Journal of Radiation Research, 56(1), 56–61. doi.org/10.1093/jrr/rrv074

INSAG. (1986). Summary report on the post-accident review meeting on the Chernobyl Accident. International Nuclear Safety Advisory Group Report INSAG-1. Vienna: IAEA

INSAG. (1992). The Chernobyl accident: Updating of INSAG-1. International Nuclear Safety Advisory Group Report INSAG-7. Vienna: IAEA international pour l'Exploration de la Mer 186, 60–69

Irlweck, K., Wicke, J. (1998). Isotopic composition of plutonium immissions in Austria after the Chernobyl accident. J Radioanal Nucl Chem 227, 133–136. doi.org/10.1007/BF02386445

ISO. (1993). Guide to the Expression of Uncertainty in Measurements, ISO, Geneva, Switzerland, Corrected and reprinted in 1995

ISO. (2000). ISO Guide 33, Uses of Certified Reference Materials, 2nd Edition, Geneva, Switzerland

Jakopič, R., Tavčar, P., Benedik, L. (2007). Sequential determination of Pu and Am radioisotopes in environmental samples: a comparison of two separation procedures. Appl. Radiat. Isot., 65(5), 504. doi:10.1016/j.apradiso.2006.12.005

Jankowska, H., and Łęczyński, L. (1993). Bottom sediments. The Puck Bay. Institute of Oceanography University of Gdańsk, Gdańsk, Poland, 320-327

Jokinen, S. A., Virtasalo, J. J., Kotilainen, A. T., Saarinen, T. (2015). Varve microfabric record of seasonal sedimentation and bottom flow-modulated mud deposition in the coastal northern Baltic Sea. Marine Geology, 366, 79–96. doi.org/10.1016/j.margeo.2015.05.003

Kaihola, L. (2000). Journal of Radioanalytical and Nuclear Chemistry, 243(2), 313–317. doi.org/10.1023/a:1016032921544

Kanisch, G. (2004). Alpha-spectrometric analysis of environmental samples (IAEA-TECDOC--1401). International Atomic Energy Agency (IAEA)

Kashparov, V. A., Lundin, S. M., Zvarych, S. I., Yoshchenko, V. I., Levchuk, S. E., Khomutinin, Y. V. (2003b). Territory contamination with the radionuclides representing the fuel component of Chernobyl fallout. Science of the Total Environment, 317, 105-119. doi:10.1016/S0048-9697(03)00336-X

Kashparov, V.A., Lundin, S.M., Zvarich, S.I. (2003a). Soil Contamination with Fuel Component of Chernobyl Radioactive Fallout. Radiochemistry 45, 189–200 doi.org/10.1023/A:1023897612740

Kaskela, A. M., and Kotilainen, A. T. (2017). Seabed geodiversity in a glaciated shelf area, the Baltic Sea. Geomorphology, 295, 419–435. doi.org/10.1016/j.geomorph.2017.07.014

Kaskela, A. M., Kotilainen, A. T., Al-Hamdani, Z., Leth, J. O., and Reker, J. (2012). Seabed geomorphic features in a glaciated shelf of the Baltic Sea. Estuarine, Coastal and Shelf Science, 100, 150–161. doi.org/10.1016/j.ecss.2012.01.008

Katz, J. I. (2008). Lessons Learned from Nonproliferation Successes and Failures. Comparative Strategy, 27(5), 426–430. doi.org/10.1080/01495930802358398

Kershaw, P. J., Pentreath, R. J., Harvey, B. R., Lovett, M. B., and Boggis, S. J. (1986). Apparent distribution coefficients of transuranium elements in UK coastal waters. In Application of distribution coefficients to radiological assessment models.

Kershaw, P., and Baxter, A. (1995). The transfer of reprocessing wastes from north-west Europe to the Arctic. Deep Sea Research Part II: Topical Studies in Oceanography, 42(6), 1413–1448. doi.org/10.1016/0967-0645(95)00048-8

Kim, C. K., Morita, S., Seki, R., Takaku, Y., Ikeda, N., and Assinder, D. J. (1992). Distribution and behaviour of ^{99}Tc, ^{237}Np, ^{239,240}Pu, and^{241}Am in the coastal and estuarine sediments of the Irish Sea. Journal of Radioanalytical and Nuclear Chemistry Articles, 156(1), 201–213. doi.org/10.1007/bf02037434

Kim, C.-K., Kim, C.-S., Sansone, U., and Martin, P. (2008). Development and application of an on-line sequential injection system for the separation of Pu, ^{210}Po and ^{210}Pb from environmental samples. Applied Radiation and Isotopes, 66(2), 223–230. doi.org/10.1016/j.apradiso.2007.08.006

Kinoshita, N., Sueki, K., Sasa, K., Kitagawa, J. i., Ikarashi, S., Nishimura, T., Wong, Y. S., Satou, Y., Handa, K., Takahashi, T., Sato, M., and Yamagata, T. (2011). Assessment of individual radionuclide distributions from the Fukushima nuclear accident covering central-east Japan. Proceedings of the National Academy of Sciences, 108(49), 19526–19529. doi.org/10.1073/pnas.1111724108

Knapinska-Skiba, D., Bojanowski, R., Radecki, Z., and Millward, G. E. (2001). Activity Concentrations and Fluxes of Radiocesium in the Southern Baltic Sea. Estuarine, Coastal and Shelf Science, 53(6), 779–786. doi.org/10.1006/ecss.2001.0812

Kolker, A. S., Goodbred, S. L., Hameed, S., and Cochran, J. K. (2009). High-resolution records of the response of coastal wetland systems to long-term and short-term sea-level variability. Estuarine, Coastal and Shelf Science, 84(4), 493–508. doi.org/10.1016/j.ecss.2009.06.030

Kowalewska G., Winterhalter B., Talbot, H., Maxwell J.R. and Konat, J. (1999). Chlorins in sediments of the Gotland Deep (Baltic Sea). Oceanologia. 41. 81-97

Krishnaswamy, S., Lal, D., Martin, J. M., and Meybeck, M. (1971). Geochronology of lake sediments. Earth and Planetary Science Letters, 11(1-5), 407–414. doi.org/10.1016/0012-821x(71)90202-0

Kuliński, K., and Pempkowiak, J. (2011). The carbon budget of the Baltic Sea. Biogeosciences, 8(11), 3219–3230. doi.org/10.5194/bg-8-3219-2011

Kurkina, O., Talipova, T., Pelinovsky, E.N., and Soomere, T. (2011). Mapping the internal wave field in the Baltic Sea in the context of sediment transport in shallow water. Journal of Coastal Research, 2042-2047

Larsen, R.J. (1985). Worldwide deposition of ^{90}Sr through 1983, Environmental Measurements Laboratory, Department of Energy, EML-444, pp. 1-159

Lee, S.-H., Povinec, P. P., Wyse, E., Pham, M. K., Hong, G.-H., Chung, C.-S., Kim, S.-H., and Lee, H.-J. (2005). Distribution and inventories of ^{90}Sr, ^{137}Cs, ^{241}Am and Pu isotopes in sediments of the Northwest Pacific Ocean. Marine Geology, 216(4), 249–263. doi.org/10.1016/j.margeo.2005.02.013

Lehto J. and Harjula R. (1999). Selective Separation of Radionuclides from Nuclear Waste Solutions with Inorganic Ion Exchangers. Radiochimica Acta. 86. doi:10.1524/ract.1999.86.12.65

Lehto, J., and Hou, X. (2010). Chemistry and Analysis of Radionuclides. Wiley-VCH Verlag GmbH and Co. KGaA. doi.org/10.1002/9783527632770

Leipe, T., Tauber, F., Vallius, H., Virtasalo, J., Uścinowicz, S., Kowalski, N., Hille, S., Lindgren, S., and Myllyvirta, T. (2010). Particulate organic carbon (POC) in surface sediments of the Baltic Sea. Geo-Marine Letters, 31(3), 175–188. doi.org/10.1007/s00367-010-0223-x

Leppäranta, M., and Myrberg, K. (2009). Physical oceanography of the Baltic Sea. Springer Science and Business Media

Levin, C. (2004). Basic Physics of Radionuclide Imaging. W Emission Tomography (s. 53–88). Elsevier. doi.org/10.1016/B978-012744482-6.50007-7

Lieser, K. H. (2008). Nuclear and radiochemistry: fundamentals and applications. John Wiley and Sons

Ligero, R. A., Barrera, M., and Casas-Ruiz, M. (2005). Levels of ^{137}Cs in muddy sediments of the seabed of the Bay of Cádiz, Spain. Part I. Vertical and spatial distribution of activities. Journal of Environmental Radioactivity, 80(1), 75–86. doi.org/10.1016/j.jenvrad.2004.05.019

Livens, F. R., and Singleton, D. L. (1989). Evaluation of methods for the radiometric measurement of americium-241 in environmental samples. The Analyst, 114(9), 1097. doi.org/10.1039/an9891401097

Livingston, H. D., and Povinec, P. P. (2000). Anthropogenic marine radioactivity. Ocean and Coastal Management, 43(8-9), 689–712. doi.org/10.1016/s0964-5691(00)00054-5

Livingston, H. D., and Povinec, P. P. (2002). A millennium perspective on the contribution of global fallout radionuclides to ocean science. Health Physics, 82(5), 656–668. doi.org/10.1097/00004032-200205000-00012

Lujanas, V., Mastauskas, A., Lujaniene, G., Spirkauskaite, N. (1994). Development of radiation in Lithuania. J. Environ. Radioact. 23, 249–263. doi.org/10.1016/ 0265-931X(94)90065-5

Lujanienė, G., Aninkevicius, V., Lujanas, V. (2009). Artificial radionuclides in the atmosphere over Lithuania. J. Environ. Radioact., 100, 108-119. doi:10.1016/j.jenvrad.2007.07.015

Lujanienė, G., Beneš, P., Štamberg, K., Jokšas, K., and Kulakauskaitė, I. (2012a). Pu and Am sorption to the Baltic Sea bottom sediments. Journal of Radioanalytical and Nuclear Chemistry, 295(3), 1957–1967. doi.org/10.1007/s10967-012-2281-1

Lujanienė, G., Byčenkienė, S., Povinec, P.P., Gera, M. (2012b). Radionuclides from the Fukushima accident in the air over Lithuania: measurement and modelling approaches. J. Environ. Radioact. 114, 71–80. doi.org/10.1016/j. jenvrad.2011.12.004

Lujanienė, G., Remeikaitė-Nikienė, N., Garnaga, G., Jokšas, K., Šilobritienė, B., Stankevičius, A., Šemčuk, S., and Kulakauskaitė, I. (2014). Transport of ^{137}Cs, ^{241}Am and Pu isotopes in the Curonian Lagoon and the Baltic Sea. Journal of Environmental Radioactivity, 127, 40–49. doi.org/10.1016/j.jenvrad.2013.09.013

Lujanienė, G., Sapolaite, J., Remeikis, V., Lujanas, V., Jermolajev, A. (2006). Cesium, americium, and plutonium isotopes in ground level air of Vilnius. Czech. J. Physics, 56(Suppl. D), D55-D61. doi:10.1007/s10582-006-1077-3

Lundberg C., (2005). Eutrophication in the Baltic Sea from area-specific biological effects to interdisciplinary consequences. Environmental and Marine Biology, Department of Biology, Åbo Akademi University, Finland

Mabit, L., Benmansour, M., Abril, J. M., Walling, D. E., Meusburger, K., Iurian, A. R., Bernard, C., Tarján, S., Owens, P. N., Blake, W. H., and Alewell, C. (2014). Fallout 210Pb as a soil and sediment tracer in catchment sediment budget investigations: A review. Earth-Science Reviews, 138, 335–351. doi.org/10.1016/j.earscirev.2014.06.007

Magill, J., Galy, J. (2005). Radioactivity, Radionuclides, Radiation. Springer-Verlag Berlin Heidelberg and European Communities, Karlsruhe, p. 62

Majewski, A. (1987). Charakterystyka wód. W: Bałtyk Południowy.(Characteristics of waters. In: The Southern Baltic)

Malátová, I., and Bečková, V. (2014). Americium. W Encyclopedia of Toxicology (s. 182–186). Elsevier. doi.org/10.1016/b978-0-12-386454-3.01162-3

Marks, L., Bitinas, A., Błaszkiewicz, M., Börner, A., Guobyte, R., Rinterknecht, V., and Tylmann, K. (2022). Glacial landscapes of Northern Central Europe. W European Glacial Landscapes (s. 45–51). Elsevier. doi.org/10.1016/b978-0-12-823498-3.00007-8

Martin, J.M., Thomas, A.J. (1990). Origins, concentrations, and distributions of artificial radionuclides discharged by the Rhone River to the Mediterranean Sea. J. Environ. Radioact. 11, 105–139. doi.org/10.1016/0265-931X(90)90056-2

Maslowski, Wieslaw and Walczowski, Waldemar. (2001). Circulation of the Baltic Sea and its connection to the Pan-Arctic region - A large scale and high-resolution modeling approach. Boreal Environmental Research. 7.

Masson, O., Baeza, A., Bieringer, J., Brudecki, K., Bucci, S., Cappai, M., Carvalho, F.P., Connan, O., Cosma, C., Dalheimer, A., Didier, D., Depuydt, G., De Geer, L.E., DeVismes, A., Gini, L., Groppi, F., Gudnason, K., Gurriaran, R., Hainz, D.,

Halldorsson, O., Hammond, D., Hanley, O., Holey, K., Homoki, Zs, Ioannidou, A., Isajenko, K., Jankovick, M., Katzlberger, C., Kettunen, M., Kierepko, R., Kontro, R., Kwakman, P.J.M., Lecomte, M., Leon Vintro, L., Leppanen, A.-P., Lind, B., Lujaniene, G., Mc Ginnity, P., Mc Mahon, C., Mala, H., Manenti, S., Manolopoulou, M., Mattila, A., Mauring, A., Mietelski, J.W., Møller, B.S., Nielsen, P., Nikolick, J., Overwater, R.M.W., Palsson, S.E., Papastefanou, C., Penev, I., Pham, M. K., Povinec, P.P., Rameback, H., Reis, M.C., Ringer, W., Rodriguez, A., Rulík, P., Saey, P.R.J., Samsonov, V., Schlosser, C., Sgorbati, G., Silobritiene, B.V., Soderstrom, C., Sogni, R., Solier, L., Sonck, M., Steinhauser, G., Steinkopff, T., Steinmann, P., Stoulos, S., Sykora, I., Todorovic, D., Tooloutalaie, N., Tositti, L., Tschiersch, J., Ugron, A., Vagena, E., Vargas, A., Wershofen, A.H., Zhukova, O. (2011). Tracking of airborne radionuclides from the damaged Fukushima Dai-ichi nuclear reactors by European Networks. Environ. Sci. Technol. 45, 7670–7677. doi.org/10.1021/es2017158

Mattsson, S., Eriksson Stenström, K., and Bernhardsson, C. (2018). Chernobyl and Fukushima – A Swedish perspective. Proceedings of the International Conference "Environmental Radioactivity – Experience from Japan and Sweden"

McKay, W., and Walker, M. (1990). Plutonium and americium behaviour in Cumbrian near-shore waters. Journal of Environmental Radioactivity, 12(3), 267–283. doi.org/10.1016/0265-931x(90)90026-r

Meier, H. E. M., Andersson, H. C., Eilola, K., Gustafsson, B. G., Kuznetsov, I., Müller-Karulis, B., Neumann, T., and Savchuk, O. P. (2011). Hypoxia in future climates: A model ensemble study for the Baltic Sea. Geophysical Research Letters, 38(24), n/a. doi.org/10.1029/2011gl049929

Meier, H. E. M., Eilola, K., Almroth-Rosell, E., Schimanke, S., Kniebusch, M., Höglund, A., Pemberton, P., Liu, Y., Väli, G., and Saraiva, S. (2018). Disentangling the impact of nutrient load and climate changes on Baltic Sea hypoxia and eutrophication since 1850. Climate Dynamics, 53(1-2), 1145–1166. doi.org/10.1007/s00382-018-4296-y

Meyer H, Lampe R (1999) The restricted buffer capacity of a South Baltic estuary–the Oder Estuary. Limnologica 29:242–248

Mietelski, J. W., Dorda, J., Wąs, B. (1999). Pu-241 in samples of forest soil from Poland. Applied Radiation and Isotopes, 51(4), 435–447. doi.org/10.1016/s0969-8043(99)00055-x

Mietelski, J. W., Gaca, P., Jasińska, M. (2000). Plutonium and other alpha-emitters in bones of wild, herbivorous animals from north-eastern Poland. Applied Radiation and Isotopes, 53(1-2), 251–257. doi.org/10.1016/s0969-8043(00)00140-8

Mietelski, J.W., Wąs, B. (1995). Plutonium from Chernobyl in Poland. Appl. Radiat. Isot., 46(11), 1203-1211. doi:10.1016/0969-8043(95)00162-7

Mihai, S., and Hurtgen, C. (1997). Plutonium and americium in sediment samples along the Romanian sector of the Danube river and the Black Sea coast. Journal of Radioanalytical and Nuclear Chemistry, 222(1-2), 275–278. doi.org/10.1007/bf02034286

Milan, C.S., Swenson, E.M., Turner, R.E., Lee, J.M. (1995). Assessment of the ^{137}Cs method for estimating sediment accretion rates: Louisiana salt marshes. J. Coast Res. 11, 296-307

Mincher, B. J., Martin, L. R., and Schmitt, N. C. (2008). Tributylphosphate Extraction Behavior of Bismuthate-Oxidized Americium. Inorganic Chemistry, 47(15), 6984–6989. doi.org/10.1021/ic800667h

Mincher, B. J., Schmitt, N. C., Tillotson, R. D., Elias, G., White, B. M., and Law, J. D. (2014). Characterizing Diamylamylphosphonate (DAAP) as an Americium Ligand for Nuclear Fuel-Cycle Applications. Solvent Extraction and Ion Exchange, 32(2), 153–166. doi.org/10.1080/07366299.2013.850288

Missiaen, T., and Noppe, L. (2009). Detailed seismic imaging of a chemical munition dumpsite in the Bornholm Basin, south-western Baltic. Environmental Earth Sciences, 60(1), 81–94. doi.org/10.1007/s12665-009-0171-9

Mitchell, P. I., Vives i. Batlle, J., Downes, A. B., Condren, O. M., León Vintró, L., and Sánchez-Cabeza, J. A. (1995). Recent observations on the physico-chemical speciation of plutonium in the Irish Sea and the western Mediterranean. Applied Radiation and Isotopes, 46(11), 1175–1190. doi.org/10.1016/0969-8043(95)00160-f

Mitchell, P.I., Batlle, J.V., Ryan, T.P., Schell, W.R., Sanchez-Cabeza, J.A., Vidal-Quadras, A. (1991). Studies on the Speciation of Plutonium and Americium in the Western Irish Sea. In: Kershaw, P.J., Woodhead, D.S. (eds) Radionuclides in the Study of Marine Processes. Springer, Dordrecht. doi.org/10.1007/978-94-011-3686-0_5

Mojski, J.E., Dadlez, R., Słowańska, B., Uścinowicz, S., Zachowicz, J. (Eds.). (1995) Geological atlas of the southern Baltic, 1:500000. (pp. 1–63). Pol. Geol. Inst., Sopot-Warszawa. (In Polish)

Molero, J., Sanchez-Cabeza, J.A., Morino, J., Vives Batlle, J., Mitchell, P.I., Vidal-Quadras, A. (1995). Particulate distribution of plutonium and americium in surface water from the Spanish Mediterranean Coast. J. Environ. Radioact. 28, 271–283. doi.org/10.1016/0265-931X(95)97299-R

Møller, J.S., and Hansen, I.S. (2011). Hydrographic processes and changes in the Baltic Sea

Moore, F. L. (1963). Separation of Americium from Other Elements. Application to the Purification and Radiochemical Determination of Americium. Analytical Chemistry, 35(6), 715–719. doi.org/10.1021/ac60199a010

Moreno, J., Vajda, N., Danesi, P.R., Larosa, J.J., Zeiller, E., Sinojmeri, M. (1997). Combined procedure for the determination of ^{90}Sr, ^{241}Am, and Pu radionuclides in soil samples. J. Radioanal. Nucl. Chem., 226, 279-284. doi:10.1007/BF02063661

Moros, M., Andersen, T. J., Schulz-Bull, D., Häusler, K., Bunke, D., Snowball, I., Kotilainen, A., Zillén, L., Jensen, J. B., Kabel, K., Hand, I., Leipe, T., Lougheed, B. C., Wagner, B., Arz, H. W. (2016). Towards an event stratigraphy for Baltic Sea sediments deposited since AD 1900: approaches and challenges. Boreas, 46(1), 129–142. doi.org/10.1111/bor.12193

Munsiri, P., Boyd, C. E., Hajek, B. F. (1995). Physical and Chemical Characteristics of Bottom Soil Profiles in Ponds at Auburn, Alabama, USA and a Proposed System for Describing Pond Soil Horizons. Journal of the World Aquaculture Society, 26(4), 346–377. doi.org/10.1111/j.1749-7345.1995.tb00831.x

Muravitsky, A.V., Razbudey, V.F., Tokarevsky, V.V., Vorona, P.N. (2005). Time-dependent ^{241}Am activity in the environment from decay of ^{241}Pu released in the

Chernobyl accident. Appl. Radiat. Isot., 63(4), 487-492. doi:10.1016/j.apradiso.2005.03.018

Murray, C. J., Müller-Karulis, B., Carstensen, J., Conley, D. J., Gustafsson, B. G., and Andersen, J. H. (2019). Past, Present, and Future Eutrophication Status of the Baltic Sea. Frontiers in Marine Science, 6. doi.org/10.3389/fmars.2019.00002

Mushtaq, A. (2004). Inorganic ion-exchangers: Their role in chromatographic radionuclide generators for the decade 1993-2002. Journal of Radioanalytical and Nuclear Chemistry, 262(3), 797–810. doi.org/10.1007/s10967-004-0513-8

Musikas, C., Le Marois, G., Fitoussi, R., and Cuillerdier, C. (1980). Properties and uses of nitrogen and sulfur donors ligands in actinide separations. W ACS symposium series (s. 131–145). American chemical society. doi.org/10.1021/bk-1980-0117.ch010

Myasoedov, B. F., Lebedev, I. A., Khizhnyak, P. L., Timofeev, G. A., and Frenkel, V. Y. (1986). Electrochemical oxidation of americium and californium in carbonate solutions. Journal of the Less Common Metals, 122, 189–193. doi.org/10.1016/0022-5088(86)90408-x

National Center for Biotechnology Information (2024). Periodic Table of Elements. Retrieved January 12, 2024 from pubchem.ncbi.nlm.nih.gov/periodic-table/

Neacsu, E. (2020). Quality Assurance of Analytical Measurements—A Vital Element in Safety Performance in the Nuclear Field. Proceedings, 55(1), 2. doi.org/10.3390/proceedings2020055002

Nealson, K. H., Belz, A., and McKee, B. (2002). Antonie van Leeuwenhoek, 81(1/4), 215–222. doi.org/10.1023/a:1020518818647

Nielsen, S. P., Bengtson, P., Bojanowsky, R., Hagel, P., Herrmann, J., Ilus, E., Jakobson, E., Motiejunas, S., Panteleev, Y., Skujina, A., and Suplinska, M. (1999). The radiological exposure of man from radioactivity in the Baltic Sea. Science of The Total Environment, 237-238, 133–141. doi.org/10.1016/s0048-9697(99)00130-8

Nielsen, S.P., Karlberg, O., and Øhlenschlæger., (1995). Modelling the transfer of radionuclides in the Baltic Sea (Baltic Sea Environment Proceedings No. 61). Helsinki Commission

Nilsson H, Ramebäck H, Skålberg M. (2001). An improved method for α-source preparation using neodymium fluoride coprecipitation. Nucl Instrum Methods Phys Res A 462:397-404. doi.org/10.1016/S0168-9002(01)00184-X

OECD, 1995. Chernobyl ten years on. NEA Committee on Radiation Protection and Public Health. OECD Nuclear Energy Agency.

Ojovan, M. I., Lee, W. E., and Kalmykov, S. N. (2019). Nuclear Decay. W An Introduction to Nuclear Waste Immobilisation (s. 9–22). Elsevier. doi.org/10.1016/b978-0-08-102702-8.00002-9

Olszewski, G., Andersson, P., Lindahl, P., and Eriksson, M. (2018). On the distribution and inventories of radionuclides in dated sediments around the Swedish coast. Journal of Environmental Radioactivity, 186, 142–151. doi.org/10.1016/j.jenvrad.2017.09.025

Osiński R., (2007) Baltic dynamics simulated by the coupled ocean-ice numerical model. PhD thesis, Institute of Oceanology, Polish Academy of Sciences.

Parrington, J.R., Knox, H.D., Breneman, S.L., Feiner, F., and Baum, E.M. (1996). Nuclides and Isotopes: Chart of the Nuclides (15th ed.). Lockheed Martin and General Electric

Penneman, R. A., and Keenan, T. K. (1960). THE RADIOCHEMISTRY OF AMERICIUM AND CURIUM. Office of Scientific and Technical Information (OSTI). doi.org/10.2172/4187189

Pentreath, R.J., Woodhead, D.S., Kershaw, P.J., Jefferies, D.F., Lovett, M.B. (1986). The behaviour of plutonium and americium in the Irish Sea. Rapports et Processes-verbaux des Re´unions du Conseil

Piechura J, Walczowski W, Beszczyńska-Möller A (1997) On the structure and dynamics of the water in the Słupsk Furrow. Oceanologia 39:35–54

Piekarz, M., Komosa, A. (2014). Rapid method for plutonium-241 determination in soil samples. Journal of Radioanalytical and Nuclear Chemistry, 299(3), 2019–2021. doi.org/10.1007/s10967-013-2907-y

Playford K., Lewis G.N., Carpenter R.C., 1990. Radioactive fallout in air and rain. Results to the end of 1989. UK Atomic Energy Authority, Environment and Energy, Harwell Laboratory, AEA-EE-0227

Polak-Juszczak, L. (2012). Bioaccumulation of mercury in the trophic chain of flatfish from the Baltic Sea. Chemosphere, 89(5), 585–591 doi.org/10.1016/j.chemosphere.2012.05.057

Polikarpov, G.G., Egorov, V.N., Gulin, S.B., Stokozov, N.A., Lazorenko, G.E., Mirzoeva, N. Yu, Tereshchenko, N.N., Tsytsugina, V.G., Kulebakina, L.G., Popovichev, V.N., Korotkov, A.A., Evtushenko, D.B., Zherko, N.V., Malakhova, L.V. (2008). Radioecological Response of the Black Sea to the Chernobyl Accident. In: Polikarpov, G.G., Egorov, V.N. (Eds.), ECOSI-gidrofizika, Sevastopol

Pöllänen, R., Valkama, I., Toivonen, H. (1997). Transport of radioactive particles from the Chernobyl accident. Atmos. Environ. 31, 3575–3590. doi.org/10.1016/ s1352-2310(97)00156-8

Prăvălie, R. (2014). Nuclear Weapons Tests and Environmental Consequences: A Global Perspective. AMBIO, 43(6), 729–744. doi.org/10.1007/s13280-014-0491-1

Qi, D. (2018). Ion-Exchange and Extraction Chromatography Separation of Rare Earth Elements. W Hydrometallurgy of Rare Earths (s. 631–669). Elsevier. doi.org/10.1016/b978-0-12-813920-2.00006-4

Quevauviller, P., Benoliel, M.-J., Andersen, K., Merry, J. (1999). New certified reference materials for the quality control of groundwater monitoring. TrAC Trends in Analytical Chemistry, 18(6), 376–383. doi.org/10.1016/s0165-9936(99)00106-5

RADNET, 1996. A freedom of nuclear information resource. Center for Biological Monitoring, Hulls Cove, ME 04644 (/home.acadia.net/user-pages/jbrown/rad.html)

Rak, D., and Wieczorek, P. (2012). Variability of temperature and salinity over the last decade in selected regions of the southern Baltic Sea. Oceanologia, 54(3), 339–354. doi.org/10.5697/oc.54-3.339

Rana, V., Milke, J., and Gałczyńska, M. (2021). Inorganic and Organic Pollutants in Baltic Sea Region and Feasible Circular Economy Perspectives for Waste Management: A Review. W Handbook of Solid Waste Management (s. 1–35). Springer Singapore. doi.org/10.1007/978-981-15-7525-9_80-1

Ray, D., Leary, P., Livens, F. R., Gray, N., Morris, K., Law, K., Fuller, A. J., Abrahamsen-Mills, L., Howe, J., Tierney, K. M., Muir, G. K., and Law, G. T. W. (2020). Controls on anthropogenic radionuclide distribution in the Sellafield-impacted Eastern Irish Sea. Science of the Total Environment, 743, 140765. doi.org/10.1016/j.scitotenv.2020.140765

Reinikainen, P., Meriläinen, J. J., Virtanen, A., Veijola, H., Äystö, J. (1997). Accuracy of ^{210}Pb dating in two annually laminated lake sediments with high Cs background. Applied Radiation and Isotopes, 48(7), 1009–1019. doi.org/10.1016/s0969-8043(96)00337-5

Renshaw, J. C., Handley-Sidhu, S., and Brookshaw, D. R. (2011). Chapter 7. Pathways of Radioactive Substances in the Environment. W Issues in Environmental Science and Technology (s. 152–176). Royal Society of Chemistry. doi.org/10.1039/9781849732888-00152

Renshaw, J. C., Lloyd, J. R., and Livens, F. R. (2007). Microbial interactions with actinides and long-lived fission products. Comptes Rendus Chimie, 10(10–11), 1067–1077. doi.org/10.1016/j.crci.2007.02.013

Reponen, A., Jantunen, M., Paatero, J., and Jaakkola, T. (1993). Plutonium fallout in Southern Finland after the Chernobyl accident. Journal of Environmental Radioactivity, 21, 119. doi:10.1016/0265-931X(93)90049-D

Ristic, M., Degetto, S., Cantallupi, C. (2002). Sample preparation for the determination of ^{241}Am in sediments utilizing gamma-spectroscopy. J. Environ. Radioact., 59(2), 179-189. doi:10.1016/s0265-931x(01)00070-4

Robbins, J. A., Edgington, D. N. (1975). Determination of recent sedimentation rates in Lake Michigan using Pb-210 and Cs-137. Geochimica et Cosmochimica Acta, 39(3), 285–304. doi.org/10.1016/0016-7037(75)90198-2

Runde, W. (2010). Americium and Curium: Radionuclides. 10.1002/0470862106.ia742.

Runde, W. H., and Mincher, B. J. (2011). Higher Oxidation States of Americium: Preparation, Characterization and Use for Separations. Chemical Reviews, 111(9), 5723–5741. doi.org/10.1021/cr100181f

Runde, W.H., Schulz, W.W. (2008). Americium. In: Morss, L.R., Edelstein, N.M., Fuger, J. The Chemistry of the Actinide and Transactinide Elements. Springer, Dordrecht. doi.org/10.1007/1-4020-3598-5_8

Sabatier, P., Dezileau, L., Blanchemanche, P., Siani, G., Condomines, M., Bentaleb, I., Piquès, G. (2010). Holocene Variations of Radiocarbon Reservoir Ages in a Mediterranean Lagoonal System. Radiocarbon, 52(1), 91–102. doi.org/10.1017/s0033822200045057

Salbu, B. (2009). Fractionation of radionuclide species in the environment. Journal of Environmental Radioactivity, 100(4), 283–289. doi.org/10.1016/j.jenvrad.2008.12.013

Saniewski, M., Zalewska, T. (2018). Budget of ^{90}Sr in the Gulf of Gdańsk (southern Baltic Sea). Oceanologia 60, 256–263. doi.org/10.1016/j.oceano.2017.11.002

Saxen, R., Ilus, E. (2001). Discharge of ^{137}Cs and ^{90}Sr by Finnish rivers to the Baltic Sea in 1986-1996. J. Environ. Radioact. 54, 275–291. 10.1016/s0265-931x(00)00154-5

Schenck L.M., and Youmans R.A. 2012. From start to finish: A historical review of nuclear arms control treaties and starting over with the new start. Journal of International and Comparative Law 20(2): 399–435

Schnetger, B., Häusler, K., and Dellwig, O. (2013). ^{241}Am supporting ^{210}Pb and ^{137}Cs dating. Paper presented at the Goldschmidt 2013 Conference, Florence, Italy

Schulz, W. W. (1976). Chemistry of americium. Office of Scientific and Technical Information (OSTI). doi.org/10.2172/7232133

Scott, R. A. (2011). Encyclopedia of Inorganic and Bioinorganic Chemistry. Wiley and Sons, Limited, John

Seaborg, G. T. (1946). The Transuranium Elements. Science, 104(2704), 379–386. doi.org/10.1126/science.104.2704.379

Seaborg, GT. (1991). Actinides and transactinides. Fourth ed., Vol. 1. Encyclopedia of chemical technology, 412-445

Seppälä, M. (Ed.) (2005). *The physical geography of Fennoscandia*. (Oxford regional environments). Oxford University Press.

Shahidi, D., Roy, R., and Azzouz, A. (2015). Advances in catalytic oxidation of organic pollutants – Prospects for thorough mineralization by natural clay catalysts. Applied Catalysis B: Environmental, 174-175, 277–292. doi.org/10.1016/j.apcatb.2015.02.042

Shehee, T. C., Martin, L. R., and Nash, K. L. (2010). Solid-liquid separation of oxidized americium from fission product lanthanides. IOP Conference Series: Materials Science and Engineering, 9, 012066. doi.org/10.1088/1757-899x/9/1/012066

Sill, C.W. (1987). Precipitation of actinides as fluorides or hydroxides for high resolution alpha spectrometry. Nuclear Chem. Waste Mgmt 7, 201

Silva, R. J., and Nitsche, H. (1995). Actinide Environmental Chemistry. Radiochimica Acta, 70-71(s1). doi.org/10.1524/ract.1995.7071.s1.377

Sinkko, K., Aatonen, H., Mustonen, R., Taipale, T.K., Juutilainen, J. (1987). Airborne Radioactivity in Finland after the Chernobyl Accident in 1986. Supplement 1 to Annual Report STUK-A55. STUK-A56, p. 42. inis.iaea.org/collection/ NCLCollectionStore/_Public/19/001/19001530.pdf

Skwarzec, B. (2010). Determination of radionuclides in aquatic environment. In J. Namieśnik P. Szefer (Eds.), Analytical Measurement in Aquatic Environments. CRC Press, Taylor Francis Group

Skwarzec, B., Jahnz-Bielawska, A., Strumińska-Parulska, D.I. (2011). The inflow of ^{238}Pu and $^{239+240}$Pu from the Vistula River catchment area to the Baltic Sea. J. Environ. Radioact., 102(8), 728-734. doi:10.1016/j.jenvrad.2011.03.017

Skwarzec, B., Strumińska, D. I., and Prucnal, M. (2003). Estimates of 239+240Pu inventories in Gdańsk bay and Gdańsk basin. Journal of Environmental Radioactivity, 70(3), 237–252. doi.org/10.1016/s0265-931x(03)00107-3

Smith, J. N. (2001). Why should we believe ^{210}Pb sediment geochronologies? Journal of Environmental Radioactivity, 55(2), 121–123. doi.org/10.1016/s0265-931x(00)00152-1

Snelgrove, P. V. R. (1999). Getting to the Bottom of Marine Biodiversity: Sedimentary Habitats. BioScience, 49(2), 129. doi.org/10.2307/1313538

Snoeijs-Leijonmalm, P., and Andrén, E. (2017). Why is the Baltic Sea so special to live in? W Biological Oceanography of the Baltic Sea (s. 23–84). Springer Netherlands. doi.org/10.1007/978-94-007-0668-2_2

Steinbauer, E., Bortels, G., Bauer, P., Biersack, J. P., Burger, P., and Ahmad, I. (1994). A survey of the physical processes which determine the response function of silicon detectors to alpha particles. Nuclear Instruments and Methods in Physics Research Section A: Accelerators, Spectrometers, Detectors and Associated Equipment, 339(1-2), 102–108. doi.org/10.1016/0168-9002(94)91787-6

Stephanou, S. E., and Penneman, R. A. (1952). Observations on Curium Valence States; A Rapid Separation of Americium and Curium1. Journal of the American Chemical Society, 74(14), 3701–3702. doi.org/10.1021/ja01134a514

Stokely, J. R., and Moore, F. L. (1967). New separation method for americium based on liquid-liquid extraction behavior of americium(V). Analytical Chemistry, 39(8), 994–997. doi.org/10.1021/ac60252a027

Strumińska-Parulska, D. I. (2014). Vertical distribution of ^{241}Pu in the southern Baltic Sea sediments. Marine Pollution Bulletin, 89(1-2), 12–15. doi.org/10.1016/j.marpolbul.2014.10.016

Strumińska-Parulska, D., Skwarzec, B., Pawlukowska, M. (2012) Plutonium fractionation in southern Baltic Sea sediments, Isot. Environ. Health Stud., 48:4, 526-542, doi:10.1080/10256016.2012.683524

Strumińska-Parulska, D.I., Skwarzec, B. (2013). Plutonium ^{241}Pu in the biggest Polish rivers. J. Radioanal. Nucl. Chem., 298(3), 1693-1703. doi:10.1007/s10967-013-2566-z

Stumpf, S., Billard, I., Gaillard, C., Panak, P. J., and Dardenne, K. (2008). TRLFS and EXAFS investigations of lanthanide and actinide complexation by triflate and

perchlorate in an ionic liquid. Radiochimica Acta, 96(1/2008), 1–10. doi.org/10.1524/ract.2008.1461

Suplińska, M. M., Pietrzak-Flis, Z. (2008). Sedimentation rates and dating of bottom sediments in the Southern Baltic Sea region. Nukleonika, 53, suppl. 2, 105–111

Suplińska, M.M., Pietrzak-Flis, Z. (2008). Sedimentation rates and dating of bottom sediments in the Southern Baltic Sea region, Nukleonika. 53, S105-S111

Suplińska, Maria. (2002). Vertical distribution of ^{137}Cs, ^{210}Pb, ^{226}Ra and ^{239,240}Pu in bottom sediments from the Southern Baltic Sea in the years 1998-2000. Nukleonika. 47. 45-52

Szefer, P. (2002). Metals, metalloids and radionuclides in the Baltic Sea ecosystem. Amsterdam-London-New York-Oxford-Paris-Shannon-Tokyo: Elsevier

Szmytkiewicz, A., and Zalewska, T. (2014). Sediment deposition and accumulation rates determined by sediment trap and 210Pb isotope methods in the Outer Puck Bay (Baltic Sea). Oceanologia, 56(1), 85–106. doi.org/10.5697/oc.56-1.085

Szymczak, E., and Galińska, D. (2013). Sedimentation of suspensions in the Vistula River mouth. Oceanological and Hydrobiological Studies, 42(2). doi.org/10.2478/s13545-013-0075-x

Szymczak-Żyła, M., Krajewska, M., Witak, M., Ciesielski, T. M., Ardelan, M. V., Jenssen, B. M., Goslar, T., Winogradow, A., Filipkowska, A., Lubecki, L., Zamojska, A., and Kowalewska, G. (2019). Present and Past-Millennial Eutrophication in the Gulf of Gdańsk (Southern Baltic Sea). Paleoceanography and Paleoclimatology, 34(2), 136–152. doi.org/10.1029/2018pa003474

Talipova, T. G., Pelinovsky, E. N., and Kouts, T. (1998). Kinematic characteristics of an internal wave field in the Gotland Deep in the Baltic Sea. Okeanologiya, 38(1), 33–42.

Taylor, J. K. (2018). Quality Assurance of Chemical Measurements. Routledge. doi.org/10.1201/9780203741610

Thakkar, A. H. (2002). Journal of Radioanalytical and Nuclear Chemistry, 252(2), 215–218. doi.org/10.1023/a:1015737516054

Thamdrup, B., Glud, R. N., and Hansen, J. W. (1994). Manganese oxidation and in situ fluxes from a coastal sediment. Geochimica et Cosmochimica Acta, 58, 2563-2570.

The BACC II Author Team (Red.). (2015). Second Assessment of Climate Change for the Baltic Sea Basin. Springer International Publishing. doi.org/10.1007/978-3-319-16006-1

Thiels G. M., Murray C. N., Vanderborght O. L. J. (1984). The effect of water acidity and seasonal variability on the distribution of ^{241}Am in the freshwater snail Lymnaea stagnalis L. Health Phys 47(3):485-487

Tian, G., Zhu, Y., Xu, J., Hu, T., and Xie, Y. (2002). Characterization of extraction complexes of Am(III) with dialkyldithiophosphinic acids by extended X-ray absorption fine structure spectroscopy. Journal of Alloys and Compounds, 334(1-2), 86–91. doi.org/10.1016/s0925-8388(01)01783-2

Uğur (Tanbay), A., and Yener, G. (2002). Journal of Radioanalytical and Nuclear Chemistry, 252(1), 47–51. doi.org/10.1023/a:1015227502483

UNSCEAR. (1982). Report to the general assembly (ANNEX E—Exposures resulting from nuclear explosions). /www.unscear.org/unscear/en/publications/1982.html. Retrieved January 2024

UNSCEAR. (1988). Report to the general assembly (Annex D—Exposures from Chernobyl accident). /www.unscear.org/docs/reports/1988/1988i_unscear.pdf.Retrieved January 2024

UNSCEAR. (1993). Report to the general assembly (Annex B—Exposures from man-made sources of radiation). /www.unscear.org/docs/reports/1993/1993c_pages%2091-120.pdf. Retrieved January, 2024

UNSCEAR. (2000). Report to the general assembly (Annex C—Exposures to the public from man-made sources of radiation). /www.unscear.org/docs/reports/annexc.pdf. Retrieved January 2024

Uścinowicz S. (1997). Basen Gdański. Przegląd Geologiczny 45(6): 589–594

Uścinowicz S., Ebbing J., Laban C. and Zachowicz J. (1998). Recent Muds of the Gulf of Gdansk. Baltica. 11. 25-32

Uścinowicz, S. (2011). Geochemistry of Baltic Sea surface sediments. Polish Geological Institute - National Research Institute

Uścinowicz, S. (2014). Chapter 7 The Baltic Sea continental shelf. Geological Society, London, Memoirs, 41(1), 69–89. doi.org/10.1144/m41.7

Uścinowicz, S., Szefer, P., and Sokołowski, K. (2011). Trace elements in the Baltic Sea sediments. Geochemistry of surface sediments of the Baltic Sea, 214-274

USSR. (1986). State committee on the utilization of atomic energy: the accident at the Chernobyl nuclear power plant and its consequences. IAEA Experts Meet. Vienna inis.iaea.org/collection/NCLCollectionStore/_Public/18/001/18 00171.pdf

Vajda, N., and Kim, C. K. (2011). Determination of Pu isotopes by alpha spectrometry: a review of analytical methodology. Journal of Radioanalytical and Nuclear Chemistry, 283(1), 203–223. doi.org/10.1007/s10967-009-0342-x

Vajda, N., Martin, P., and Kim, C.-K. (2012). Alpha Spectrometry. W Handbook of Radioactivity Analysis (s. 363–422). Elsevier. doi.org/10.1016/b978-0-12-384873-4.00006-2

Vajda, N., Pöllänen, R., Martin, P., and Kim, C.-K. (2020). Alpha spectrometry. W Handbook of Radioactivity Analysis (s. 493–573). Elsevier. doi.org/10.1016/b978-0-12-814397-1.00005-4

Vives i Batlle, J., Wilson, R. C., Watts, S. J., Jones, S. R., McDonald, P., and Vives-Lynch, S. (2008). Dynamic model for the assessment of radiological exposure to marine biota. Journal of Environmental Radioactivity, 99(11), 1711–1730. doi.org/10.1016/j.jenvrad.2007.11.002

Vreček, P., Benedik, L. Evaluation of measurement uncertainty in the determination of ^{210}Pb and ^{210}Po using beta counting and alpha spectrometry. Accred Qual Assur 8, 134–137 (2003). doi.org/10.1007/s00769-002-0577-5

Vuorinen, I. (2018). Post-Glacial Baltic Sea Ecosystems. Oxford University Press. doi.org/10.1093/acrefore/9780190228620.013.675

Walker, R., Lumley, I. (1999). Pitfalls in terminology and use of reference materials. TrAC Trends in Analytical Chemistry, 18(9-10), 594–616. doi.org/10.1016/s0165-9936(99)00158-2

Wang, H., Ni, Y., Men, W., Wang, Z., Liu, M., Xiao, D., Zheng, J. (2022). Distributions of fallout ^{137}Cs, $^{239+240}Pu$ and ^{241}Am in a soil core from South Central China. Journal of Environmental Radioactivity, 251-252, 106971. doi.org/10.1016/j.jenvrad.2022.106971

Warren, L. A., and Haack, E. A. (2001). Biogeochemical controls on metal behaviour in freshwater environments. Earth-Science Reviews, 54(4), 261–320. doi.org/10.1016/s0012-8252(01)00032-0

Warwick, P. E., Croudace, I. W., and Carpenter, R. (1996). Review of analytical techniques for the determination of americium-241 in soils and sediments. Applied Radiation and Isotopes, 47(7), 627–642. doi.org/10.1016/0969-8043(96)00023-1

Warwick, P. E., Croudace, I. W., and Oh, J. S. (2001). Radiochemical Determination of ^{241}Am and Pu(α) in Environmental Materials. Analytical Chemistry, 73(14), 3410–3416. doi.org/10.1021/ac001510e

Waugh, W. J., Carroll, J., Abraham, J. D., and Landeen, D. S. (1998). Applications of dendrochronology and sediment geochronology to establish reference episodes for evaluations of environmental radioactivity. Journal of Environmental Radioactivity, 41(3), 269–286. doi.org/10.1016/s0265-931x(98)00002-2

Werner, L. B., and Perlman, I. (1951). The Pentavalent State of Americium. Journal of the American Chemical Society, 73(1), 495–496. doi.org/10.1021/ja01145a540

WHO. (1989). Health hazards from radiocesium following the Chernobyl nuclear accident, J. Environ. Radioact., 10, 257-295. doi.org/10.1016/0265-931x(89)90029-5

WHO. (2010). Concise international chemical assessment document 77 (strontium an strontium compounds)

Winsor, P., Rodhe, J., and Omstedt, A. (2001). Baltic Sea ocean climate: an analysis of 100 yr of hydrographic data with focus on the freshwater budget. Climate Research, 18, 5–15. doi.org/10.3354/cr018005

Winterhalter, B. (1992). Late-Quaternary stratigraphy of Baltic Sea basins - a review. Bulletin of the Geological Society of Finland, 64(2), 189–194. doi.org/10.17741/bgsf/64.2.007

Winterhalter, Boris. (2001). On sediment patchiness at the BASYS coring site, Gotland Deep, the Baltic Sea. Baltica. 14. 18-23

Yamato, A. (1982). An anion exchange method for the determination of ^{241}Am and plutonium in environmental and biological samples. J.Radioanal. Nucl. Chem., 75(1-2), 265-273. doi:10.1007/BF02519996

Yoshimochi, H., Nemoto, M., Mondo, K., Koyama, S., and Namekawa, T. (2004). Fabrication Technology for MOX Fuel Containing AmO_2 by an In-cell Remote Process. Journal of Nuclear Science and Technology, 41(8), 850–856. doi.org/10.1080/18811248.2004.9715556

Zaborska, A., Carroll, J., Papucci, C., and Pempkowiak, J. (2007). Intercomparison of alpha and gamma spectrometry techniques used in ^{210}Pb geochronology. Journal of Environmental Radioactivity, 93(1), 38–50. doi.org/10.1016/j.jenvrad.2006.11.007

Zaborska, A., Kosakowska, A., Bełdowski, J., Bełdowska, M., Szubska, M., Walkusz-Miotk, J., Żak, A., Ciechanowicz, A., and Wdowiak, M. (2017). The distribution of heavy metals and ^{137}Cs in the central part of the Polish maritime zone (Baltic Sea) – the area selected for wind farm acquisition. Estuarine, Coastal and Shelf Science, 198, 471–481. doi.org/10.1016/j.ecss.2016.12.007

Zaborska, A., Winogradow, A., Pempkowiak, J. (2014). Caesium-137 distribution, inventories, and accumulation history in the Baltic Sea sediments. J. Environ. Radioact., 127, 11-25. doi:10.1016/j.jenvrad.2013.09.003

Zalewska, T., and Saniewski, M. (2011). Bioaccumulation of ^{137}Cs by benthic plants and macroinvertebrates. Oceanological and Hydrobiological Studies, 40(3), 1–8. doi.org/10.2478/s13545-011-0023-6

Zalewska, T., Lipska, J. (2006). Contamination of the southern Baltic Sea with ^{137}Cs and ^{90}Sr over the period 2000–2004. Journal of Environmental Radioactivity, 91(1-2), 1–14. doi.org/10.1016/j.jenvrad.2006.08.001

Zalewska, T., Przygrodzki, P., Suplińska, M., and Saniewski, M. (2020). Geochronology of the southern Baltic Sea sediments derived from 210Pb dating. Quaternary Geochronology, 56, 101039. doi.org/10.1016/j.quageo.2019.101039

Zalewska, T., Woroń, J., Danowska, B., and Suplińska, M. (2015). Temporal changes in Hg, Pb, Cd, and Zn environmental concentrations in the southern Baltic Sea sediments dated with ^{210}Pb method. Oceanologia, 57(1), 32–43. doi.org/10.1016/j.oceano.2014.06.003

Żarnowiecki, K. (1988). Analiza skażeń promieniotwórczych i zagrożenia radiologicznego w Polsce po awarii elektrowni jądrowej w Czarnobylu; Raport CLOR Nr 120/D

Żbikowski, R., Szefer, P., and Latała, A. (2006). Distribution and relationships between selected chemical elements in green alga Enteromorpha sp. from the southern Baltic. Environmental Pollution, 143(3), 435–448. doi.org/10.1016/j.envpol.2005.12.007

Zhang, H., Hou, X., Qiao, J., Lin, J. (2022) Determination of ^{241}Am in Environmental Samples: A Review. Molecules 27, 4536. doi.org/10.3390/molecules27144536

List of Figures

Figure 1. Periodic table of elements - element of americium highlighted by a bold border (National Center for Biotechnology Information, 2024)..... 12
Figure 2. Production table for ^{241}Am (Parrington et al. 1996)..... 14
Figure 3. Standard reduction potentials of Am at the acidic solution (E_0/V) (Schulz, 1976; Silva et al., 1995)..... 19
Figure 4. Standard reduction potentials of Am at the basic solution (E_0/V) (Penneman and Keenan, 1960; Schulz, 1976)..... 19
Figure 5. Pourbaix diagram (Eh-pH) in a solution in the Am-H_2O-CO_2 system by Runde and Mincher, 2011..... 24
Figure 6. The primary sources of radionuclides in the environment and the fundamental processes that control their mobility in the environment (based on Renshaw et al., 2011)..... 25
Figure 7. In-growth of ^{241}Am from ^{241}Pu as a function of time..... 31
Figure 8. The Baltic Sea drainage basin and location of nuclear reactors and dumping sites for radioactive waste in the area (outline of Baltic Sea from HELCOM website maps.helcom.fi/website/mapservice/)..... 33
Figure 9. The fate of radionuclides in the marine environment, including the principal processes of dry and wet deposition, advection and dispersion, particulate transfer, sedimentation, seabed remobilization, and biological uptake (Batlle et al., 2018)..... 37
Figure 10. A summary of the key geochemical processes controlling radionuclide speciation and some of the factors influencing these processes (Renshaw et al., 2011) 38
Figure 11. Paths of alpha particles in source-detector system (Vajda, 2012)..... 51
Figure 12. Alpha energies of the interfering radionuclides..... 52
Figure 13. Map of the Baltic Sea and the sampling area; P1 – Gdańsk Basin; 78M – Bornholm Basin; BY15 – Gotland Basin (based on HELCOM, 2006)..... 54
Figure 14. OCEANIA Research vessel..... 68
Figure 15. Plexiglas coring tube from GEMAX gravity corer..... 68
Figure 16. Precipitate and filtrate after oxalate precipitation..... 73
Figure 17. Ion exchange columns..... 74
Figure 18. Tandem column arrangement of the UTEVA/TRU resins..... 75
Figure 19. Capacity factors k' for various actinides on UTEVA resin concerning the acid concentration (23–25°C) (www.eichrom.com)..... 76

Figure 20. Capacity factors k' for various actinides on TRU resin concerning the acid concentration (23–25°C) (www.eichrom.com) 77
Figure 21. Ice bath in the microprecipitation process 79
Figure 22. Source of ^{241}Am for Alpha Particle Spectrometry 79
Figure 23. Flow diagram of general steps of the total analytical process 80
Figure 24. Alpha spectrum of a commercially available calibration source containing ^{237}Np, ^{241}Am, and ^{244}Cm 82
Figure 25. Alpha spectrometer at the University of Gdańsk 83
Figure 26. Alpha spectrum of americium isotopes 84
Figure 27. Approach and structure of the specific guidance for quantifying uncertainty 89
Figure 28. Depth profiles for dry bulk density 100
Figure 29. Age-depth model for Gotland Basin sediment core. From left to right: $^{210}Pb_{ex}$ and the CF:CS age model 102
Figure 30. Age-depth model for Gdańsk Basin sediment core. From left to right: $^{210}Pb_{ex}$ and the CF:CS age model 103
Figure 31. Age-depth model for Bornholm Basin sediment core. From left to right: $^{210}Pb_{ex}$ and the CF:CS age model 103
Figure 32. Comparison of CF:CS and CRS age models in analyzed sediments 106
Figure 33. Deposition histories of ^{137}Cs in sediments from the southern Baltic Sea ... 111
Figure 34. The activity concentrations of ^{241}Am in sediment collected in 2010 from the Gotland Basin 114
Figure 35. The activity concentrations of ^{241}Am in sediment collected in 2010 from the Gdańsk Basin 115
Figure 36. The activity concentrations of ^{241}Am in sediments collected in 2019 from Bornholm Basin 118
Figure 37. The activity concentrations of ^{241}Am in sediments collected in 2019 from the Gdańsk Basin 119
Figure 38. The activity concentrations of ^{241}Am in sediments collected in 2019 from Gotland Basin 121
Figure 39. Boxplot of ^{241}Am concentration in all studied samples from different areas. 78M: Bornholm Basin, BY15: Gotland Basin, P1: Gdańsk Basin 125
Figure 40. The activity concentrations of ^{241}Am in sediments from Gotland Basin collected in 2010 and 2019 129

Figure 41. The activity concentrations of ^{241}Am in sediments from Gdańsk Basin in reference to the history of atmospheric nuclear weapon tests 130
Figure 42. The activity concentrations of ^{241}Am in sediments from Bornholm Basin in reference to the history of atmospheric nuclear weapon tests 131
Figure 43. The activity concentrations of ^{241}Am in sediments from Gotland Basin in reference to the history of atmospheric nuclear weapon tests 132

List of Tables

Table 1. ^{241}Am decay scheme - minimum intensity 2%, up to five energies, with at least one entry per radiation type (ATSDR, 2004) 14
Table 2. ^{243}Am decay scheme - minimum intensity 2%, up to five energies, with at least one entry per radiation type (ATSDR, 2004) 16
Table 3. Physical and chemical properties of americium and selected americium compounds (ATSDR, 2004) 20
Table 4. Summarized stability constants of the most stable complexes of Am(III) with inorganic and simple organic complexes (according to Runde and Schulz, 2008) 22
Table 5. Summary of dating models highlighting key assumptions of each of the two dating models used..... 46
Table 6. Advantages and disadvantages of alpha spectrometry (Vajda et al., 2020) 50
Table 7. The ten largest rivers (according to drainage area) feed into the Baltic Sea region (The BACC Author Team, 2015; Kulinski and Pempkowiak, 2011). The Göta River drains into the Kattegat, sometimes included in the Baltic Sea region..... 56
Table 8. Sampling locations..... 65
Table 9. Mass and porosity of the samples 69
Table 10. Characteristics of the calibrated solid mixed nuclide source..... 81
Table 11. List of available reference materials produced by IAEA for analysis of ^{241}Am radionuclides in the soil and sediment (extended uncertainty at k=2)..... 93
Table 12. List of available standard reference materials from NIST for analysis of ^{241}Am radionuclides in the soil and sediment (extended uncertainty at k=2)..... 94
Table 13. Activity concentrations in Bq·kg^{-1} dry weight for ^{241}Am radioisotope in IAEA references materials (decay ^{241}Pu corrected value and extended uncertainty at k=2) 95
Table 14. Activities of ^{210}Pb total, supported, excess, and porosity concerning the depth of the sediment cores 78M, BY15, and P1 (extended uncertainty at k=2); NA – not available 97
Table 15. Sediment accumulation rates and mass accumulation rates calculated from radiolead-dated cores from the Baltic Sea, CS:CF model (extended uncertainty at k=2) 101
Table 16. The age model (CFCS, CRS), sediment accumulation rates, and mass accumulation rates (CRS model) calculated from radiolead-dated cores from the Baltic Sea (extended uncertainty at k=2) 104

Table 17. Activity concentration of ^{137}Cs in southern Baltic Sea bottom sediments (extended uncertainty at k=2) 108
Table 18. Activity concentrations of ^{241}Am in sediments from 2010 (extended uncertainty at k=2) 113
Table 19. Activities of ^{241}Am and the estimated age concerning the depth of the sediment cores 78M, BY15, and P1 (extended uncertainty at k=2) 116
Table 20. Distributions of ^{241}Am in sediments in some specific locations..... 122
Table 21. Descriptive statistics of radionuclide ^{241}Am concentration in bottom sediments of the southern Baltic Sea 126
Table 22. Summary of Kruskal-Wallis Test and Dunn's Method Pairwise Comparisons for radionuclide ^{241}Am concentration in bottom sediments of the southern Baltic Sea 127

DOROBEK NAUKOWY

DANE LICZBOWE

Sumaryczny IF wszystkich publikacji	**31,763**
Sumaryczna liczba cytowań[1] wszystkich publikacji	**25 / 31**
Sumaryczna punktacja MEiN	**750**
Indeks Hirscha[2]	**3**

[1]Liczba cytowań publikacji według bazy Web of Science (WoS) / Google Scholar

[2]Indeks Hirscha według bazy Web of Science (WoS)

Lista publikacji

1. **Block, K**., Qiao, J., Zaborska, A., & Strumińska-Parulska, D. (2024). Vertical distribution of ^{241}Am in the southern Baltic Sea sediment profiles. *Marine Pollution Bulletin* , *202* , 1–11. https://doi.org/10.1016/j.marpolbul.2024.116305
2. Moniakowska, A., Konieczyński, P., **Block, K**., Lysiuk, R., Shapovalova, N., & Strumińska-Parulska, D. (2024). The presence of radiotoxic ^{210}Po and ^{210}Pb in Ukrainian wild medicinal plants and the assessment of related dose and cancer risk. *Journal of Environmental Quality* , 1–12. doi.org/10.1002/jeq2.20555
3. **Block-Łaszewska, K**., Benedik, L., & Strumińska-Parulska, D. (2023). Advancing environmental monitoring: A comparative analysis of sequential radiochemical methods for precise alpha-particle spectrometry analysis of ^{241}Am in soil and marine sediment samples. *Marine Environmental Research* , *192* , 1–10. doi.org/10.1016/j.marenvres.2023.106243
4. Zhang, D., Niemczyk, A., Moniakowska, A., **Block, K**., Olszewski, G., & Strumińska-Parulska, D. (2023). On ^{210}Po and ^{210}Pb in algae diet supplements - the assessed radiation hazard of aquatic superfoods. *Marine Pollution Bulletin* , *188* , 1–5. doi.org/10.1016/j.marpolbul.2023.114591
5. Moniakowska, A., **Block-Łaszewska, K**., & Strumińska-Parulska, D. (2022). Determination of natural thorium isotopes (^{230}Th and ^{232}Th) in calcium and magnesium supplements and the potential effective exposure radiation dose for

human. *Journal of Food Composition and Analysis* , *105* , 1–5. doi.org/10.1016/j.jfca.2021.104263

6. Moniakowska, A., Zhang, D., **Block-Łaszewska, K**., Olszewski, G., Zaborska, A., & Strumińska-Parulska, D. (2022). Radioactive isotopes ^{40}K, ^{137}Cs, ^{226}Ra, ^{228}Ra, ^{234}Th in algae supplements - potential radiotoxicity of aquatic superfoods. *Journal of Food Composition and Analysis* , *114* , 1–5. doi.org/10.1016/j.jfca.2022.104862
7. Moniakowska, A., Olszewski, G., **Block, K**., & Strumińska-Parulska, D. (2020). The level of ^{210}Pb extraction efficiency in Polish herbal teas and the possible effective dose to consumers. *Journal of Environmental Science and Health. Part A, Toxic/Hazardous Substances & Environmental Engineering* , *55* , 161–167. doi.org/10.1080/10934529.2019.1678323
8. Olszewski, G., Szymańska, M., Westa, M., Moniakowska, A., **Block, K**., & Strumińska-Parulska, D. (2019). On the extraction efficiency of highly radiotoxic ^{210}Po in Polish herbal teas and possible related dose assessment. *Microchemical Journal* , *144* , 431–435. doi.org/10.1016/j.microc.2018.10.005

Konferencje naukowe

Udział w 43 konferencjach naukowych, w tym 27 krajowych i 16 międzynarodowych, na których zaprezentowano:

• 5 wystąpień ustnych

• 38 postery

Staże i szkolenia

1. Szkolenie „*Towards effective radiation protection based on improved scientific evidence and social considerations – focus on radon and NORM*” organizowane przez Główny Instytut Górnictwa, Katowice - w ramach projektu *RadoNORM*. 12.03–23.03.2021

2. 3-krotny staż naukowy w ramach projektu *Erasmus+*, Jožef Stefan Institute (Słowenia), 03.10.2022–03.03.2023, 01.06.2023-14.06.2023 oraz 09.2022–01.2023

3. SEA-EU DOC Szkolenie „*Entrepreneurship Skills*”, Kadyks, Hiszpania, 17-21.04.2023

4. SEA-EU DOC Training Event "*The problem-solving skills for higher education learners*", Split, 23-28.05.2022

Projekty badawcze

1. Projekt nr BMN 539-T030-B484-20 w ramach Badań Naukowych Służących Rozwojowi Młodych Naukowców oraz Uczestników Studiów Doktoranckich w 2020 roku.
2. Projekt nr BMN 539-T030-B878-21 w ramach Badań Naukowych Służących Rozwojowi Młodych Naukowców oraz Uczestników Studiów Doktoranckich w 2021 roku.
3. Projekt nr BMN 539-T030-B005-22 w ramach Badań Naukowych Służących Rozwojowi Młodych Naukowców oraz Uczestników Studiów Doktoranckich w 2022 roku.